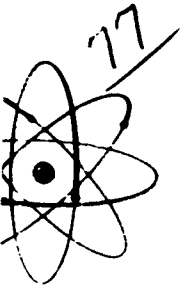

633-1

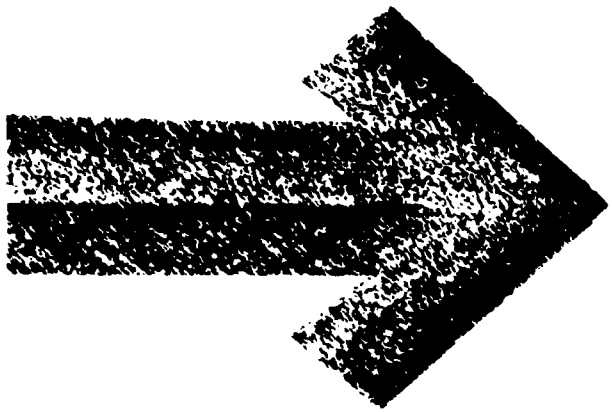

NP-12445
Report Number

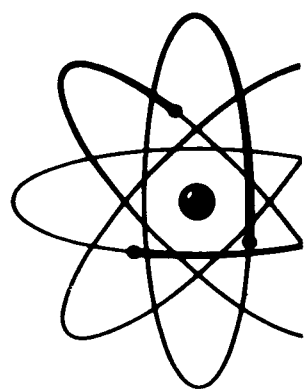

$8.10

United States Atomic Energy Commission
Division of Technical Information

OTI-131(May 1962)

LRSM Final Report

ARMADILLO

Job Assignment 6-62

PROJECT VT/074
Contract AF33(600)-41694
Captain Nancy G. Madden, Project Officer

The Geotechnical Corporation
3401 Shiloh Road
Garland, Texas

30 July 1962

ARMADILLO

INTRODUCTION

The primary aim of this report is to present in both tabular and graphic form, information pertaining to travel times and amplitudes of the principle phases generated by the ARMADILLO detonation. A secondary goal is to make a tentative interpretation of the data in the hope of providing avenues of further research. The interpretations made in this paper should be considered as one of several hypotheses available for explaining the anomalies in LRSM data.

METHODS

Visual Analysis: The data used in the visual phase of this investigation were obtained primarily from 35-mm film recordings. However, 16-mm film composites and paper records made from magnetic-tape playbacks were also examined. The team designator code used in this paper and the techniques of visual data reduction are described in Appendix A. The magnifications and time corrections obtained using these techniques are listed in table 1.

Machine Analysis

The data used in the machine analysis phase of this investigation were obtained from a composite magnetic tape edited from the original LRSM field tapes. The techniques of data processing are discussed in the report furnished by Texas Instruments Incorporated included as Appendix B in this report.

UTILITY OF DATA

The utility of the data provided for the visual analysis phase was discussed previously in the Preliminary Analysis of ARMADILLO. The utility of the data provided for the machine analysis is discussed in the Texas Instruments report included in Appendix B.

RESULTS: VISUAL ANALYSIS:

General

Twenty-nine LRSM stations recorded one or more phases of the ARMADILLO detonation. The distribution of these stations is shown in figure 1. The two stations inside 200 kilometers recorded a P_g first arrival. All stations from 200 to 1000 kilometers with

the exception of SV AZ, ML NM, TC NM and MV CL recorded a reliable P_n first arrival. Six stations recorded weak arrivals attributed to a P path, however, they are considered to be reliable only at SE MN and MP AR.

Travel Times

Certain revisions have been made in the distances, travel times, and residuals originally reported in the Preliminary Report on ARMADILLO. The values listed in table 2 to the best of our knowledge are correct and should be considered to be the final times for ARMADILLO.

P_n

Twenty LRSM stations between 200 and 1000 km recorded a first arrival attributed to a P_n type travel path. Of these the SV AZ, ML NM, TC NM and MV CL arrivals are considered unreliable because of emergent starts or excessive noise conditions during the onset of the phase. The travel times and residuals for P_n or P arrivals are listed in table 2, column 1. Unreliable values are indicated by parentheses. The residuals, obtained by

subtracting Δ/8.1 from the observed travel times are plotted versus epicentral distance in figure 2.

From the observed scatter it is apparent that the travel times cannot be fitted to any single velocity and intercept. Excluding operator error, there are several possible explanations for the observed scatter.

1. Local variations in geology and elevation between individual recording sites will result in some scatter. No corrections were made for these factors and it is possible that deviations of several tenths of seconds may result from them.

2. Regional variations in either the velocity of P_n in the upper mantle or changes in the dip and strike of the refracting discontinuity could be the major cause of the scatter. In the LRSM report on STILLWATER, dated 15 June 1962, the relationship between P_n velocities and structural provinces was pointed out. As shown in figure 3, a similar relation is found for ARMADILLO. The location of the LRSM stations

with respect to the structural provinces of the western United States are shown in figure 4. In figures 5 through 7 the signals recorded in the various provinces are aligned according to the following travel-time equation:

$$T = 7.2 + \Delta/8.1 \quad (1)$$

The travel times to the six stations in the Basin and Range province can be fitted to the following straight line

$$T = 5.4 + \Delta/7.6 \quad (2)$$

The travel times to stations in the Colorado Plateau province can be fitted to

$$T = 7.6 + \Delta/7.9 \quad (3)$$

Three of the 5 other stations having reliable P_n arrivals can be fitted to the Colorado Plateau travel times with little scatter. The remaining two, MV CL and VN UT, are late with respect to the Colorado Plateau travel-time curve. The VN UT time fits the Basin and Range travel times. Berg et al (1960) found similar P_n velocities in that same general region. MV CL is late to both curves, however, noise may have obscured the onset. Another possibility is that the late arrival may be due to the local

geological conditions mentioned previously in the STILLWATER report.

3. Regional differences in crustal thickness may also contribute to the scatter in the P_n data. The difference in intercept times for the P_n travel-time curves indicate that the crust beneath areas outside the Basin and Range is approximately 1.5 times thicker than beneath the Basin and Range. The late arrival at MV CL may alternately be interpreted as indicative of an abnormally thick crustal section in that region, perhaps associated with the Sierra Nevada root.

4. Another possible cause for scatter is the association of arrivals from deeper zones with P_n arrivals. This may have happened at HL ID and DR CO. Both stations are approximately 730 kilometers from the epicenter and both are characterized by very weak first motion followed by prominent second arrivals (see figure 8). The travel time of the second arrival at HL ID is consistent with

Basin and Range P_n travel times and suggests that this velocity zone may extend beneath the Idaho Batholith.

The travel time of the prominent second arrival at DR CO may be associated with first arrival travel times at WM AZ, FS AZ and SF AZ.

P

At epicentral distances greater than 1000 kilometers weak first arrivals were recorded at 6 LRSM stations. However, they can only be considered to be reliable at the two stations approximately 2000 kilometers from the epicenter. At the remainder of the stations beyond 1000 kilometers the first arrivals are of dubious quality. As indicated in figure 2, these arrivals are characterized by a higher apparent velocity than the P_n arrivals. This factor, coupled with a change in character, is according to Romney (1959), indicative of a wave which has traveled a deeper path in the mantle.

P_g

The travel times and residuals for P_g are listed in table 2, column 2. The residuals, obtained by subtracting $\Delta/6.0$ from the observed travel time, are plotted versus epicentral distance in figure 9.

With the exception of the travel times to N2 NV and DV CL , the data points shown are for later arrivals.

Although there is considerable scatter, the travel times can be fitted generally to the following equation:

$$T = 1.5 + \Delta/6.0 \qquad (4)$$

The large intercept time and the difference in character between P_g first and later arrivals, discussed previously in the STILLWATER report, suggests that the true onset of P_g is rarely recognized when it is recorded as a later arrival.

P_{g2}

Waves arbitrarily identified as P_{g2} in the STILLWATER report were also found on a number of the ARMADILLO records. The travel times and residuals for this phase are listed in table 2, column 4. The residuals, obtained by subtracting $\Delta/6.0$ from the observed time are plotted versus distance in figure 10.

L_g

The travel times and residuals for L_g are listed in table 2, column 3. The residuals obtained by subtracting $\Delta/3.5$ from

the observed time, are plotted versus epicentral distance in figure 11. The scatter of the data points is in part related to the difficulty in determining the actual onset of the L_g arrival.

P?

Bursts of energy occurring between the P_n and P_g phases were noted on a number of the ARMADILLO records and at present the origin of these arrivals is unknown. Until further progress can be made in the identification of these waves, no further data on them will be included in the LRSM reports.

AMPLITUDES

General

The following techniques were used to obtain raw data for the amplitude study: The a, b, c and d, peak-to-peak trace amplitudes were measured for first arrivals. For later arrivals only the maximum (d) peak-to-peak amplitude was measured due to the uncertainty involved in determining the first motion of a later arrival. These values, together with the computed earth motion ,and the earth motion divided by the period, hereinafter referred

to as the A/T ratio, are listed in tables 4 through 8. The final value plotted versus distance in figures 12 through 16, was obtained by dividing the A/T ratio by 2 to obtain the zero-to-peak value.

P_n

Data concerning P_n amplitudes are listed in table 4. The zero-to-peak A/T ratios for the first and maximum motion are plotted versus epicentral distance in figures 12 and 13 respectively.

The considerable scatter of the data points in figure 12 is partially the result of two factors. At distances less than 500 km, even though the true first motion could be positively identified, the signal-to-noise ratio was generally low enough to introduce some errors. At greater distances the true first motion was more than likely lost in the background noise, and the value reported for the "a" amplitude probably represents a value for the "b" or "c" amplitude. As might be expected, the data is more closely grouped in figure 13, and in this plot the rate of attenuation with distance is approximated by an inverse cube slope. A straight line with an inverse cube slope

is also shown in figure 12 but primarily for reference. It is interesting to note that if in figure 12 only the data inside 450 km is considered a higher attenuation rate is obtained.

Later Arrivals

The maximum amplitudes for P_g and L_g are listed in tables 4 and 5. The zero-to-peak A/T ratios are plotted versus distance in figures 14 and 15. For P_g the attenuation rate is best approximated by an inverse cube slope while an inverse 4th power slope seems to fit the L_g data better.

Separation of Amplitude by Structural Province

In figure 16, the maximum zero-to-peak A/T ratios for P_n, P_g and L_g are replotted by structural province. By presenting the data in this fashion, several interesting points become more apparent.

1. The attenuation rate for all phases can be approximated by an inverse cube slope.

2. The position of an individual data point relative to the position of adjacent data points is generally constant

for both the P_n and P_g phases. This suggests that the scatter is not completely due to random error.

3. The L_g amplitudes in general are lower at stations outside the Basin and Range province.

AFTERSHOCK

General

The ARMADILLO detonation was followed by a series of minor tremors culminating in a major crater collapse at 16:42:23.6Z. The travel times and amplitude of the principal phases of this event were compared to those of the main shock in order to bring to light any significant differences between the two. The results are tabulated in tables 6 through 8 and plotted in figures 17 through 26.

Travel Times

The travel times and residuals for the P_n, P_g and L_g phases are listed in table 6 and plotted in figures 17 through 19. The scatter of points in these figures is probably due to poor picks rather than differences in travel time.

Amplitudes

The periods and maximum amplitudes for the P_n, P_g and L_g phases are listed in table 7. The ratio at zero-to-peak A/T ratios for each are plotted versus epicentral distance in figures 20 through 22. The best fit to data obtained from the main shock is shown for comparative purposes.

The ratio of the maximum P_n, P_g and L_g A/T ratios for the main event are compared in table 8 to those of the aftershock. In figures 23 through 25 these values are plotted versus bearing and distance.

L_g/P_g Amplitude Ratios

The L_g/P_g amplitude ratios for the main event and aftershock were computed and are listed in table 8. In figure 26 the ratio of the L_g/P_g ratios and aftershock are plotted versus distance. Although there is considerable scatter, the results suggest that the L_g/P_g amplitude ratio tends to be higher for the aftershock than for the main detonation. However, further investigation is necessary before any positive statement can be made.

Period Ratios

The ratio of the period of the maximum amplitude for the main event was compared to that of the aftershock. The results are tabulated in table 8 and plotted versus distance in figures 27 through 29. As can be seen, the periods of the aftershock are significantly higher than those of the main event.

RESULTS: MACHINE PROCESSING

The following section is drawn largely from the report submitted by Texas Instruments Incorporated concerning the results of the machine processing of the seismic data from 18 LRSM stations which recorded the ARMADILLO detonation. A copy of this report is included as Appendix B, Part 1.

The principal goal of the machine processing was to analyse the spectral content of the P_n, P_g and L_g phases. Unfortunately, due to the relatively short distances involved, little spectral separation of the phases was noted. Therefore, spectral analysis of individual phases was precluded.

The data processing results for each station include the following:

1. Spectral-energy density analyses taken over a time interval extending from the predicted P_n arrival time to a point beyond which no signal is discernible.

2. Noise-power density spectra taken from an 81.92 second time interval immediately prior to the predicted P_n time.

3. Signal-to-noise ratio spectra obtained by computing the ratio of signal-energy density to the noise-power spectra at 0.1 cps intervals.

4. Octave-band width integrations of the signal-energy density spectra obtained by integrating the signal-energy density spectra over octave-band widths having center frequencies ranging from 0.15 to 9.3 cps.

The results for individual stations are presented graphically in Appendix B, plates 1 through 18. The abscissa in all figures is given in cps. The ordinates for the signal energy and noise-power density spectra are expressed in millimicrons^2 per cps (mμ^2/cps). The ordinate for the octave-band width integration

is expressed in millimicrons^2 ($m\mu^2$). The ordinate for the signal-to-noise ratio density spectra is expressed in db where db = 10 $\log_{10}$(S/N).

In addition, Texas Instruments Incorporated submitted several large time-domain displays, the nature of which is discussed in Appendix B. However, due to their size they are not included in this report.

In figures 30A through 30D, the maximum signal-energy density and the signal-energy densities at 1.0, 2.0 and 3.0 cps are plotted versus epicentral distances. The rate of attenuation for each is best approximated by an inverse 7th power slope.

There is some suggestion that the scatter in total signal strength may be azimuthally controlled. However, with the exception of the stations along the southeast profile, the data are inconsistent.

In figure 31, the maximum signal-energy densities were reduced to db equivalents where db = 10 $\log_{10}$(maximum signal-energy density) and contoured at a 10 db interval.

The result is an assymetric radiation pattern indicating that more energy was directed to the north than in other directions.

An alternate approach to explaining the anomalies in total signal strength is by examining the signal-energy densities in a given province.

In figures 32 through 34, the signal-energy densities recorded within a given province are arranged in order of increasing distance. The graph on the right is a plot of the maximum signal-energy density recorded at each station within that province.

The results indicate that in the Basin and Range province the total signal energy is a factor of 7.5 higher to the north and northeast than it is in other directions. A less likely assumption is that the attenuation rate is approximated by a lower slope and that there is no azimuthal variation.

In the Colorado Plateau province the data can be fitted to an inverse 7th power slope with little scatter.

The data recorded in other provinces, as might be expected, shows considerable scatter. The signal-energy densities are

abnormally low at CP CL, MV CL, HL ID and LC NM. At the remaining two stations, VN UT and TC NM, the data could be fitted to the Colorado Plateau data.

In figure 35 the frequency at which the maximum signal-energy density occurs is plotted versus distance. It should be noted that this frequency shows a definite tendency to shift towards lower values as the distance is increased.

SIGNAL ENVELOPE STUDIES

The strong similarity between signals recorded in the same structural province was pointed out earlier in the STILLWATER final report. As can be seen from figure 36, a similar phenomena is noted for ARMADILLO. Furthermore, the signal envelope retains the same general character as noted in the STILLWATER report (i.e; a relatively simple envelope in the Basin and Range and a more complex envelope in adjacent regions.)

SUMMARY OF RESULTS AND CONCLUSIONS

1. The apparent P_n velocities derived from the ARMADILLO data vary from 7.6 km/sec in the Basin and Range to 7.9 km/sec in the Colorado Plateau. This variation in velocity may result from real variations in the properties of the upper mantle or from variations in the strike and dip of the refracting discontinuity. Without reversed profiles a unique solution to the problem cannot be found.

2. The difference in intercept times between the Basin and Range and Colorado Plateau P_n travel-time equations indicate that the crust is approximately 1.5 times thicker beneath the Basin and Range than beneath the Colorado Plateau. Insufficient data from other provinces also indicate a relatively thick crust in those regions. The relatively low L_g signal strength in regions adjacent to the Basin and Range also indicates a thicker crust in those areas.

3. The scatter of the P_g travel-time data and the large intercept time suggests that the true onset of P_g is rarely identified when P_g is recorded as a later arrival.

4. The scatter of the L_g data may be the result of inconsistent picks rather than real variations in velocity.

5. The P_{g2} phase which is characterized by strong vertical and transverse motion, was recorded at a number of stations, but the data is too scattered to provide a reliable velocity.

6. The P? phase or phases are generally recorded as arrivals between the P_n and P_g phases, at distances greater than 300 km. However, the travel times of these phases show no consistency and their origin and travel path is questionable.

7. The ARMADILLO amplitude data indicates that the attenuation rate for P_n and P_g phases with distance can be approximated by an inverse cube slope. The L_g amplitude attenuation rate can be approximated by

an inverse 4th power slope. There also appears to be a tendency for the ratio of the maximum amplitudes of P_g and P_n to remain relatively constant regardless of the scatter of points. This may be due to undetected variations in instrument constants or to a local focusing phenomena in the vicinity of the recording site.

8 Comparison of the aftershock data to that of the main event brought to light a wide variation in amplitude ratios. The cause for this is not yet understood. Also, an apparent increase in the L_g/P_g ratios and the period of the principal phases was noted for the aftershock.

The results of the machine analysis phase are less concrete since the spectra were averaged over the whole signal. However, certain statements can be made concerning the entire signal.

1. Although the data shows considerable scatter, the average rate of attenuation for the entire signal-energy density can be approximated by an inverse 7th power slope

2. The variation in total signal-energy density from station to station may be related to azimuth but the data is consistent only along the southeast profile. Alternatively, the variation in signal-energy density may be related to structural province. A more likely possibility is that both factors play a role in determining the amount of energy recorded at a give . station.

3. The frequency at which the maximum signal-energy density occurs tends to decrease with distance.

REFERENCES

Berg, J. W., Jr., K. L. Cook, H. D. Narcns and W. M. Dolan (1960), Seismic Investigation of Crustal Structure in the Eastern Part of the Basin and Range Province; Bull. Seism. Soc. Am., v. 50, no. 4, pp 511-536.

Romney, C. F. (1959), Amplitudes of Seismic Body Waves from Underground Nuclear Explosions; Jour. Geophys. Research, v. 64, no. 10, pp 1489-1498.

Table 1. ARMADILLO.
Time corrections and magnifications of film recordings (at 10X view)

Station	Distance (Km)	Time corr. (sec)	Short Period Magnification in thousands at 1 sec period Z	R	T	Long Period Magnification in thousands at 25 sec period Z	Z Le	R	T
N2 NV	45.8	+0.2	4.7	5.1	5.9	-	-	-	-
DV CL	134.4	0.0	22	19	42	33.8	3.4	24.6	32.6
MN NV	241.8	-0.6	39	39	39	17.0	1.8	16.5	15.3
AT NV	285.4	-0.2	90	78	78	18.9	2.0	18.9	12.8
KN UT	285.8	-0.4	69	56	56	9.3	1.0	13.1	23.2
BF CL	295.9	+2.4	98	110	99	12.2	1.2	12.4	13.2
TN CL	315.8	0 0	160	152	142	9.5	1.2	7.0	7.2
WM AZ	388.2	-1.2	207	232	226	15.0	1.5	15.4	16.1
FM UT	413.7	+0.0	55	29	30	12.7	1.0	5.3	4.9
FS AZ	479.1	0.0	352	367	360	26.7	3.3	23.6	24.8
CP CL	479.6	-0.5	349	336	326	6.2	0.6	5.9	6.7
WI NV	493.7	-0.3	312	287	279	14.5	1.5	13.5	12.9
MV CL	521.1	+1.6	331	320	348	7.3	0.7	7.5	8.3
SF AZ	577.2	0.0	222	212	228	13.6	1.3	14.1	8.4
VN UT	680.3	+20.3	150	157	190	23.6	2.9	13.0	12.2
SV AZ	700.6	0.0	90	90	90	16.2	1.5	-	16.6
VT OR	707.6	+0.1	349	296	296	15.6	1.7	18.3	16.7
DR CO	733.7	+0.2	377(S)	394(S)	405(S)	20.9	2.4	14.9	14.2
HL ID	748.8	0.0	358	331	369	17.2	0.9	9.5	10.7
ML NM	769.1	-8.4	217	218	186	2.7	0.6	2.3	3.0
TC NM	890.9	0.0	135	140	123	7.7	0.7	7.7	7.4
PT OR	981.0	0.0	195	253	300	9.7	0.9	1.3	3.8
LC NM	1005.5	+0.7	392	412	392	14.8	1.5	13.1	13.0
PM WY	1031.8	+0.6	143	131	114	9.3	0.8	8.1	8.8
RT NM	1041.1	+0.2	123(S)	142(S)	108(S)	3.6	0.4	3.0	2.9
EP T.:	1084.1	-0.6	282	320	255(S)	9.5	1.0	16.2	10.2
EF TX	1197.2	-0.4	370	415	426	8.6	0.9	7.7	11.1
GN NM	1234.1	+15.3	78	86	71	5.2	0.5	5.1	1.5
BM TX	1312.7	0.0	186	250	253	9.0	1.0	9.4	15.2
SS TX	1490.3	0.0	435	416	416	18.4	1.5	16.9	21.8
WN SD	1512.8	-1.2	54	50	45	3.2	0.2	3.5	3.7
HB OK	1554.0	+1.6	81	105	99	19.5	2.0	4.0	6.6
WM SO	1594.4	0.0	820	860	760	-	-	-	-
LP TX	1754.8	0.0	395	416	304	26.2	2.8	5.0	8.9
SJ TX	1964.2	-0.2	38	41	44	7.4	0.6	5.2	5.0
SE MI	1975.4	0.0	208(S)	219	214	15.8	1.6	15.1	17.2
MP AR	2081.4	-1.0	140	106	111	5.8	0.7	10.8	8.2
NG WS	2509.3	-0.2	55	80	73	3.8	0.3	4.1	4.1
MM TN	2728.4	-0.7	102	129	82	11.7	0.8	13.7	16.1
BL WY	3058.0	-0.4	68	52	58	5.2	0.7	4.8	7 1
DH NY	3545.2	+0.1	59	82	99	-	-	11.6	7.2
BG ME	3982.4	+1.6	54	59(S)	66	6.0	0.6	-	6.6

(S) Magnification from 1 cps sine wave calibration

Table 2. ARMADILLO. Travel Times and Residuals of Principal Phases (in seconds)

Station	Distance (Km)	1 Pn or P T	1 Pn or P Residual	2 P_g T	2 P_g Residual	3 S_g or L_g T	3 S_g or L_g Residual	4 P_{g2} T	4 P_{g2} Residual	Remarks
NZ NV	65.8	-	-	8.3	0.7	16	2.9	-	-	
DV CL	134.4	-	-	22.9	0.5	40	1.6	-	-	
MN NV	241.8	37.6	7.0	41.8	0.7	69.5	0.4	42.9	+ 2.6	
AT NV	285.4	43.5	8.3	48.0	0.4	82.4	0.9	50.2	+ 2.6	
KN UT	285.8	43.2	7.9	48.3	0.7	83	1.3	50.8	+ 3.2	
BF CL	295.9	44.8	8.3	50.3	1.0	-	-	53.5	+ 4.2	
TH CL	315.8	46.6	7.6	54.1	1.5	91	0.8	57.0	+ 4.4	Good P_{g2}
WM AZ	388.2	57.0	9.1	65.0	0.3	-	-	70.1	+ 5.4	Poorly defined P_{g2}
FM UT	413.7	59.4	8.3	69.9	1.0	117	-1.2	74.4	+ 5.5	Very poor P_{g2}
FS AZ	479.1	68.4	9.3	79.5	-0.3	-	-	90.8	11.0	Good P_{g2}
CP CL	479.6	66.9	7.7	80	0.1	136	-1.0	86.8	+ 6.9	Good P_{g2}
WI NV	493.7	70.0	9.1	81	-1.3	144	2.9	84.4	2.1	
MV CL	521.1	75.4	11.1	89	2.2	147	-1.9	-	-	
SF AZ	577.2	81.0	9.8	97	0.8	167	2.1	99.4	+ 3.2	Poorly defined P_{g2}
VN UT	600.3	95.3	11.4	117	3.6	192	-2.4	125.1	11.7	Poorly defined P_{g2}
SV AZ	700.6	102.3	15.8	116.2	-0.6	200	-0.2	-	-	High-noise level
VT OR	707.6	98.9	11.6	117	-0.9	200	-2.2	122.2	+ 4.3	
DR CO	733.7	99.9	9.4	121	-1.3	207	-2.6	-	-	Strong arrival 1.1 seconds after P_n
NL ID	748.8	101.3	9.9	124.3	-0.5	-	-	129.9	+ 5.1	Strong arrival 2.8 seconds after P_n
ML NM	769.1	107.5	12.5	130.6	2.4	-	-	138.8	+10.6	Very doubtful Pn, possible background
TC NM	898.9	126.7	16.8	150	1.5	255	0.5	156.7	+ 8.2	Very doubtful Pn
PT OR	981.8	135.8	13.9	-	-	281	0.7	-	-	No P_g recognized
LC NM	1005.5	(149.0)	24.9	170	2.4	291	3.3	176.6	+ 9.0	Start time in doubt
PM WY	1031.8	-	-	-	-	-	-	-	-	
RT NM	1041.1	(161.0)	32.5	176	2.5	293	-4.4	-	-	Start time in doubt
EP TX	1084.1	-	-	182	1.3	-	-	-	-	Start time in doubt
EF TX	1197.2	-	-	206	4.5	-	-	-	-	
GN NM	1234.1	-	-	206	0.3	-	-	-	-	
BM TX	1312.7	-	-	-	-	-	-	-	-	
SS TX	1490.3	-	-	-	-	-	-	-	-	
WN SD	1512.8	-	-	-	-	-	-	-	-	
NB OK	1554.0	-	-	-	-	-	-	-	-	
WM SO	1594.4	(210.0)	14.1	271	5.3	-	-	-	-	
LP TX	1754.8	(227.0)	10.5	-	-	-	-	-	-	
SJ TX	1964.2	-	-	-	-	-	-	-	-	
SE MN	1975.4	251.0	7.2	-	-	-	-	-	-	
MP AR	2081.4	262.3	5.5	-	-	-	-	-	-	
NG WS	2509.3	-	-	-	-	-	-	-	-	
MM TN	2720.4	-	-	-	-	-	-	-	-	
BL WV	3050.0	-	-	-	-	-	-	-	-	
SH NY	3545.2	-	-	-	-	-	-	-	-	
BG ME	3982.4	-	-	-	-	-	-	-	-	

Residuals

Pn or P = T - Δ /8.1
Pg = T - Δ /6.0
Lg = T - Δ /3.5
Parentheses indicate doubtful values

Table 3. ARMADILLO. Periods and amplitudes of Pn or P

Station	Distance (Km)	Period (sec)	Trace amplitude (mm) a	b	c	d	Ground motion (mμ) a	b	c	d	Ground motion/period (mμ/sec) a	b	c	d
NZ NV	65.8	-	-	-	-	-	-	-	-	-	-	-	-	-
DV CL	134.4	-	-	-	-	-	-	-	-	-	-	-	-	-
MN NV	241.8	0.6	2	7	12	12	22	76	130	130	37	126	220	220
AT NV	285.4	0.5	0.5	8	16	16	6.1	33	66	66	12	66	132	130
KN UT	285.8	0.5	2	8	10	26	11	42	54	138	22	84	108	280
BF CL	295.9	0.6	2	8	16	16	8.6	34	70	70	14	56	116	116
TH CL	315.8	0.5	1.5	8	16	16	3.5	18	36	36	7.0	36	72	72
WM AZ	388.2	0.6	1	4	7	12	2.0	8.1	14.2	24	3.3	13	24	40
FM UT	413.7	0.3	0.5	1	4	4	2.9	5.9	24	24	9.6	2.0	80	80
FS AZ	479.1	0.6	8	16	16	16	9.6	19	19	19	16	32	32	32
CP CL	479.6	0.4	2	6	12	13	1.9	5.8	11	12	4.8	15	28	30
WI NV	493.7	0.8	3.5	5	4	6	7.0	10	8.0	12	8.8	13	10	15
MV CL	521.1	0.5	-	6	-	6	-	6.6	-	6.6	-	13	-	13
SF AZ	577.2	0.4	2	4	4	11	3.0	6.0	6.0	16	7.5	15	15	40
VN UT	600.3	0.4	1	3	4	4	2.2	6.6	8.8	8.8	5.5	16	22	22
SV AZ	700.6	-	-	-	-	-	-	-	-	-	-	-	-	-
VT OR	707.6	0.6	4	6	4	6	4.8	8.4	4.8	8.4	8.0	14	8.0	14
DR CO	733.7	0.5	1	1	1	3	1.0	1.0	1.0	3.0	2.0	2.0	2.0	6.0
NL ID	748.8	0.7	1	2	2	3	1.4	2.8	2.8	4.2	2.0	4.0	4.0	6.0
ML NM	769.1	0.4	0.5	1	1	1	0.8	1.5	1.5	1.5	2.0	3.8	3.8	3.8
TC NM	898.9	0.7	1	1	1	1	3.7	3.7	3.7	3.7	5.3	5.3	5.3	5.3
PT OR	981.8	0.6	1.5	2	2	2	2.5	4.3	4.3	4.3	4.2	5.5	5.5	7.2
LC NM	1005.5	0.7	0.5	1	1	1	0.6	1.3	1.3	1.3	0.8	1.8	1.8	1.8
PM WY	1031.8	-	-	-	-	-	-	-	-	-	-	-	-	-
RT NM	1041.1	-	-	-	-	-	-	-	-	-	-	-	-	-
EP TX	1084.1	-	-	-	-	-	-	-	-	-	-	-	-	-
EF TX	1197.2	0.8	-	-	-	2	-	-	-	3.4	-	-	-	6.2
GN NM	1234.1	0.6	-	-	-	-	-	-	-	-	-	-	-	-
BM TX	1312.7	-	-	-	-	-	-	-	-	-	-	-	-	-
SS TX	1490.3	-	-	-	-	-	-	-	-	-	-	-	-	-
WN SD	1512.8	-	-	-	-	-	-	-	-	-	-	-	-	-
NB OK	1554.0	-	-	-	-	-	-	-	-	-	-	-	-	-
WM SO	1594.4	0.6	-	-	-	2	-	-	-	1.0	-	-	-	1.7
LP TX	1754.8	0.5	-	2	-	2	-	1.9	-	1.9	-	3.8	-	3.8
SJ TX	1964.2	-	-	-	-	-	-	-	-	-	-	-	-	-
SE MN	1975.4	0.6	-	1	1.5	2	-	2.0	3.0	4.0	-	3.4	5.8	6.7
MP AR	2081.4	0.8	0.5	0.5	1	1	2.2	2.2	4.5	4.5	2.7	2.7	5.6	5.6
NG WS	2509.3	-	-	-	-	-	-	-	-	-	-	-	-	-
MM TN	2720.4	-	-	-	-	-	-	-	-	-	-	-	-	-
BL WV	3050.0	-	-	-	-	-	-	-	-	-	-	-	-	-
SH NY	3545.2	-	-	-	-	-	-	-	-	-	-	-	-	-
BG ME	3982.4	-	-	-	-	-	-	-	-	-	-	-	-	-

Table 4. ARMADILLO. Periods and amplitudes of P_g

Station	Distance (KM)	Period (sec)	Trace Amplitude (mm)	Ground motion (mμ)	Ground motion/ period (mμ/sec)
N2 NV	45.8	0.5	10	780	1560
DV CL	134.4	0.6	55	1050	1750
MN NV	241.8	0.6	42	460	760
AT NV	285.4	0.6	48	220	380
KN UT	285.8	0.6	54	330	550
BF CL	295.9	0.7	32	164	240
TN CL	315.8	0.6	58	150	260
WM AZ	388.2	0.6	70	140	230
FM UT	413.7	0.7	22	200	280
FS AZ	479.1	0.7	45	65	92
CP CL	479.6	1.0	30	86	86
WI NV	493.7	0.6	22	30	50
MV CL	521.1	0.8	25	48	60
SF AZ	577.2	0.6	42	80	134
VN UT	680.3	0.7	15	50	72
SV AZ	700.6	0.6	6	28	48
VT OR	707.6	0.6	19	36	60
DR CO	733.7	0.6	12	13	29
HL ID	748.8	0.6	20	32	54
ML NM	769.1	0.6	16	31	52
TC NM	890.9	1.0	8	60	60
PT OR	981.0	-	-	-	-
LC NM	1005.5	1.0	4	10	10
PM WY	1031.8	-	-	-	-
RT NM	1041.1	0.7	3	12	18
EP TX	1084.1	0.8	6	15	19
EF TX	1197.2	0.8	2	3.4	4.2
GN NM	1234.1	0.4	2	8.6	22
BM TX	1312.7	-	-	-	-
SS TX	1490.3	-	-	-	-
WN SD	1512.8	-	-	-	-
HB OK	1554.0	-	-	-	-
WM SO	1594.4	1.0	4	5	5
LP TX	1754.8	-	-	-	-
SJ TX	1964.2	-	-	-	-
SE MN	1975.4	-	-	-	-
MP AR	2081.4	-	-	-	-
NG WS	2509.3	-	-	-	-
MM TN	2728.4	-	-	-	-
BL WV	3058.0	-	-	-	-
DH NY	3545.2	-	-	-	-
BG ME	3982.4	-	-	-	-

Table 5. ARMADILLO. Periods and amplitudes of L_g

Station	Distance (KM)	Period (sec)	Trace amplitude (mm)	Ground motion (mμ)	Ground motion/ period (mμ/sec)
N2 NV	45 8	0.7	80	6850	9800
DV CL	134.4	Too high to measure			
MN NV	241.8	0.8	87	1890	2300
AT NV	285 4	0.5	140	660	1320
KN UT	285.8	0.5	64	422	844
BF CL	295.9	-	-	-	-
TN CL	315.8	0.7	150	535	770
WM AZ	388.2	-	-	-	-
FM UT	413.7	0.6	40	560	940
FS AZ	479.1	-	-	-	-
CP CL	479 6	0.5	20	72	144
WI NV	493.7	Too high to measure			
MV CL	521.1	0 7	37	54	77
SF AZ	577 2	0.6	52	100	168
VN UT	680.3	1.0	13	68	114
SV AZ	700 6	0.6	14	66	110
VT OR	707 6	0.7	60	102	146
DR CO	733.7	0.8	50	78	98
HL ID	748 8	-	-	-	-
ML NM	769.1	-	-	-	-
TC NM	890.9	0 8	10	52	64
PT OR	981 0	0 6	4	5 6	9.4
LC NM	1005.5	1 2	5	15	13
PM WY	1031.8	-	-	-	-
RT NM	1041.1	1.0	3	16	16
EP TX	1084.1	-	-	-	-
EF TX	1197 2	-	-	-	-
GN NM	1234.1	-	-	-	-
BM TX	1312 7	-	-	-	-
SS TX	1490.3	-	-	-	-
WN SD	1512.8	-	-	-	-
HB OK	1554.0	-	-	-	-
WM SO	1594.4	-	-	-	-
LP TX	1754.8	-	-	-	-
SJ TX	1964.2	-	-	-	-
SE MN	1975.4	-	-	-	-
MP AR	2081.4	-	-	-	-
NG WS	2509.3	-	-	-	-
MM TN	2728.4	-	-	-	-
BL WV	3058.0	-	-	-	-
DH NY	3545.2	-	-	-	-
BG ME	3982.4	-	-	-	-

Table 6. ARMADILLO. Aftershock. Times of principal phases

Station	Distance (KM)	First arrival minus event m.	s.	Pn or P T	Pn or P Residual	Pg T	Pg Residual	Lg T	Lg Residual
N2 NV	45.8	12:23.7		-	-	8.4	0.8	15	2
DV CL	134.4	12:23.6		-	-	22.9	0.5	42.4	4.0
MN NV	241.8	12:22		36.4	6.5	40.4	0.1	73.4	4.3
AT NV	285.4	12:23.7		43.6	8.4	49.4	1.8	84.9	3.4
KN UT	285.8	12:23.4		43.0	7.7	47.9	0.3	82.4	0.7
BF CL	295.9	12:23.3		44.5	8.0	-	-	79.4	- 5.1
TN CL	315.8	12:24		(47.4)	8.4	54.4	1.8	91.6	1.4
WM AZ	388.2	12:23.4		(56.8)	8.9	65.3	0 6	-	-
FM UT	413.7	12:34		-	-	69.4	0.4	102.4	-15.8
FS AZ	479.1	12:33		-	-	77.4	-2.4	141.4	4.5
CP CL	479.6	12:24		(64.9)	5.7	79.9	0.0	138 4	1.4
WI NV	493.7	12:34		(69.4)	8.4	80.4	-1.9	143.9	2.8
MV CL	521.1	12:38		-	-	89.4	2 6	150.4	1.5
SF AZ	577.2	12:40		-	-	97.4	1.2	-	-
VN UT	680.3	12:28		(99.4)	15.4	117.4	4.0	192 4	- 2 0
SV AZ	700.6	12:41		-	-	119.4	2.6	-	-
VT OR	707.6	12:44		-	-	119.1	1.2	200.4	- 1.8
DR CO	733.7	12:24		(101.4)	10.8	123.9	1.6	210.4	0.8
HL ID	748.8	12:43		(105.5)	13.1	123.4	-1,4	-	-
ML NM	769.1	12:45		-	-	129.8	1.6	-	-
TC NM	890.9	12:55		(128.4)	18.4	149.4	0.9	254.4	- 0.1
PT OR	981.0	-		-	-	-	-	-	-
LC NM	1005.5	12:42		-	-	168.4	0.8	290.4	3.2
PM WY	1031.8	-		-	-	-	-	-	-
RT NM	1041.1	12:39		-	-	176.4	2.9	-	-

Best origin time for aftershock = 12m 23.5s after event

T = Travel time in seconds from origin time of aftershock

Residuals
Pn or P = T - Δ/8.1
Pg = T - Δ/6.0
Lg = T - Δ/3.5
Parentheses indicate doubtful value

Table 7. ARMADILLO. Aftershock Periods and Amplitudes of Principal Phases

Station	Dist. (KM)	P_n Period (sec)	P_n Trace amplitude (mm)	P_n Ground motion ($m\mu$)	P_n Ground motion/ period ($m\mu$/sec)	P_g Period (sec)	P_g Trace amplitude (mm)	P_g Ground motion ($m\mu$)	P_g Ground motion period ($m\mu$/sec)	L_g Period (sec)	L_g Trace amplitude (mm)	L_g Ground motion ($m\mu$)	L_g Ground motion/ period ($m\mu$/sec)
N2 NV	45.8	---	----	----	----	0.7	2	22	31	0.7	12		130
DV CL	134.4	---	----	----	----	0.6	0.8	9.5	16	0.8	75	1120	1400
MN NV	241.8	0.5	0.5	4.7	9.4	0.8	7	113	141	1.0	9	230	230
AT NV	285.4	1.0	2	22	22	0.9	7	63	70	0.7	20	130	186
KN UT	285.8	0.6	2	12	20	0.7	7.5	55	78	0.7	12	108	155
BF CL	295.9	0.8	3	19	24	0.8	11	70	88	0.8	8.5	56	70
TN CL	315.8	0.7	1	3.2	4.5	0.7	4	13	18	0.7	22	78	112
WM AZ	388.2	0.7	2	4.9	7.0	1.1	12	75	68	---	---	----	---
FM UT	413.7	---	----	----	----	0.7	3	6.5	10	1.0	8	34	34
FS AZ	479.1	---	----	----	----	0.8	7	12	16	0.9	18	41	45
CP CL	479.6	0.6	1	1.2	2.0	0.8	7	12.6	16	0.8	9	17	22
WI NV	493.7	0.8	1.5	----	----	0.8	2	4.0	5.0	0.8	45	100	127
MV CL	521.1	---	----	----	----	0.8	4	7.6	95	1.0	7	20	20
SF AZ	577.2	---	----	----	----	0.8	5	14	18	---	---	----	---
VN UT	680.3	0.7	0.5	1.7	2.4	0.7	2	6.7	9.6	1.0	2	10	10
SV AZ	700.6	---	----	----	----	0.8	2	14	17	---	---	----	---
VT OR	707.6	---	----	----	----	0.7	4	5.8	8.2	0.7	8	14	19
DR CO	733.7	0.5	0.5	.5	1.0	0.8	3	5.0	6.2	0.7	9	11	16
HL ID	748.8	0.6	0.5	.6	1.0	0.6	1	1.2	2.0	---	---	----	---
ML NM	769.1	---	----	----	----	1.3	4	38	30	---	---	----	---
TC NM	890.9	0.6	0.5	1.6	2.6	1.0	2	15	15	1.4	3	61	44
PT OR	981.0	---	----	----	----	---	--	---	---	---	---	----	---
LC NM	1005.5	---	----	----	----	1.2	2	8.3	6.9	1.3	2	11	8.2
PM WY	1031.8	---	----	----	----	---	--	---	---	---	---	----	---
RT NM	1041.1	---	----	----	----	0.9	0.5	3.3	3.6	---	---	----	---

Table 8. ARMADILLO. Comparison of Aftershock to Main Event

Station	Dist.	Amplitude Ratio MF/AS P_n	Amplitude Ratio MF/AS P_g	Amplitude Ratio MF/AS L_g	Period Ratio AS/MF P_n	Period Ratio AS/MF P_g	Period Ratio AS/MF L_g	$L_g P_g$ Ratio Main Event	$L_g P_g$ Ratio Aftershock	$L_g P_g$ Aftershock / $L_g P_g$ Main Event
N2 NV	45.8	--	2.6	8.4	--	1.2	1.0	6.5	5.9	.91
DV CL	134.4	--	2.4	2.1	--	1.5	--	--	--	--
MN NV	241.8	23.4	5.4	2.6	0.8	1.3	1.25	3.0	1.6	.53
AT NV	285.4	6.0	9.4	7.1	2.0	1.5	1.4	3.5	2.7	.77
KN UT	285.8	14.0	6.9	5.4	1.2	1.2	1.4	1.5	2.0	1.3
BF CL	295.9	4.8	2.7	--	1.3	1.1	--	--	--	--
TN CL	315.8	16.0	14.4	8.2	1.4	1.2	1.0	3.0	6.2	2.1
WM AZ	388.2	5.7	2.9	--	1.2	1.8	--	--	--	--
FM UT	413.7	--	7.2	3.5	--	1.0	1.7	3.4	6.9	2.0
FS AZ	479.1	--	5.7	--	--	1.1	--	--	--	--
CP CL	479.6	15.0	5.4	2.8	1.5	0.8	1.6	1.7	1.4	.82
WI NV	493.7	--	16.4	--	1.0	1.3	--	--	--	--
MV CL	521.1	--	6.3	--	--	1	1.4	1.3	2.1	1.6
SF AZ	577.2	--	14.0	--	--	1.3	--	1.3	--	--
VN UT	680.3	9.2	7.5	--	1.7	1	1.0	1.6	1.0	.62
SV AZ	700.6	--	2.8	--	--	1.3	--	2.3	--	--
VT OR	707.6	--	7.3	9.0	--	1.2	1.0	2.4	2.3	.96
DR CO	733.7	6.0	3.6	6.1	1.0	1.3	0.9	4.5	2.6	.58
HL ID	748.8	6.0	27.0	--	0.9	1.0	--	--	--	--
ML NM	769.1	--	1.7	--	--	2.2	--	--	--	--
TC NM	890.9	2.0	4.0	1.4	0.9	1.0	1.75	1.1	2.9	2.6
PT OR	981.0	--	--	--	--	--	--	--	--	--
LC NM	1005.5	--	1.4	1.6	--	1.2	1.1	1.3	1.6	1.2
PM WY	1031.8	--	--	--	--	--	--	--		--
RT NM	1041.1	--	5.0	--	--	1.3	--	0.9		--
	Average	9.8	7.1	4.8						

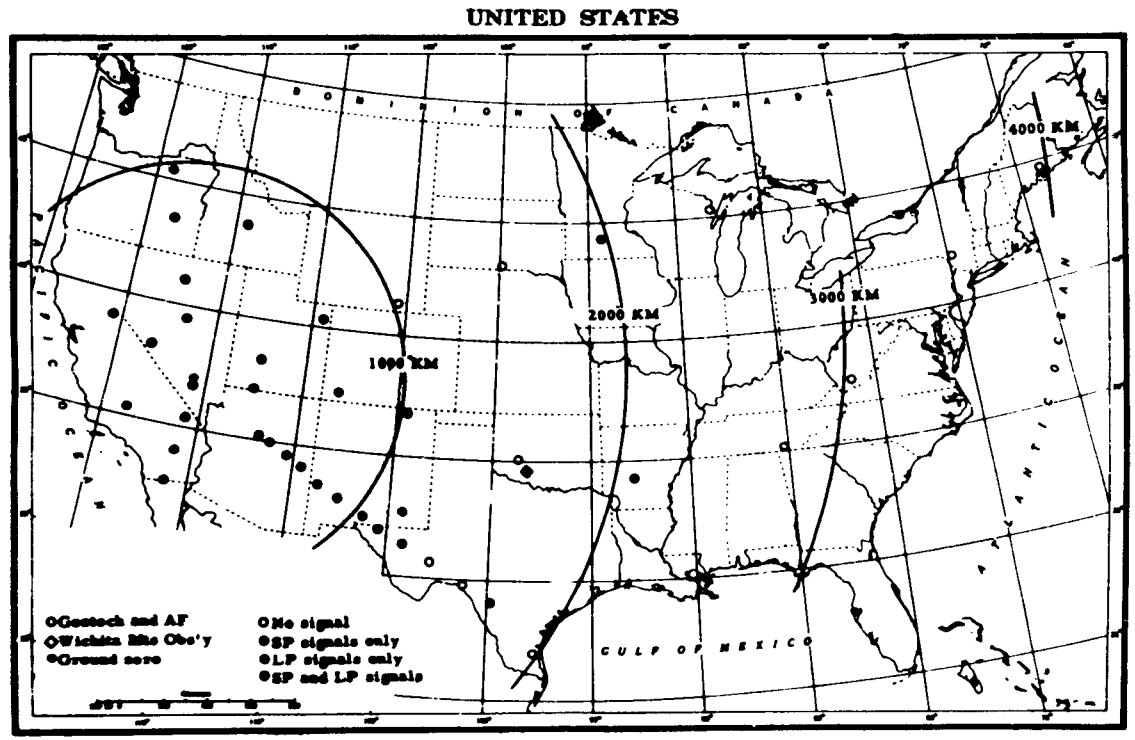

Figure 1. ARMADILLO. VELA-UNIFORM seismic measurement stations.

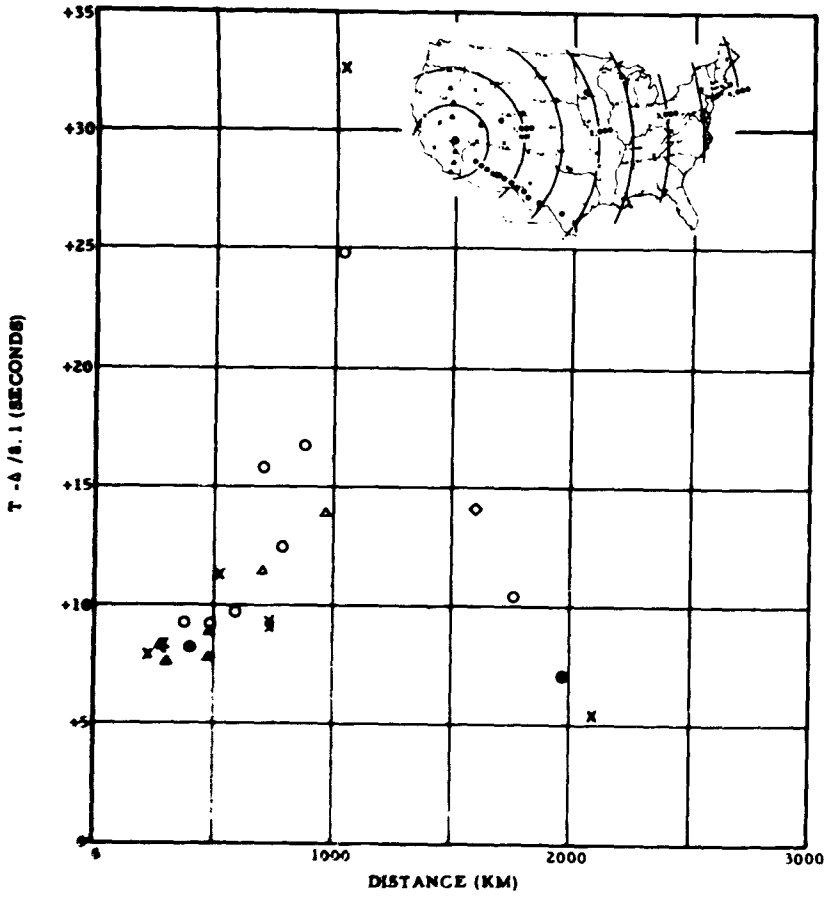

Figure 2. ARMADILLO. Travel times of Pn or P

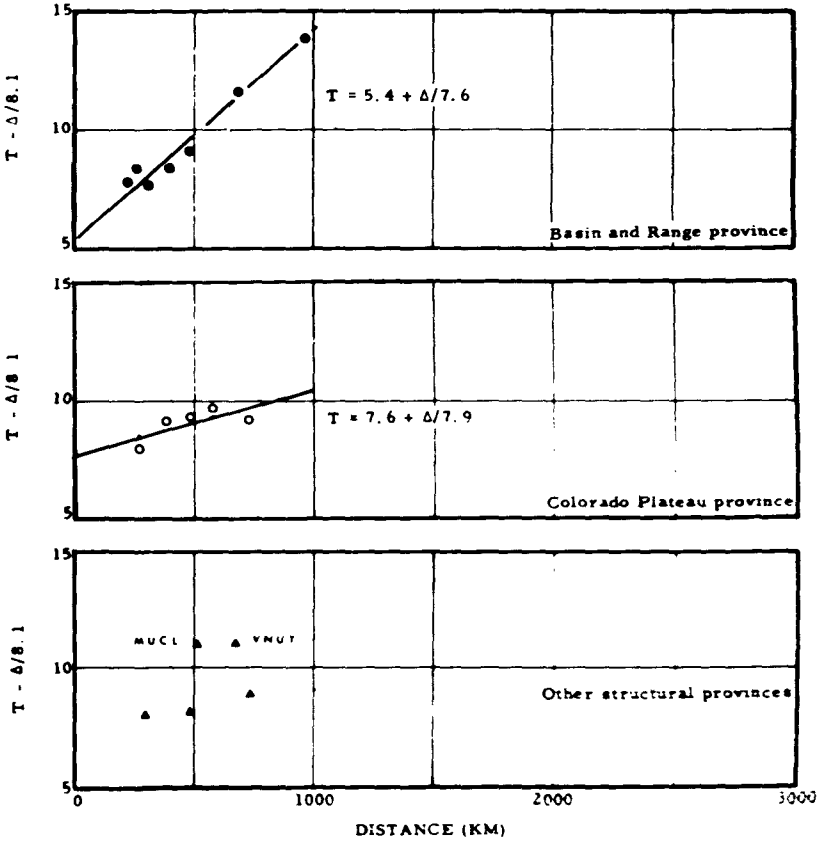

Figure 3. ARMADILLO Reliable Pn arrivals inside 1000 km by Geologic Province.

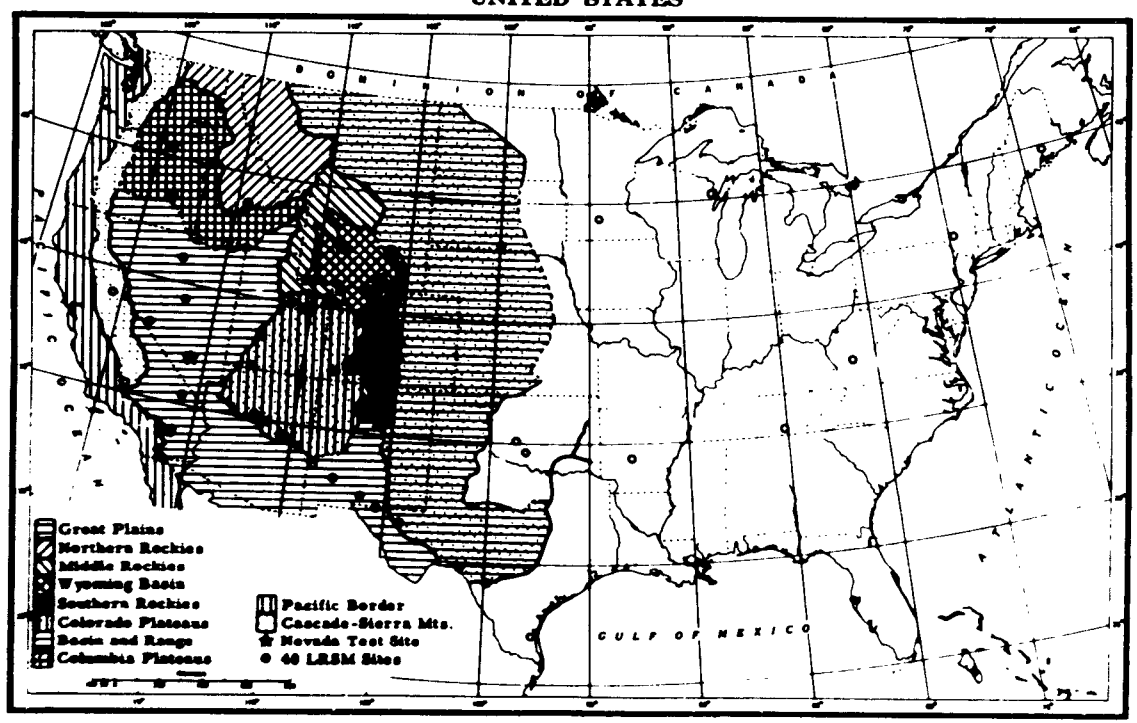

Figure 4. ARMADILLO Physiographic provinces of Western United States (after Ryall, 1962) showing approximate LRSM team locations

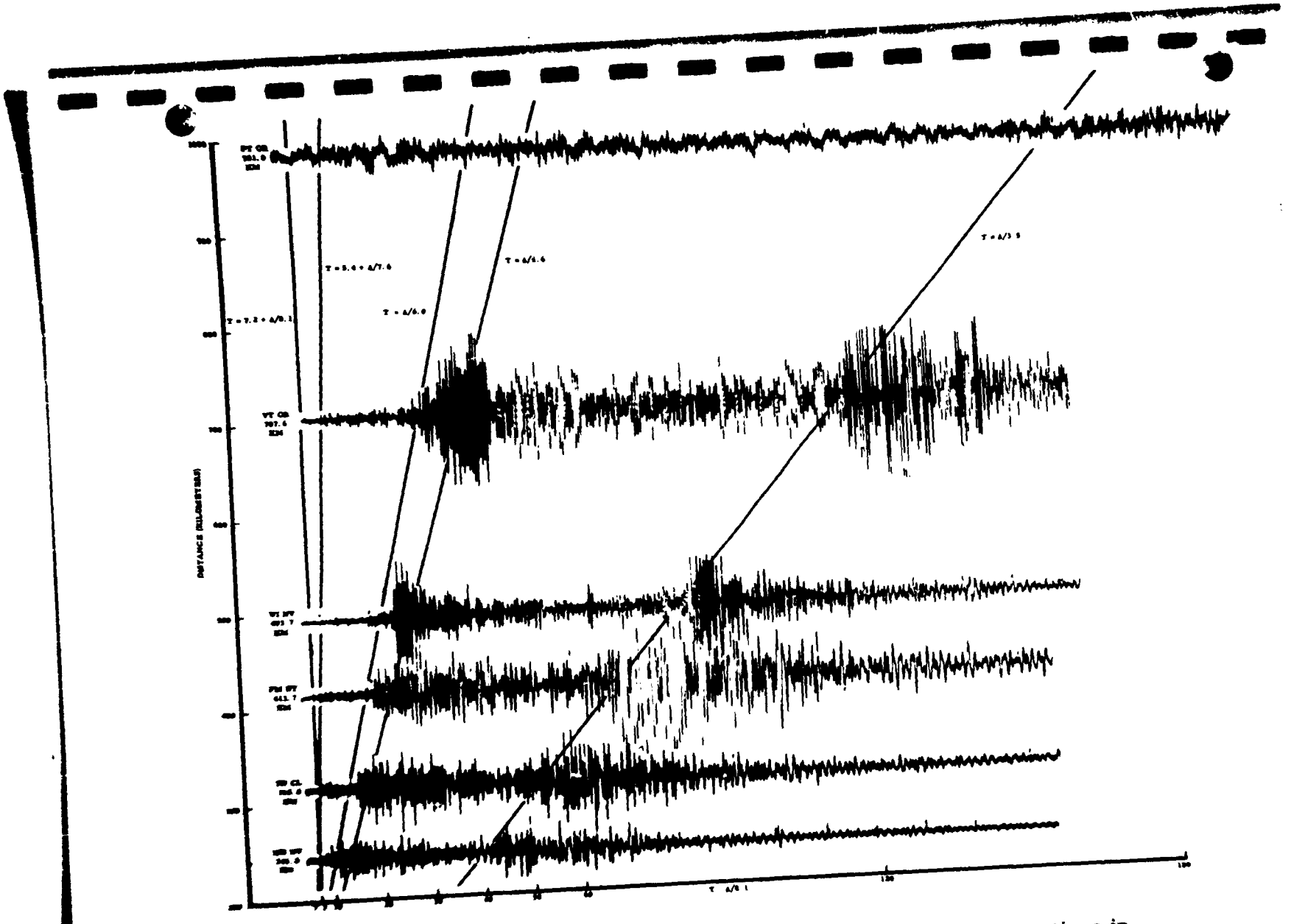

Figure 5. ARMADILLO. Short-period vertical signals recorded at stations in the Basin and Range province.

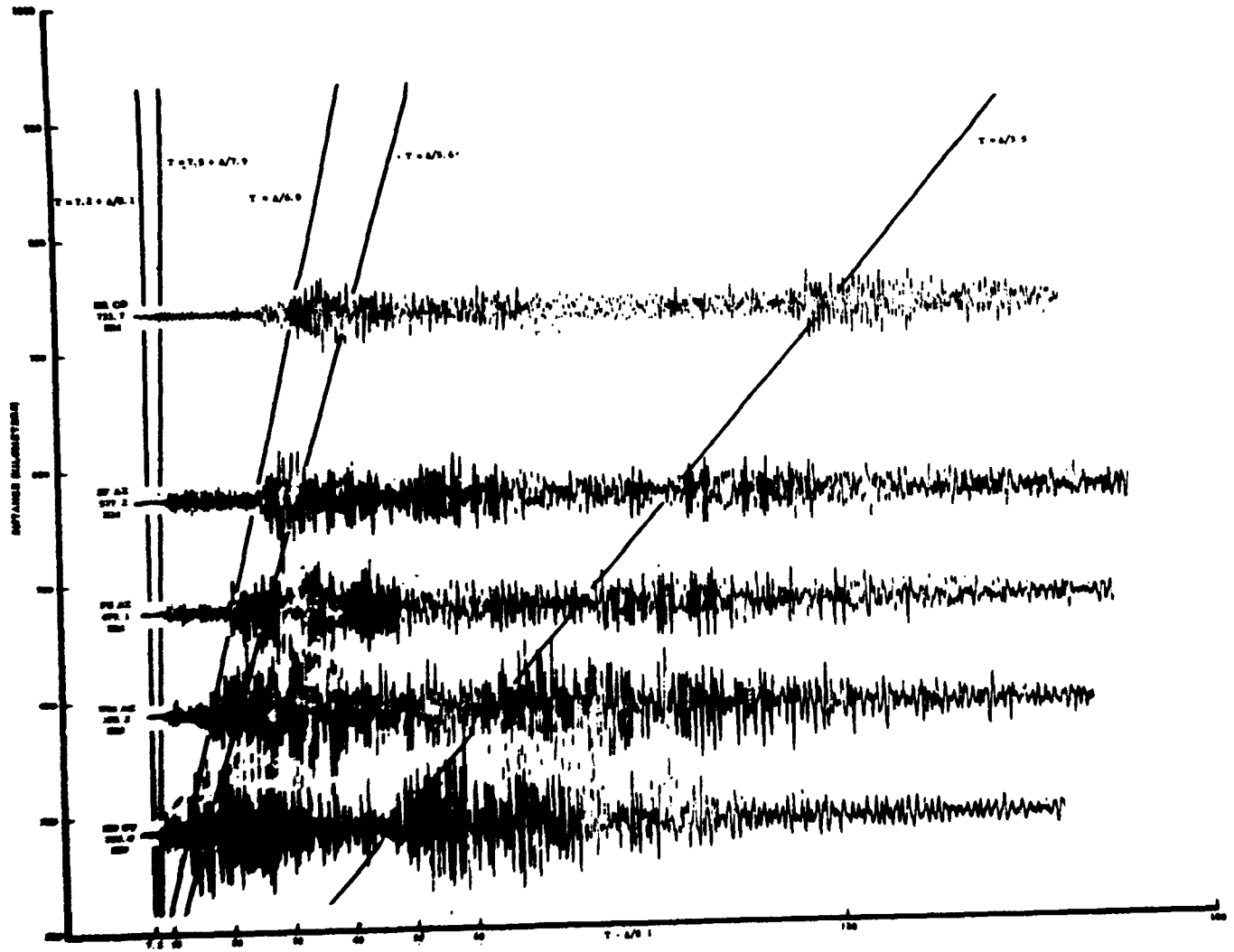

Figure 6. ARMADILLO. Short-period vertical signals recorded at stations in the Colorado Plateau province.

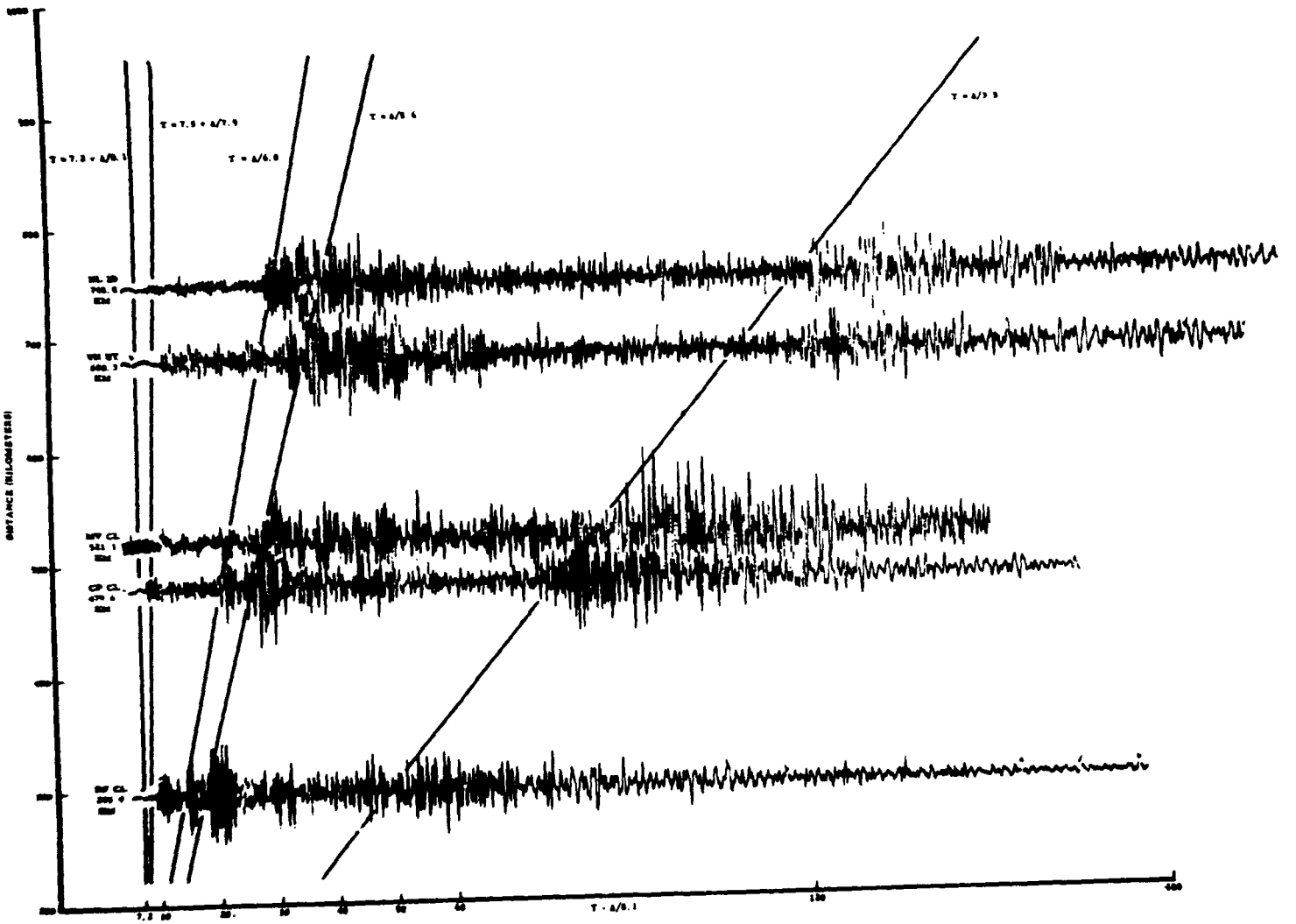

Figure 7. ARMADILLO. Short-period vertical signals recorded at stations in other structural provinces.

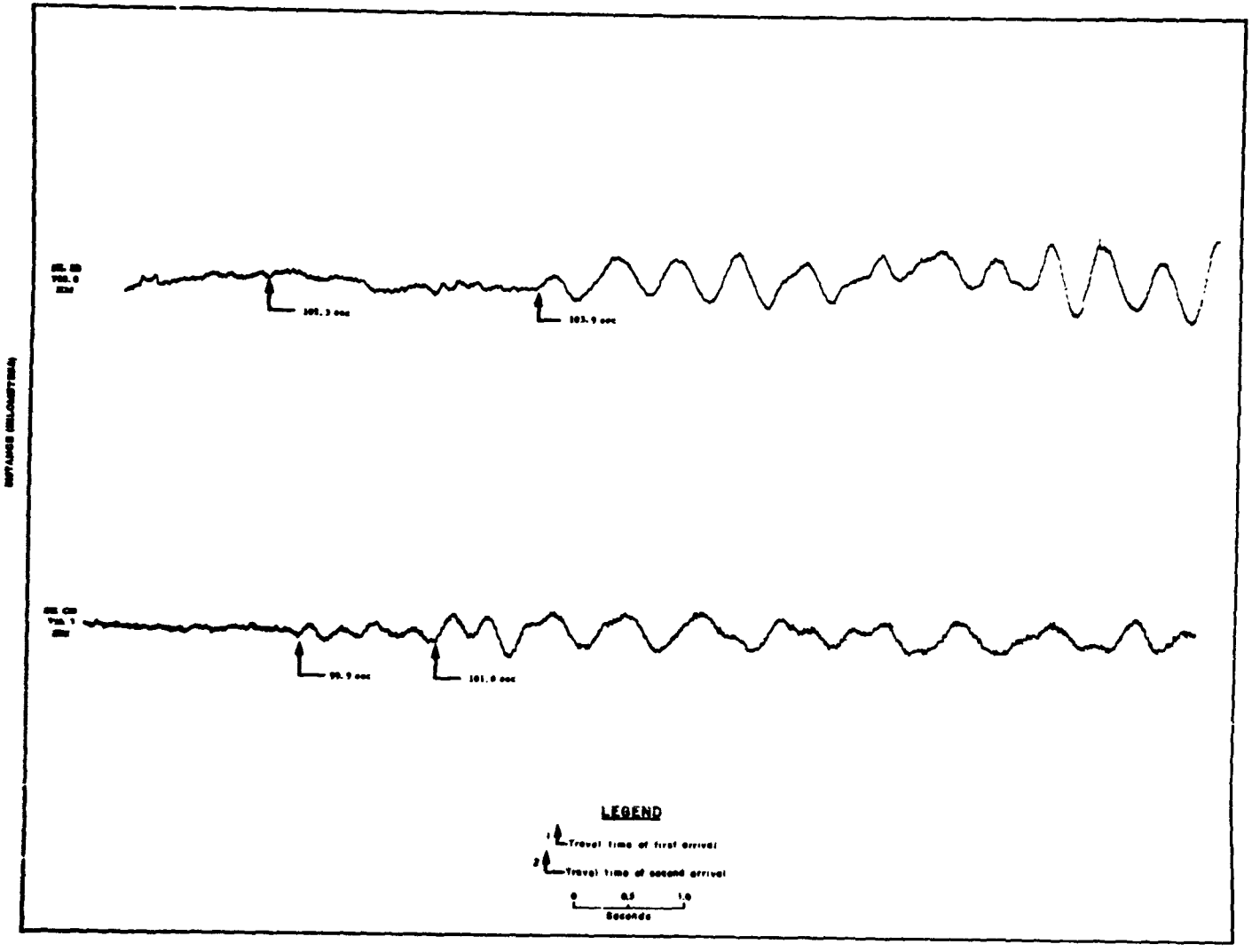

Figure 8. ARMADILLO. Early arrivals at Hailey, Idaho and Durango, Colorado

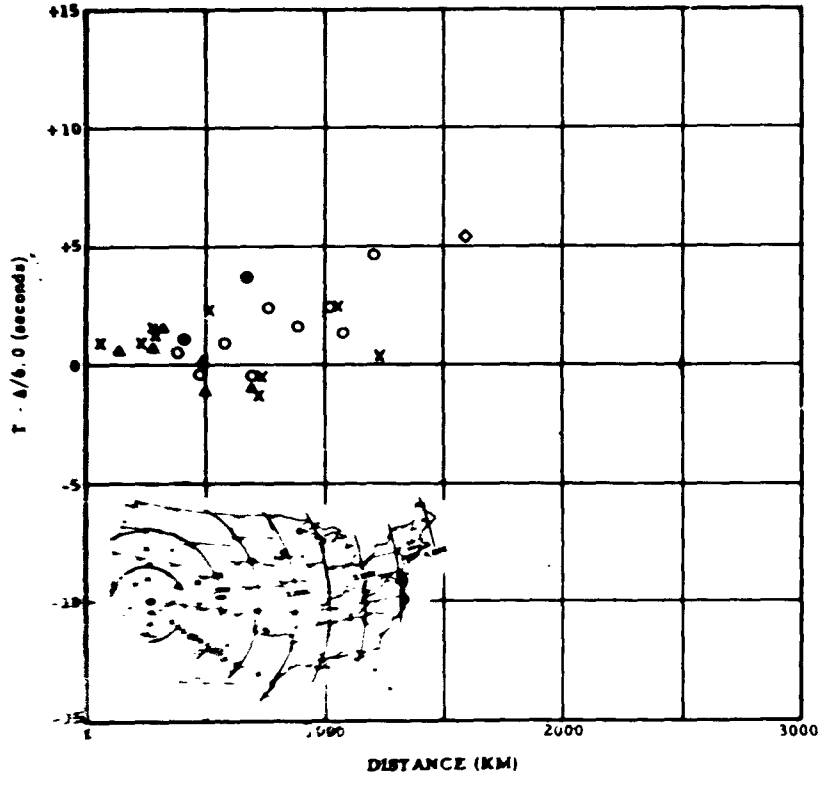

Figure 9. ARMADILLO. Travel times of Pg

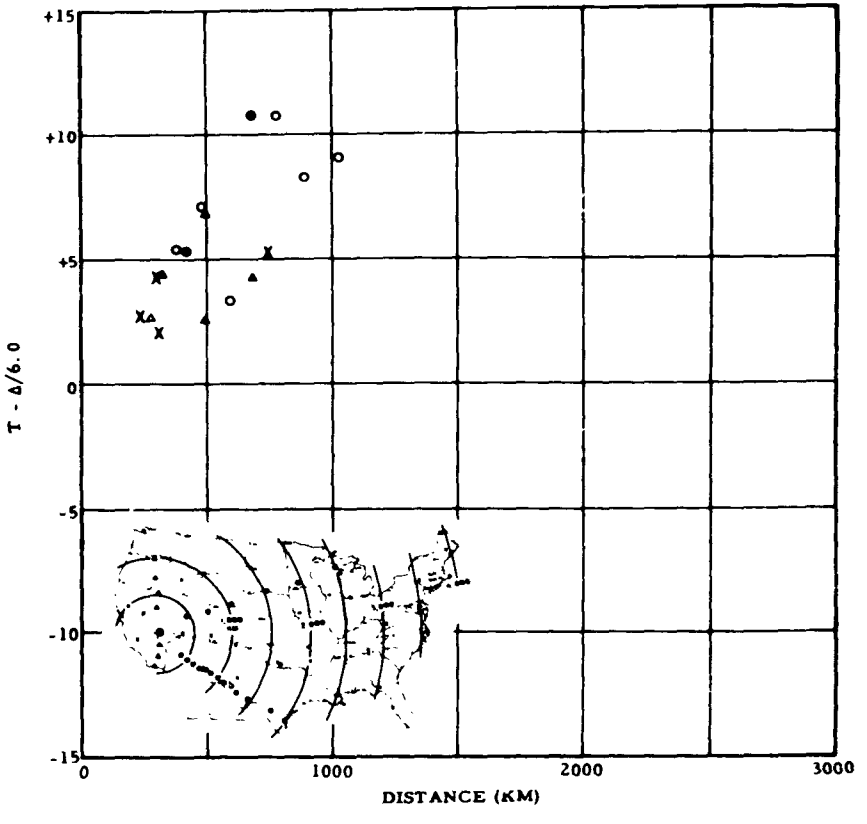

Figure 10. ARMADILLO. Travel times of Pg_2

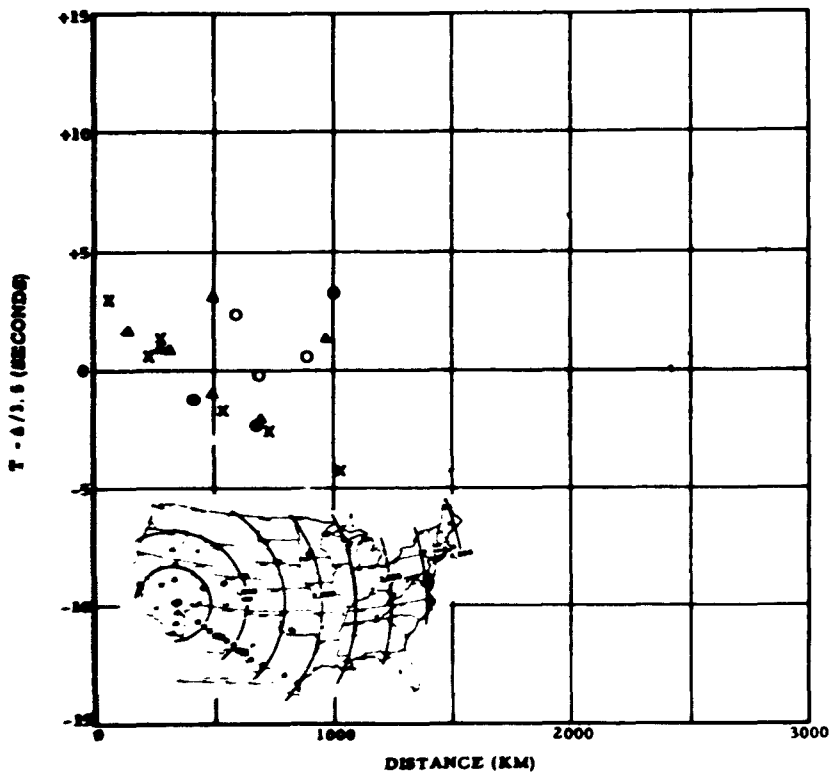

Figure 11. ARMADILLO. Travel times of Lg.

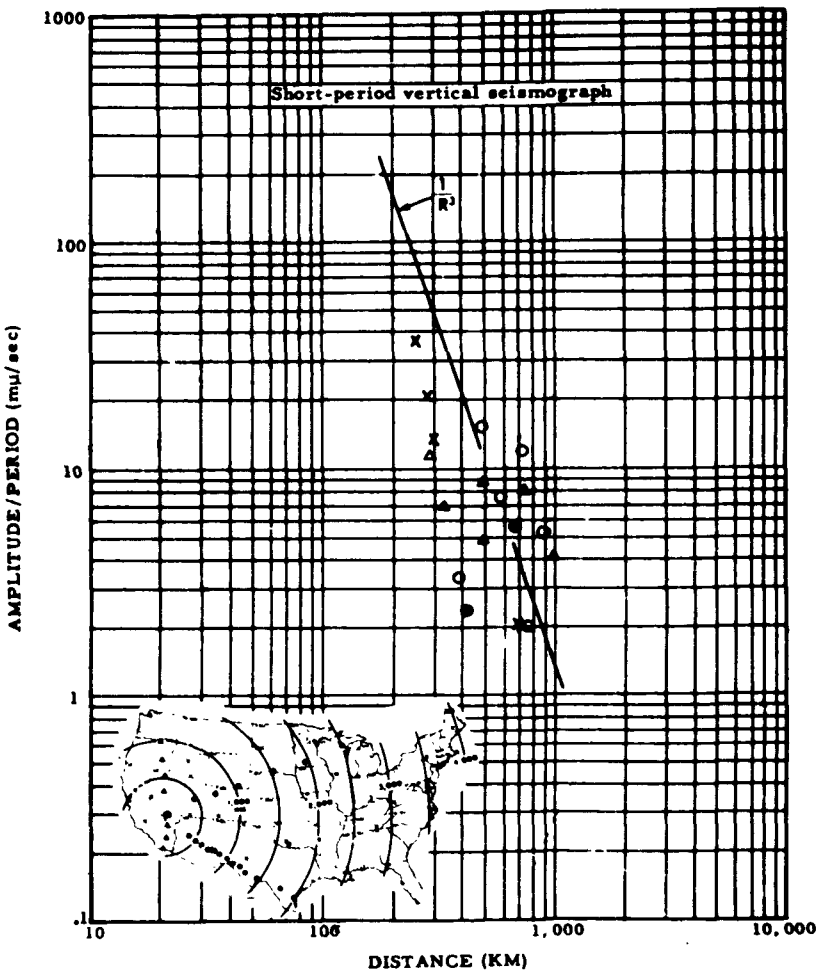

Figure 12. ARMADILLO. First motion amplitudes of Pn or P

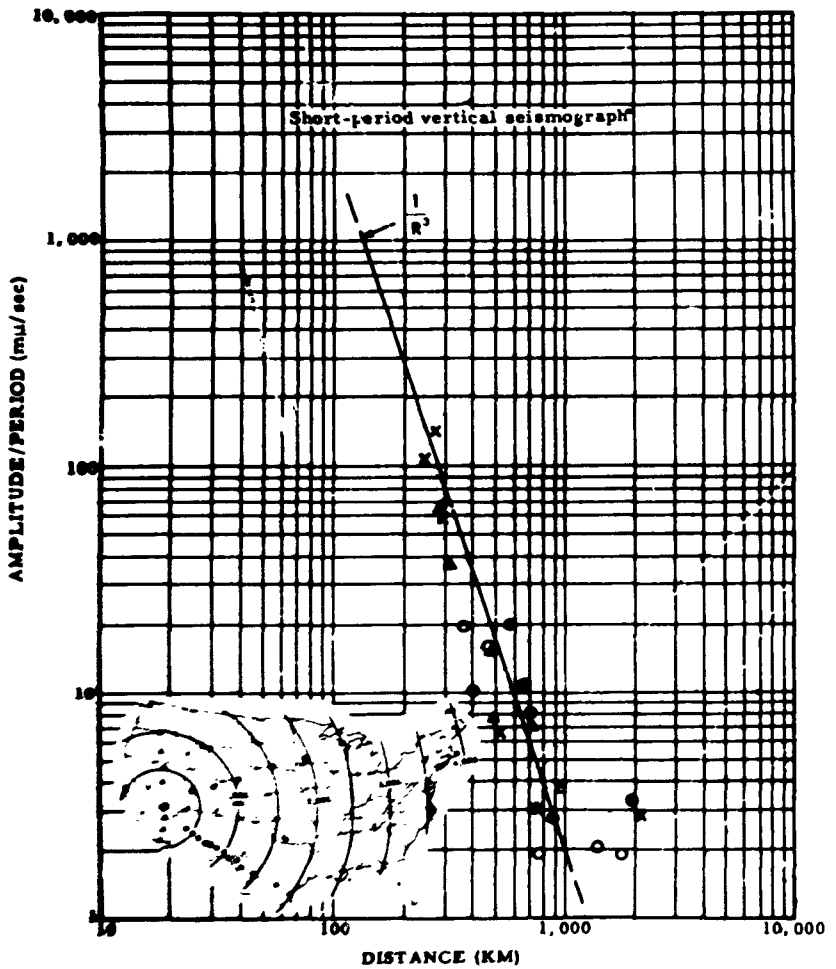

Figure 13. ARMADILLO. Maximum amplitude of Pn or P

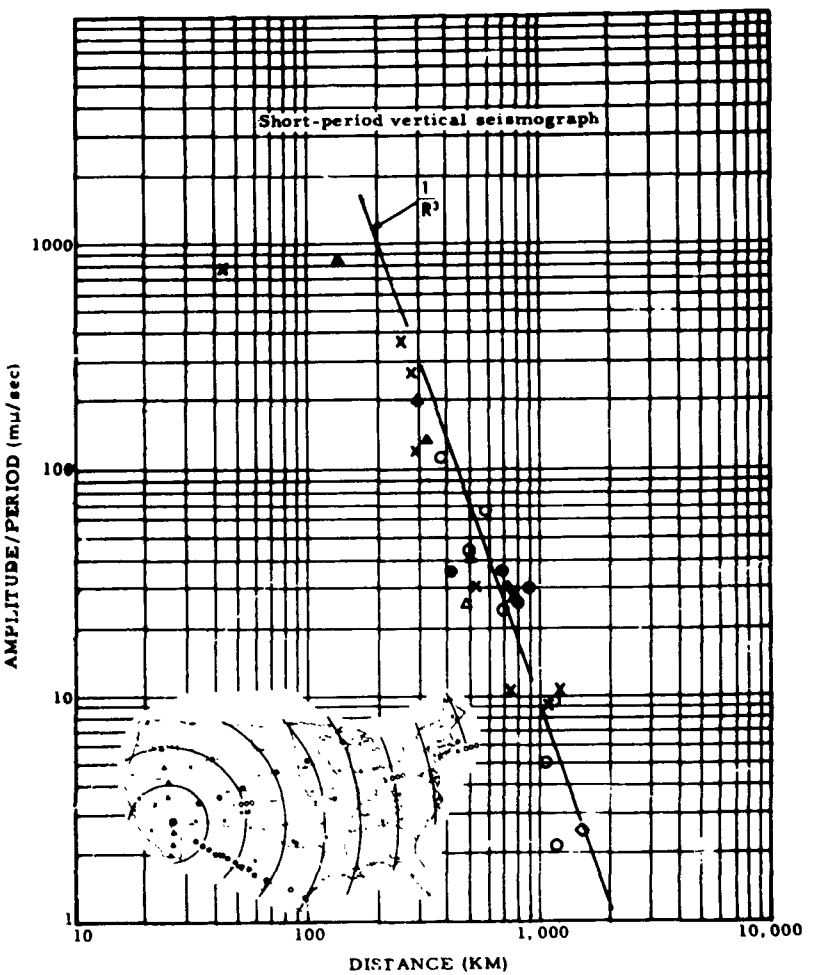

Figure 14 ARMADILLO. Maximum amplitudes of Pg

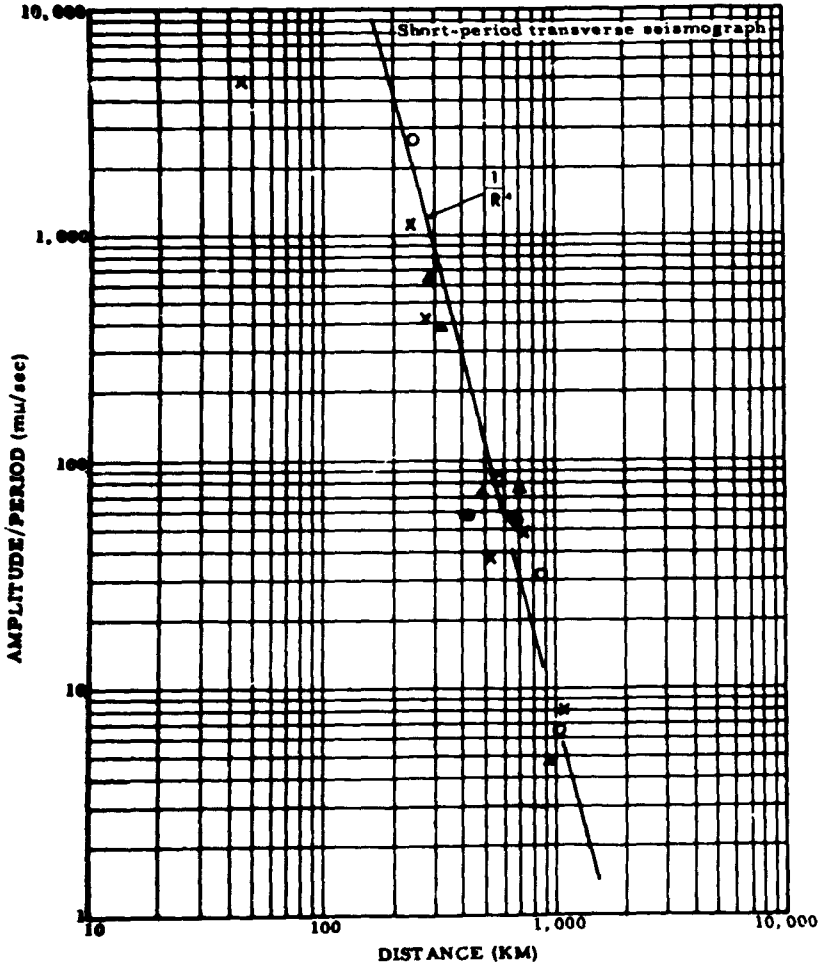

Figure 15. ARMADILLO. Maximum amplitudes of Lg

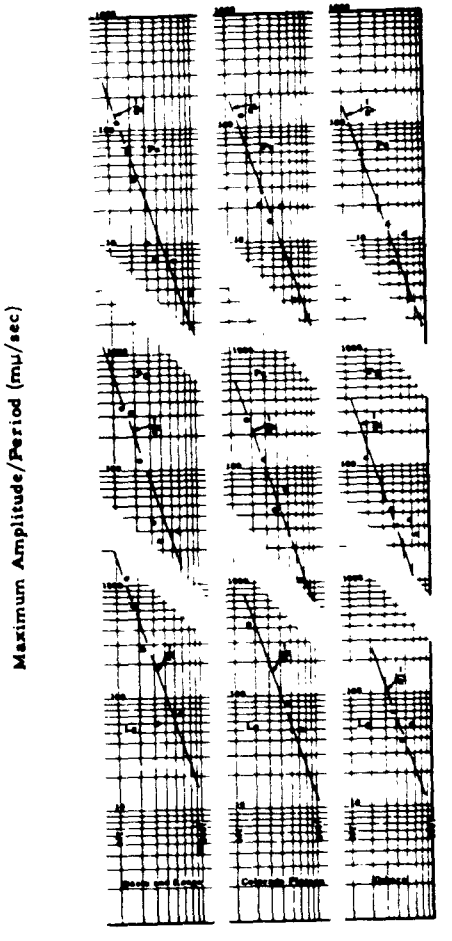

Figure 16. ARMADILLO. Amplitudes of principal phases by structural province.

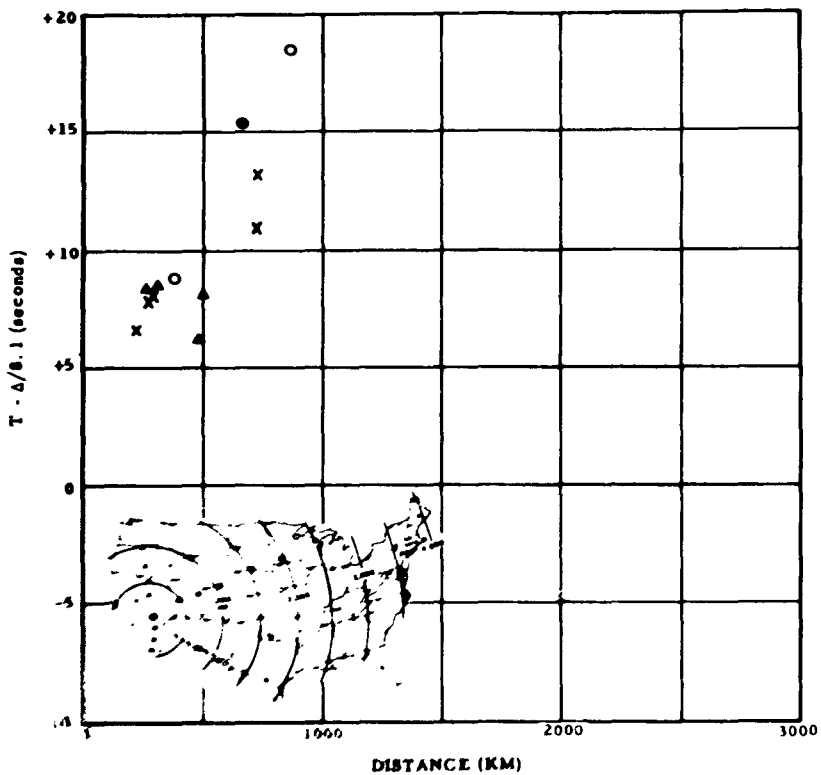

Figure 17. ARMADILLO aftershock Travel times of Pn

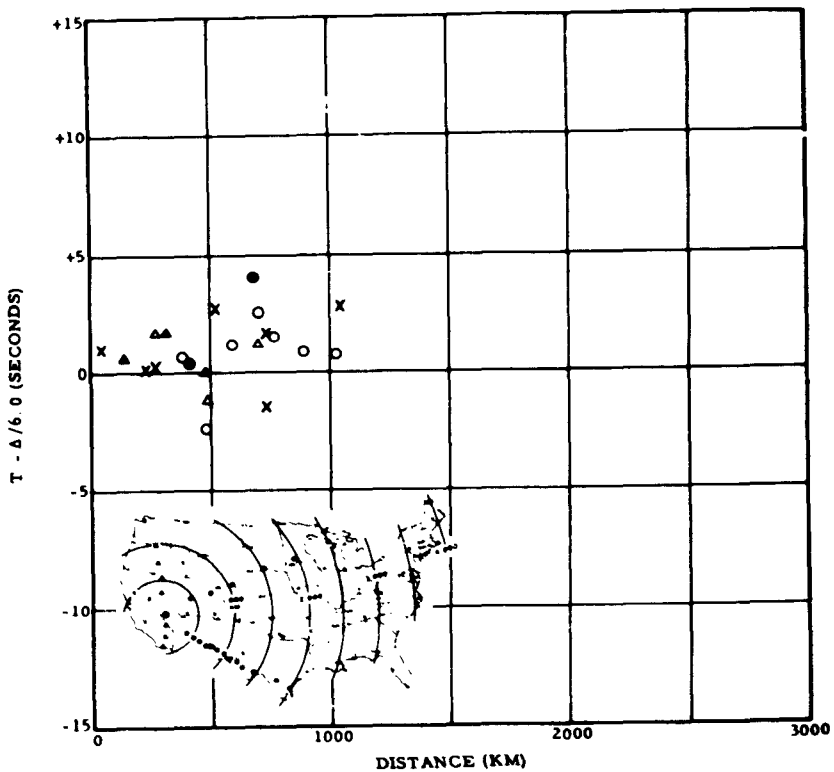

Figure 18. ARMADILLO aftershock. Travel times of Pg

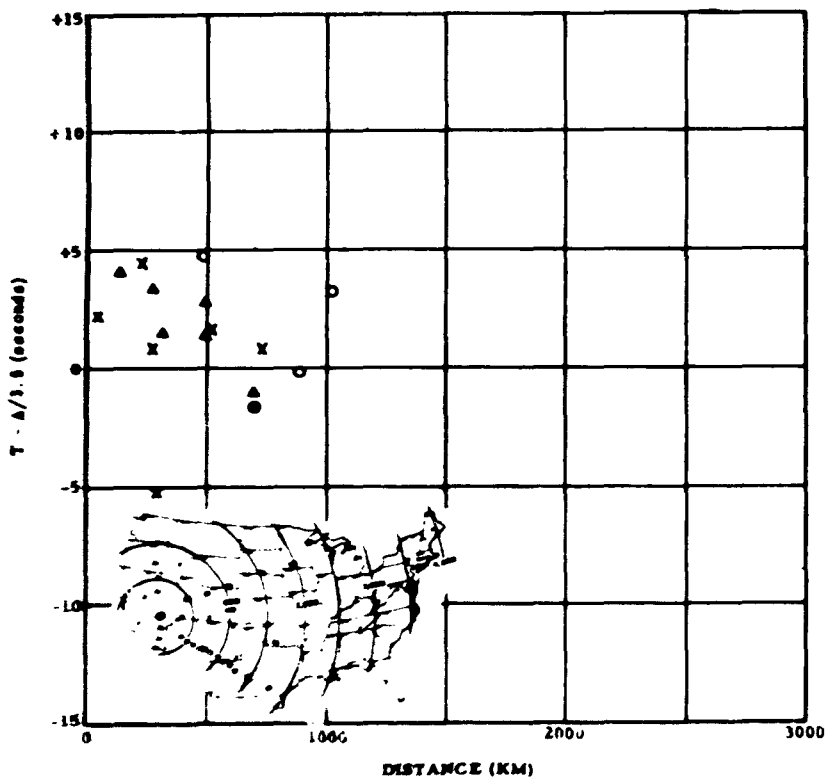

Figure 19. ARMADILLO aftershock Travel times of Lg.

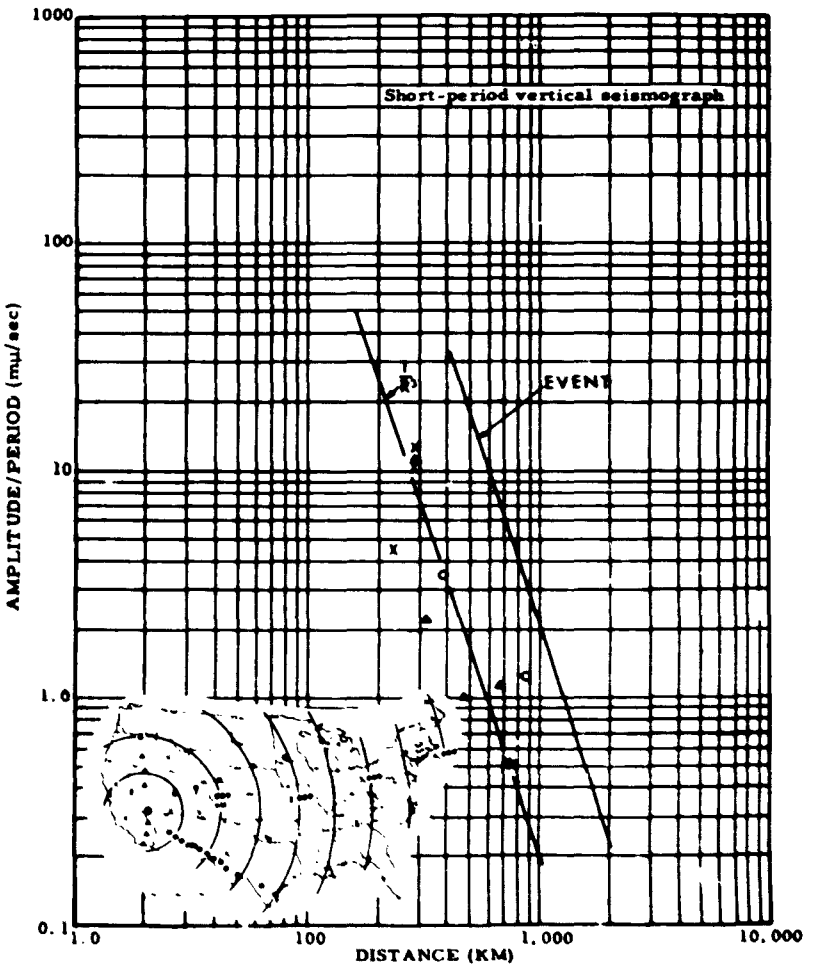

Figure 20. ARMADILLO. Maximum amplitudes of Pn for the aftershock

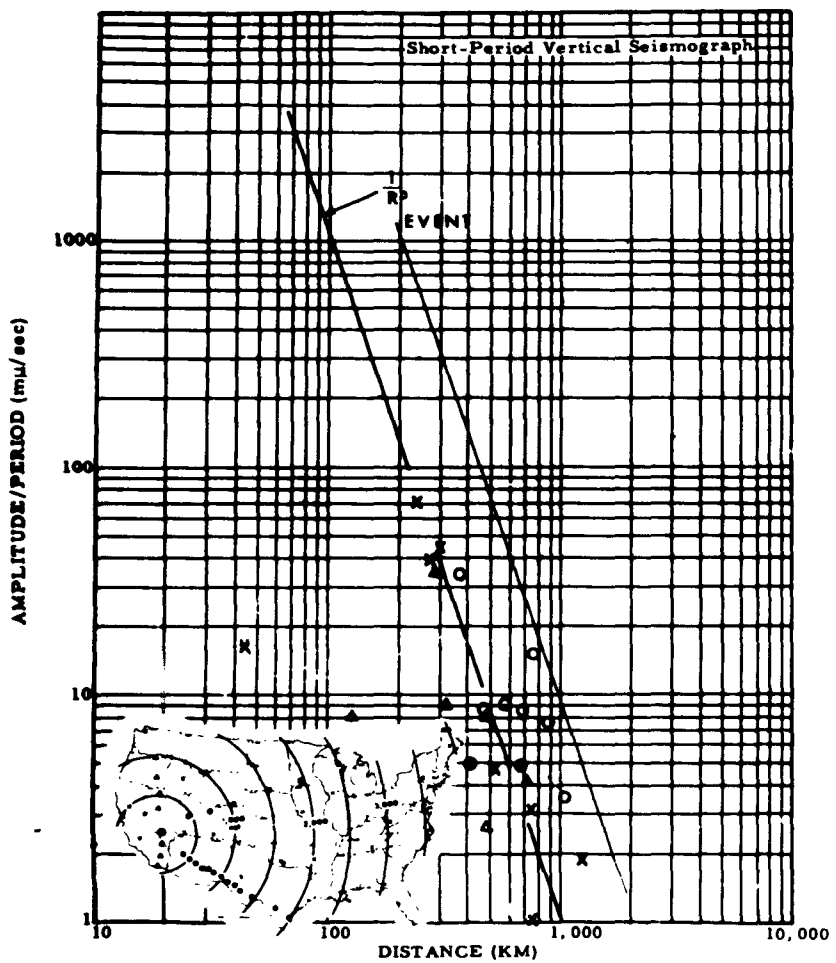

Figure 21. ARMADILLO. Maximum amplitudes of Pg for aftershock.

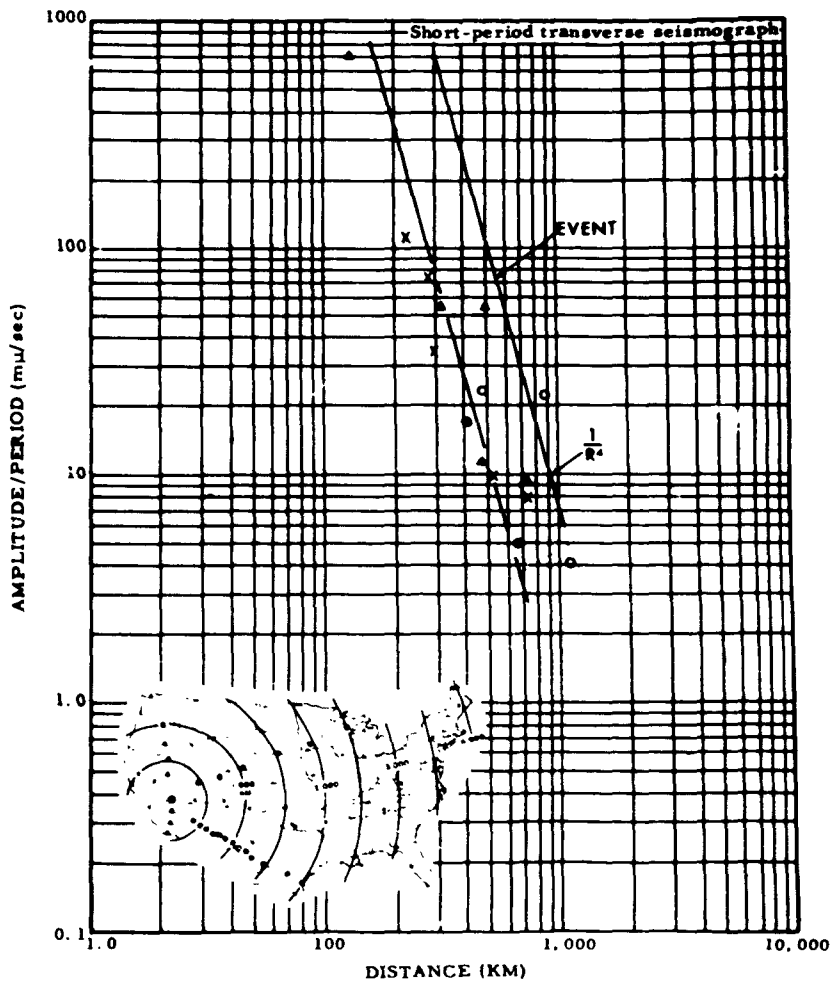

Figure 22 ARMADILLO. Maximum amplitude of Lg for the aftershock

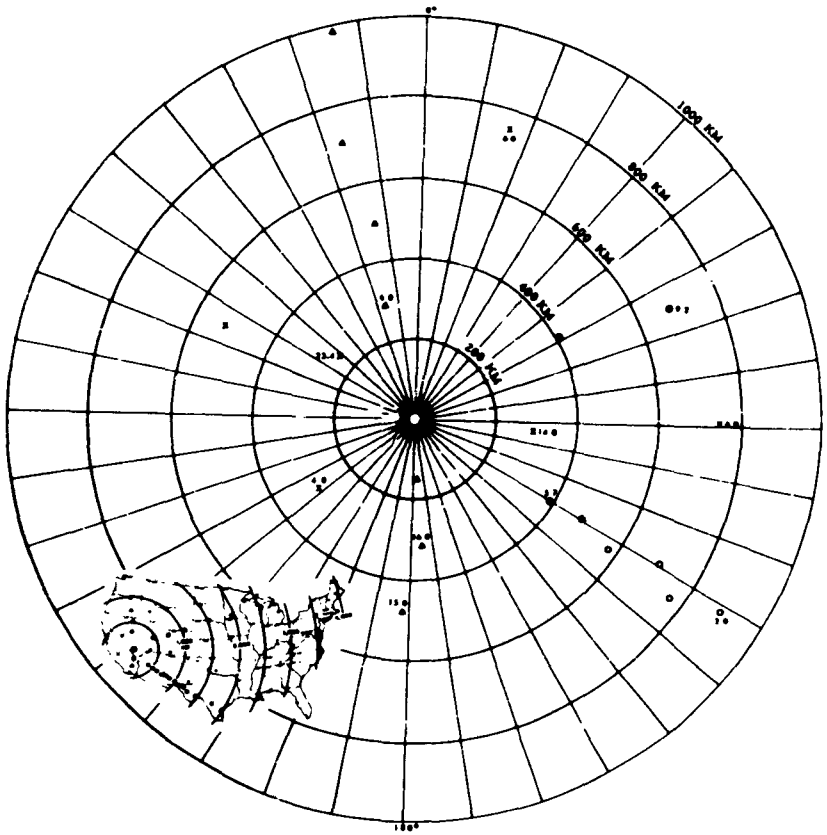

Figure 23. ARMADILLO. Pn amplitude ratios vs bearing and distance.

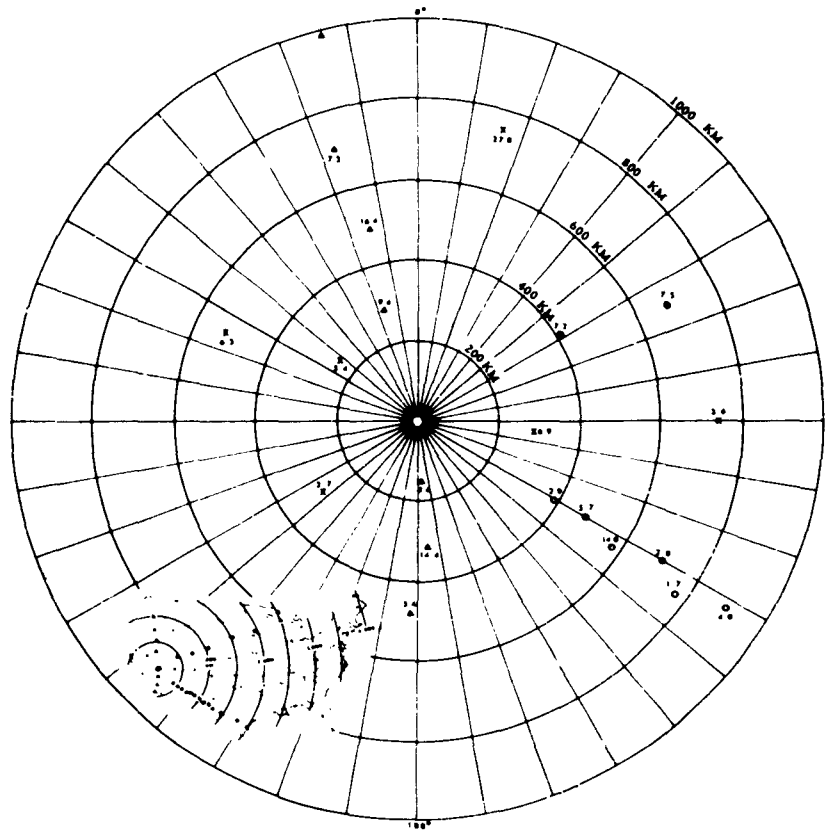

Figure 24. ARMADILLO. Pg amplitude ratios vs bearing and distance.

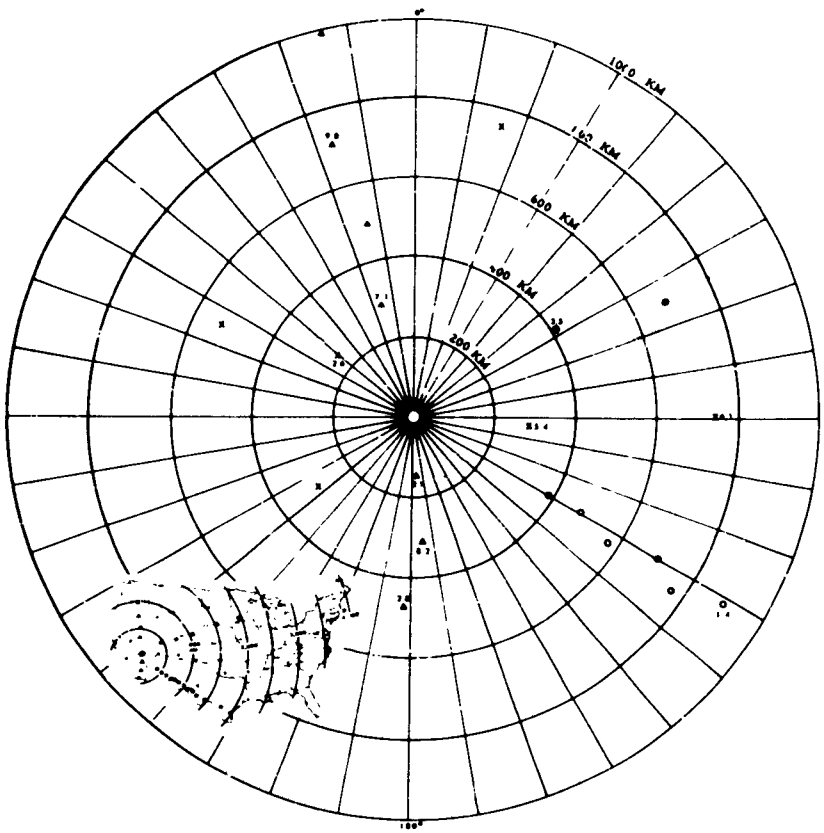

Figure 25. ARMADILLO. Lg amplitude ratios vs bearing and distance.

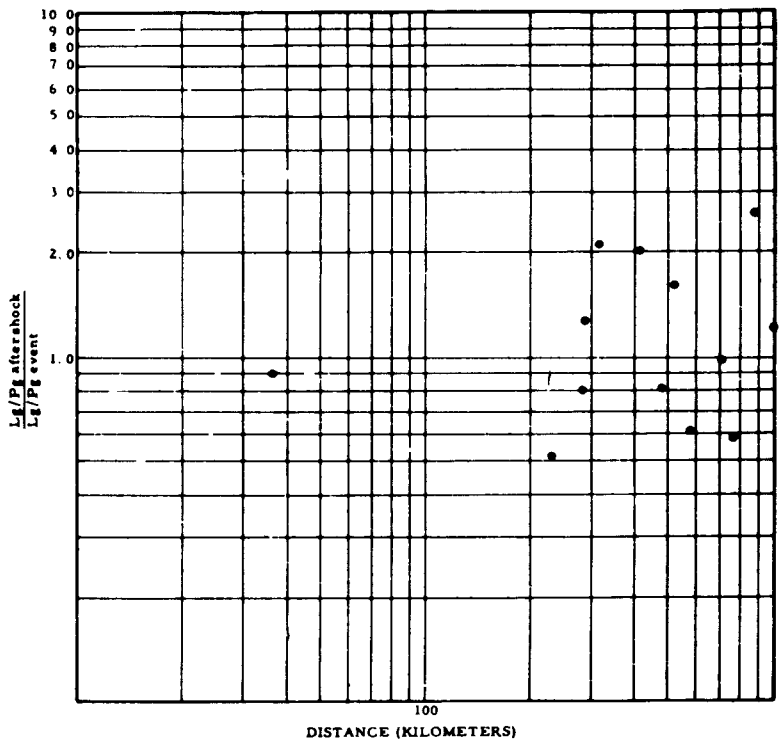

Figure 26. ARMADILLO. Comparison of Lg/Pg ratios for event and aftershock

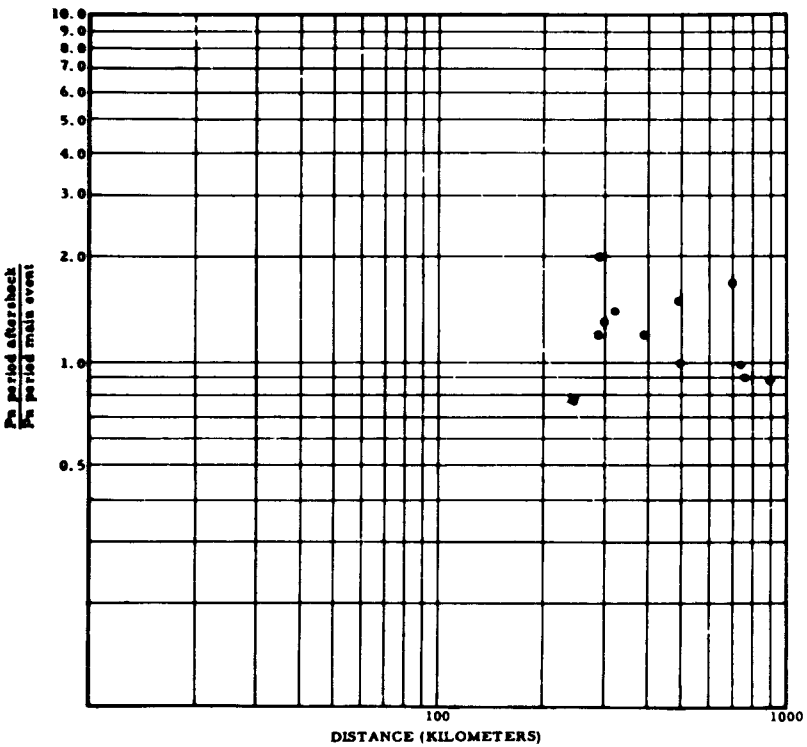

Figure 27. ARMADILLO. Comparison of Pn period for event and aftershock.

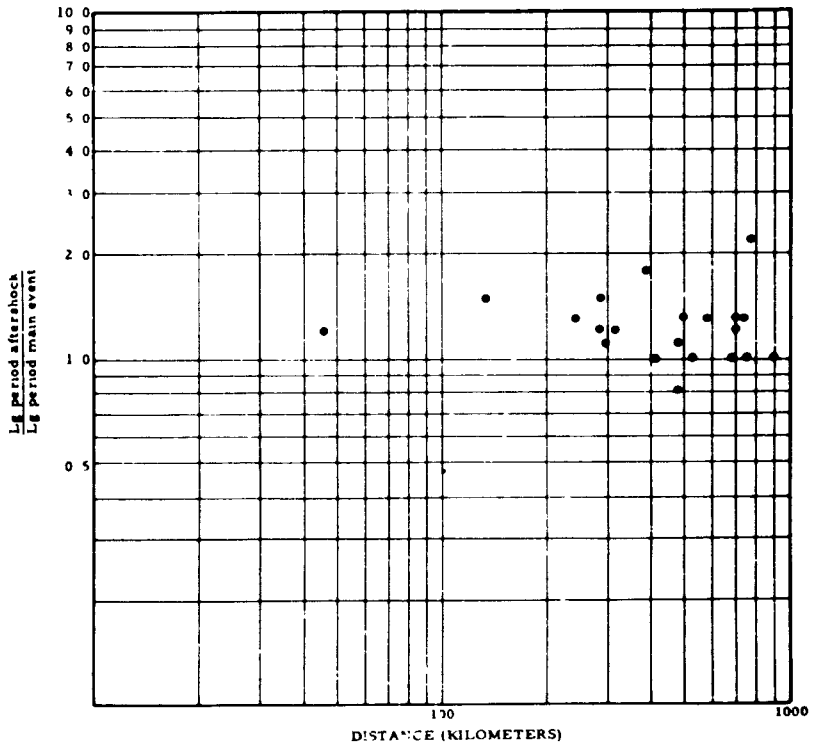

Figure 28. ARMADILLO. Comparison of Pg period for event and aftershock.

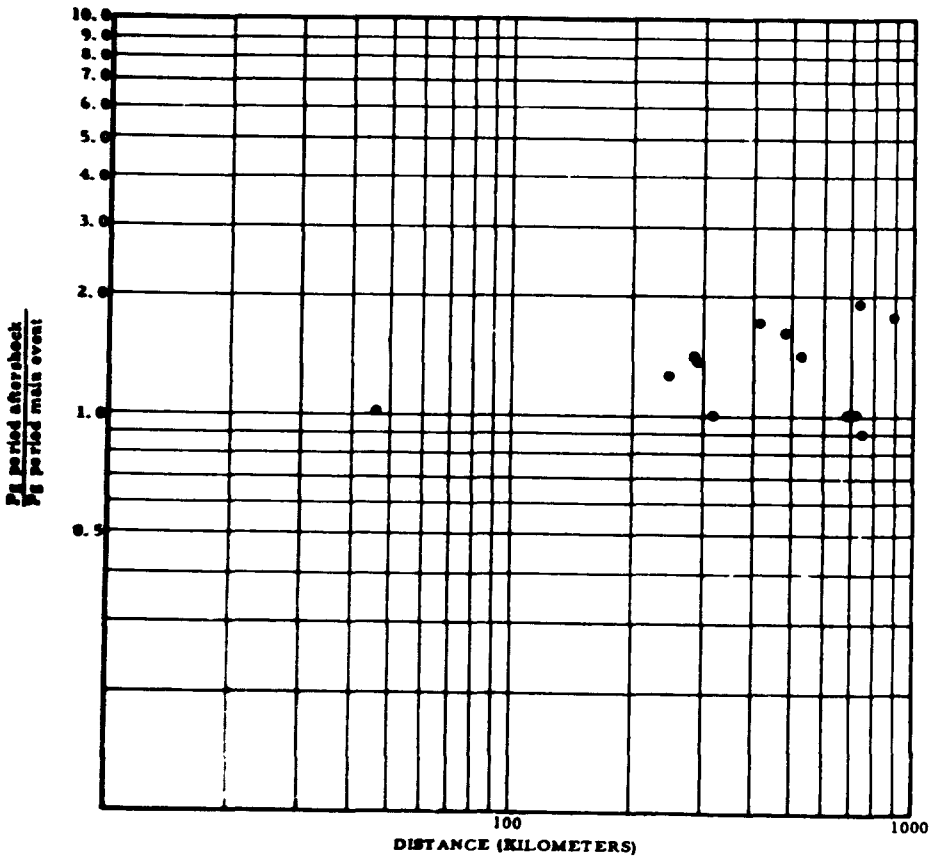

Figure 29. ARMADILLO. Comparison of Lg period for event and aftershock

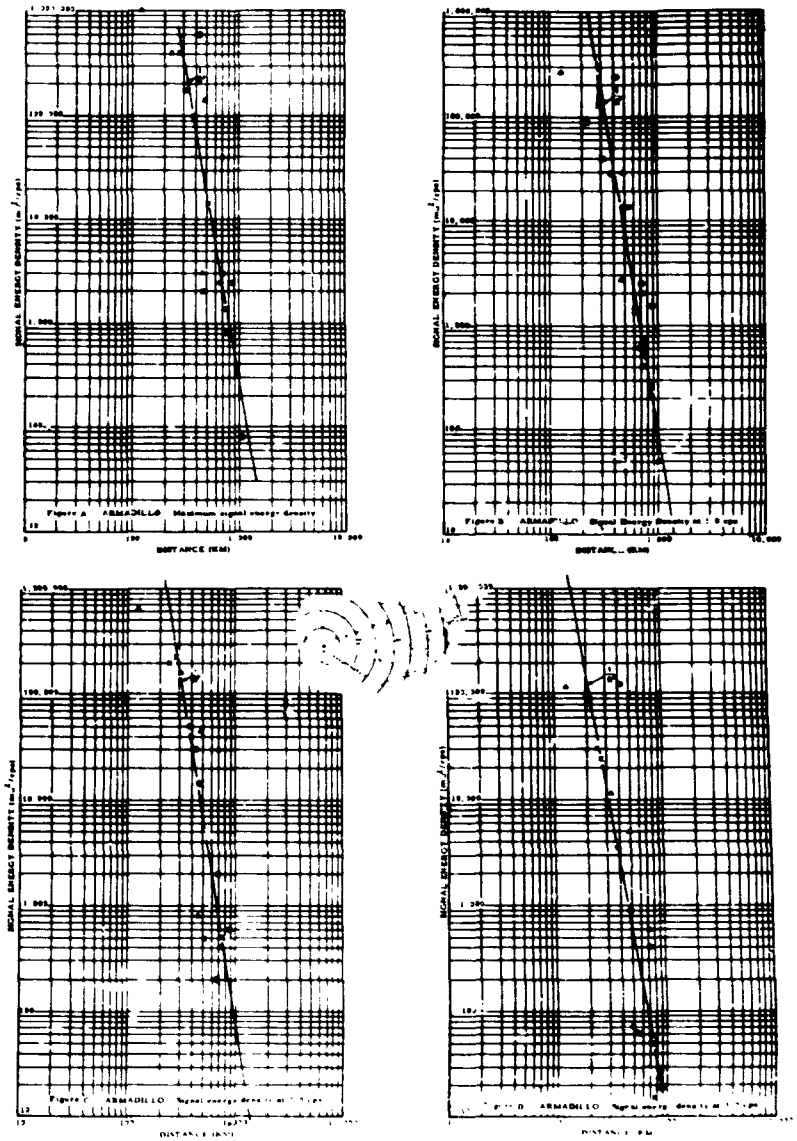

Figure 30. ARMADILLO. Maximum signal-energy density and signal-energy density at 1.0, 2.0 and 3.0 cps versus

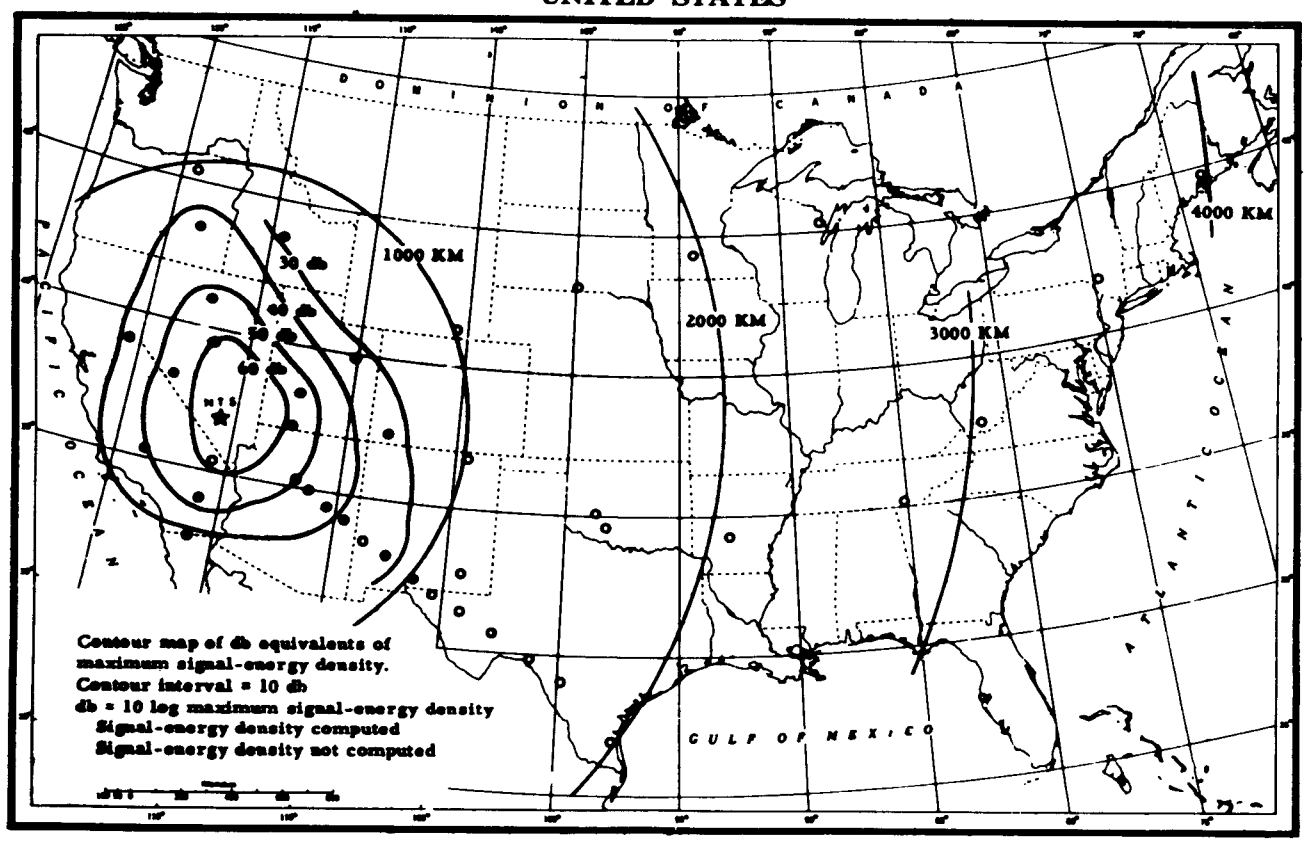

Figure 31. ARMADILLO. Contour map of maximum signal-energy density

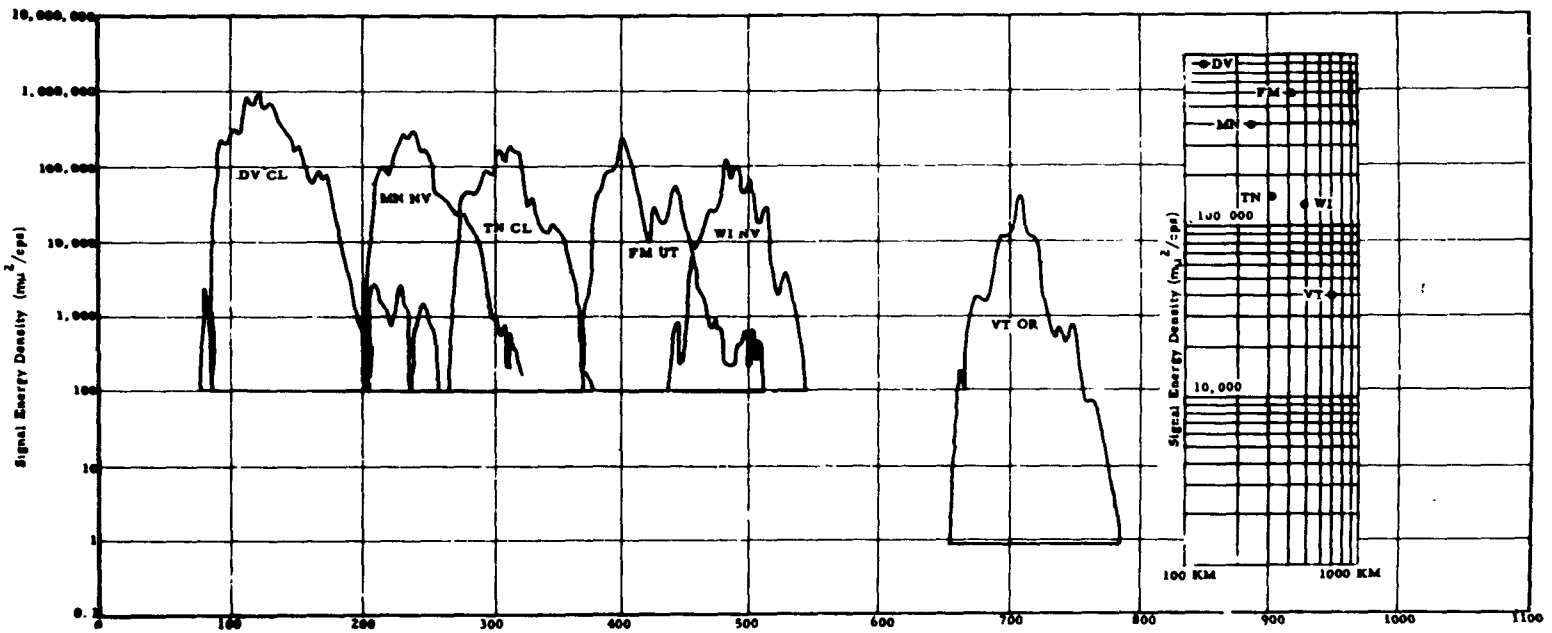

Figure 32. ARMADILLO. Signal energy density vs distance: Basin and Range province

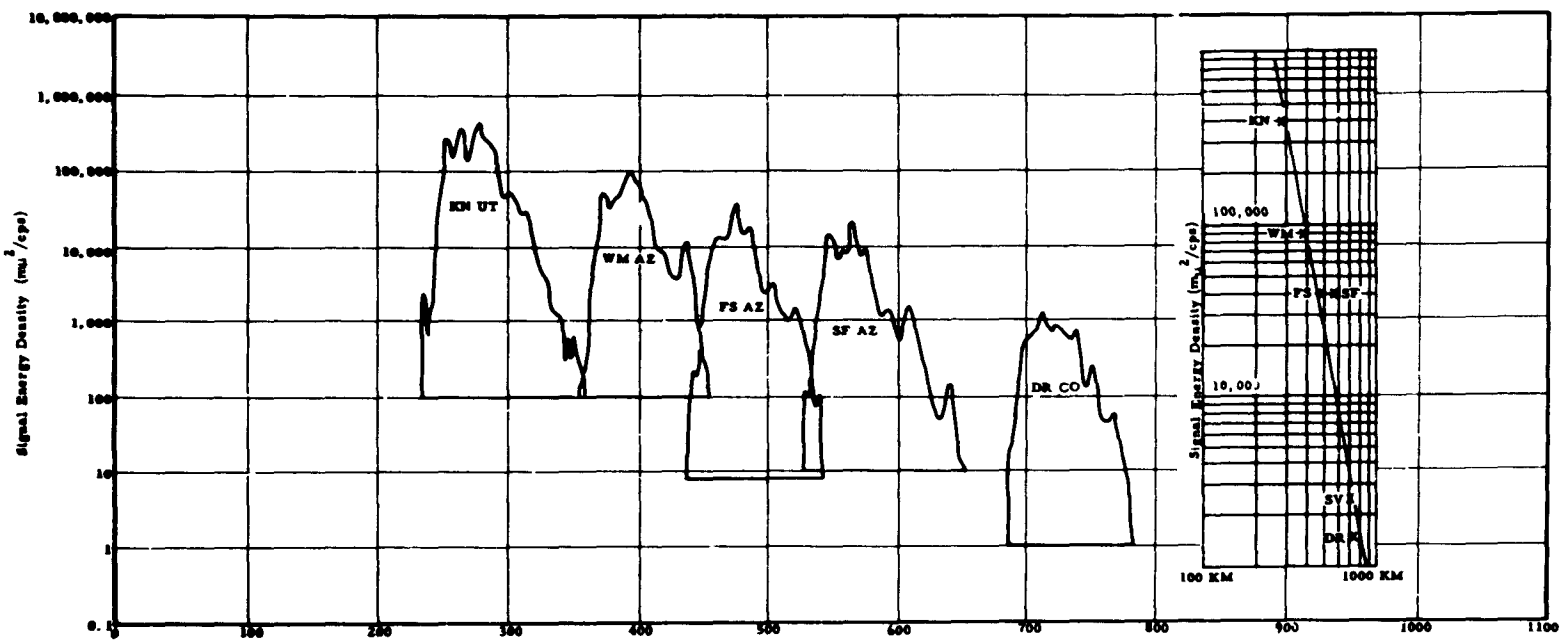

Figure 33. ARMADILLO. Signal energy density vs distance: Colorado Plateau province

Figure 34. ARMADILLO. Signal energy density vs distance: Other structural provinces

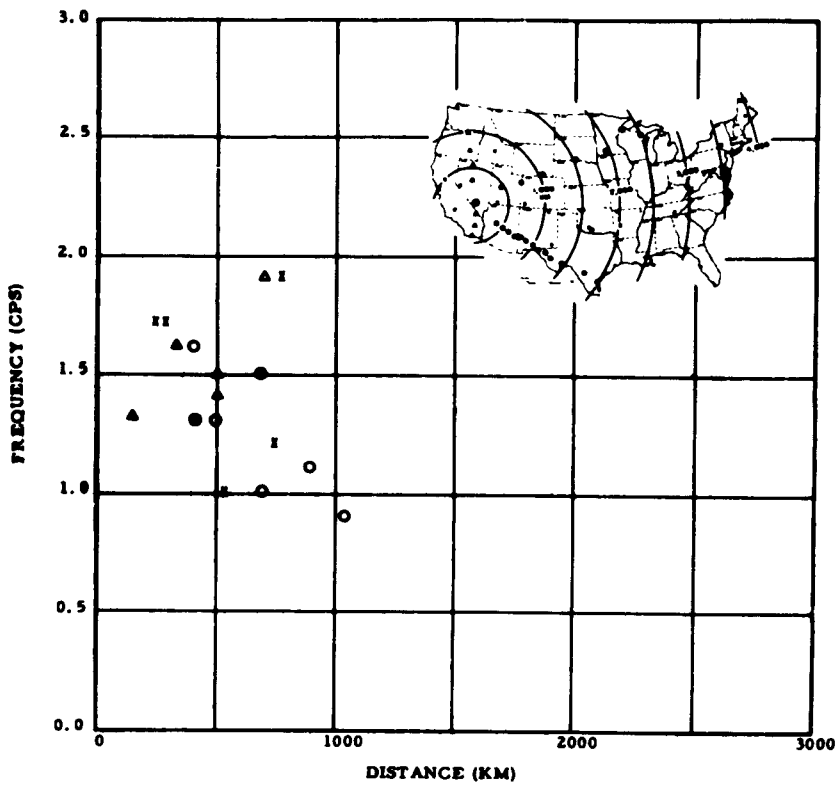

Figure 35. ARMADILLO. Frequency of the maximum signal energy density.

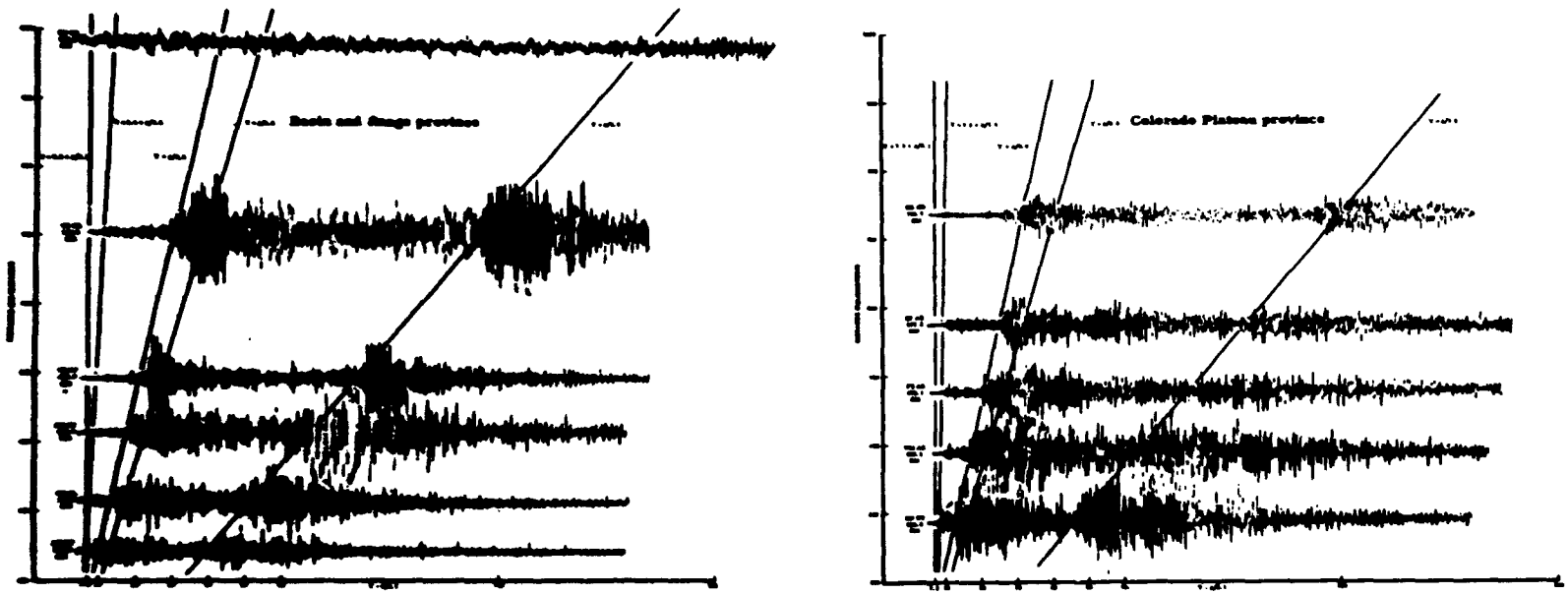

Figure 36. Comparison of Signal Envelopes Recorded in the Basin and Range and Colorado Plateau provinces

APPENDIX A

TECHNIQUES OF VISUAL DATA REDUCTION

TECHNIQUES OF VISUAL DATA REDUCTION

Magnification

Magnification is the ratio of trace deflection (at X10 view on film recordings) to ground displacement. Magnification may be calculated for LRSM recordings from either the ball-lift or sine-wave calibrations. The details of calculation are presented in the Routine Operating Instructions manual, Project VT/074. Unless otherwise noted, magnifications are obtained from ball-lift calibration.

Time Corrections

Time corrections are obtained from the radio trace which is a comparison of station program time with WWV. Time corrections are measured to a tenth of a second, and are taken as close in time to the event studied as is practical. Time corrections are taken at 10 seconds past a five-minute mark. Illustrations of time corrections on LRSM film records are given in the Routine Operating Instructions manual, Project VT/074.

Observed Travel Time (T) and Residuals

The observed travel time (T) of a phase is obtained by subtracting the origin time of the event from the arrival time of the phase. Travel time is expressed in seconds.

The residual is the algebraic difference obtained by subtracting a calculated travel time from an observed travel time. Travel times are calculated for phases by dividing the epicentral distance by a standard designated velocity.

The times thus calculated are not necessarily the best predicted time, but provide a standard for ready comparison between stations and events, and facilitates plotting and presentation of data.

Period Correction Factors

Period correction factors are used in amplitude calculations to remove the effect of instrument response. They are obtained from the response curve of the instrument by normalising the relative magnifications to the magnification at a 1-second period for the short-period system, and to a 25-second period for the long-period system. The period correction factors for the two

systems are as follows:

Short Period		Long Period			
Period (sec)	Factor	Period (sec)	Factor	Period (sec)	Factor
0.2	0.444	10	5.154	60	5.952
0.3	0.326	15	1.579	65	7.518
0.4	0.332	20	1.010	70	8.928
0.5	0.368	25	1 000	75	11.111
0.6	0 422	30	1 180	80	13.157
0 7	0 505	35	1 555	85	16.393
0 8	0 629	40	2.132	90	18.181
0.9	0 813	45	2.881	95	21.739
1.0	1 000	50	3.623	100	23 255
1.1	1.299	55	4 901		
1.2	1 639				
1 3	2.083				
1 4	2 564				

These factors multiplied by the magnifications at 1-second period give magnification at the desired periods

Amplitude Measurements and Calculations

1. Trace Amplitude

Trace amplitude is measured in millimeters on the record of specified component (Z, R, T, N, or E). Measurement is accomplished according to the following scheme.

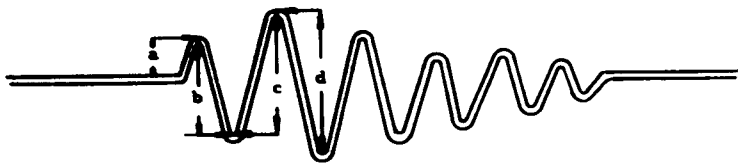

Measurements a, b, and c are always as shown; d is the maximum trace amplitude in the first 3 or 4 cycles, and may or may not be the same measurement as b or c.

2. Amplitude

Amplitude used by itself refers to ground motion and is measured in millimicrons. Amplitude is calculated from trace amplitude by the formula A (in millimicrons) = $\frac{\text{A Trace X } 10^6}{\text{Magnification}}$ X period correction factor.

3. Amplitude/Period (A/Period)

Amplitude divided by period is a measure of the velocity of ground motion, expressed in millimicrons/second. It is the final value obtained in amplitude studies, and in general is the value to be plotted.

4. Amplitude of Phases

In practice it is often difficult to apply the scheme described above rigorously. The a, b, c, and d measurements can generally be made for the first arrivals accurately, or at least be well approximated. The period used in calculations should be the predominant period of the phase, and it may be necessary to average this, or, in extreme cases, approximate it.

It is generally difficult to identify the first cycle of a later phase, so only a d measurement is commonly made. This measurement may be a single measurement or an average of several cycles

LRSM Stations

LRSM stations are occupied by mobile vans which can move from site to site as needed. There are at present 55 prepared sites and 40 mobile vans. The instrumentation in each van is the same. Summary information on the 55 sites presently prepared is given in the accompanying tabulation entitled LRSM SITE INFORMATION.

LRSM Recordings

Seismic data from both long-period and short-period seismometers is routinely recorded on 35-millimeter film and magnetic tape. The

film records provide the basic data for analysis, and playbacks from the magnetic tape are used for special presentations and processing.

Eight film records are routinely available, as follows:

1) SP-Z	4) Radio	5) LP-Z
2) SP-R	(WWV and	6) LP-Z Low (1/10 of LP-Z)
3) SP-T	Station Timing)	7) LP-R
		8) LP-T

Each film record shows both ball-lift and sine-wave calibrations. Polarity is correct when the first ball lift has a downward initial deflection, indicating dilatation from NTS, on the vertical, movement to the left as viewed from NTS on the transverse, and movement toward NTS on the radial.

Each film record is identified by the four-letter station designation, trace identification, date, time interval covered, run number, magnification, motor constant (G) and calibration current (i).

The magnetic-tape recordings have 14 channels as follows:

1. Station Time	8. SP-T-High
2. SP-T-Low	9. LP-Z-High
3. SP-R-High	10. LP-Z-Low
4. SP-R-Low	11. LP-R-High
5. SP-Z-High	12. LP-R-Low
6. SP-Z-Low	13. LP-T-High
7. Wow and Flutter	14. WWV and voice comments.

LRSM SITE INFORMATION

Site designation	Site location	Bearings from true north in degrees from NTS		Site coordinates in deg, min, sec.		Elevation	Large or Small Benioffs
		Radial	Transverse	N. Lat.	W. Long.		
AMOK	Ardmore, Oklahoma	107	197	34 02 52	97 24 41	900	L
ATNV	Austin, Nevada	343	073	39 28 51	117 04 26	6500	L
BFCL	Bakersfield, California	233	323	35 39 12	118 51 06	1850	L
BGME	Bangor, Maine	095	185	44 38 04	69 13 17	600	S
BLWV	Beckley, West Virginia	100	190	37 47 56	81 18 36	2000	S
BMTX	Balmorhea, Texas	125	215	30 55 35	103 51 18	3500	L
CNWS	Cornell, Wisconsin	076	166	45 09 50	91 08 48	1000	S
CPCL	Campo, California	182	272	32 43 44	116 22 16	3900	L
CVTN	Centerville, Tennessee	102	192	35 46 12	87 23 04	600	S
CWAR	Conway, Arkansas	103	193	35 08 08	91 58 40	500	L
DMNY	Delhi, New York	095	185	42 14 39	74 53 18	2140	S
DRCO	Durango, Colorado	090	180	37 27 53	107 47 00	7300	S
DVCL	Death Valley, California	177	267	35 50 00	116 06 06	2600	L
EFTX	Eagle Flat, Texas	126	216	31 10 35	105 07 48	4700	L
EPTX	El Paso, Texas	125	215	31 55 58	105 58 00	5300	L
FMUT	Fillmore, Utah	058	148	39 13 06	112 12 25	6200	S
FSAZ	Flagstaff, Arizona	120	210	35 04 09	111 18 34	6200	L
GLTX	Garland, Texas	110	200	32 58 20	96 38 06	450	S
GNNM	Carlsbad, New Mexico	119	209	32 15 45	103 51 25	3400	L
GTPA	Galeton, Pennsylvania	094	184	41 37 54	77 48 40	2000	S
HBOK	Hobart, Oklahoma	103	193	35 10 35	98 54 37	1612	S
HLID	Hailey, Idaho	016	106	43 38 52	114 16 02	6000	L
HSNB	Hay Springs, Nebraska	068	158	42 25 32	102 42 52	3900	S
JSTN	Jackson, Tennessee	102	192	35 39 20	88 36 46	500	S
KNUT	Kanab, Utah	095	185	37 01 22	112 49 39	5700	L
LCNM	Las Cruces, New Mexico	124	214	32 24 08	106 35 58	5200	L
LMNV	Lake Mead, Nevada	116	206	36 34 10	114 33 03	2450	L
LPTX	La Pryor, Texas	124	214	29 10 47	99 40 35	900	L
MCSD	Mitchell, South Dakota	071	161	43 39 16	97 55 10	1200	S
MLNM	Mogollon, New Mexico	124	214	33 24 53	108 50 11	5400	S
MMTN	McMinnville, Tennessee	103	193	35 33 52	85 35 20	1250	S
MNNV	Mina, Nevada	308	038	38 26 10	118 08 53	5000	L
MPAR	Mountain Pine, Arkansas	105	195	34 36 06	93 08 45	1100	S
MVCL	Marysville, California	295	025	39 13 36	121 18 05	2000	L
NGWS	Niagara, Wisconsin	078	168	45 45 34	88 09 15	1300	S
PMWY	Laramie, Wyoming	068	158	41 12 27	105 21 39	8100	S
POTX	Post, Texas	111	201	33 28 32	101 21 44	3000	L
PTOR	Pendleton, Oregon	346	076	45 36 40	118 53 02	1350	L
RTNM	Raton, New Mexico	096	186	36 43 46	104 21 37	6400	S
SEMN	Sleepy Eye, Minnesota	073	163	44 24 51	94 39 55	800	S
SFAZ	Snowflake, Arizona	123	213	34 26 19	110 30 52	6500	L
SJTX	San Jose, Texas	127	217	27 36 43	98 18 46	375	S
SMTX	Seymour, Texas	109	199	33 40 56	99 11 23	1300	L
SSTX	Sanderson, Texas	126	216	30 01 17	102 19 41	2400	L
SVAZ	Springerville, Arizona	120	210	34 10 32	109 08 49	7000	L
TCNM	Truth or Consequences, N. Mex.	122	212	33 11 03	107 27 42	5000	L
TNCL	Twentynine Palms, California	176	266	34 11 54	115 57 00	1750	L
TOOK	Tishomingo, Oklahoma	106	196	34 21 23	96 34 05	850	L
TPNV	Tippipah, Nevada	-	-	37 12 01	116 13 34	7400	L
VNUT	Vernal, Utah	065	155	40 30 31	109 34 45	6200	S
VTOR	Venator, Oregon	343	073	45 08 49	118 25 23	4700	L
WINV	Winnemucca, Nevada	346	076	41 21 02	117 27 30	5000	L
WMAZ	Williams, Arizona	120	210	35 25 04	112 32 56	6300	L
WNSD	Winner, South Dakota	069	159	43 15 08	100 31 46	2600	S
WRAR	Walnut Ridge, Arkansas	101	191	36 03 30	91 13 19	400	L

APPENDIX B

DIGITAL PROCESSING OF LRSM STATION DATA

DIGITAL PROCESSING OF LRSM STATION DATA

ARMADILLO EVENT

I INTRODUCTION

This report describes the methods employed and presents the results obtained in a program of digital data processing applied to events produced by the ARMADILLO nuclear detonation and recorded at 18 of the 40 LRSM stations.

The aim of the processing program has been to make available for study those elements of the magnetic-tape data most efficiently obtainable through digital data processing. Accordingly, this report should be viewed not as a seismic interpretation of the data, but rather as a means for its presentation in formats designed to facilitate comparisons and encourage further study. In order that most effective use can be made of the data, detailed description is provided of the processing methods employed.

A principal goal of the program was the analysis, in both the time and frequency domains, of the P_n, P_g and L_g signal phases. Unfortunately, the comparatively short distances between the

Nevada Test Site (NTS) and the various stations (about 1000 km maximum) resulted in little or no spectral separation among the various phases and accordingly, spectral analysis of the individual phases was precluded. Nonetheless, considerable insight into their detailed character and properties may be gained from the time domain studies. Additionally, the spectral studies contribute substantially to the characterization of the entire received signal and the microseism noise background at each station.

A. Summary of Results

Data processing results include for each station spectral density analyses of the entire received signal and of the microseismic noise background, computation of signal-to-noise spectral density ratios, and computation of total signal energy per octave bandwidth. In each case spectral intensities are presented in units of absolute earth motion to facilitate comparisons not only among the data for the ARMADILLO event, but also between the STILLWATER and ARMADILLO events.

In the time domain, presentations are made of the entire short-period vertical signals received at each of the 18 stations processed.

In addition, enlarged sections of each signal event showing the P_n, P_g and L_g phases are displayed by radials of stations with the traces aligned in time according to standard North American velocities of 8.11, 6.0, and 3.5 km/sec, respectively. Individual traces are displayed with their normalized amplitudes set proportional to the cube of the surface distance from the Nevada Test Site to the particular station and inversely proportional to the gain of the short-period vertical system at the station, and to the yield of the nuclear detonation. As with the spectra, all time traces of the P_n, P_g and L_g phases for both the STILLWATER and the ARMADILLO events are commensurable.

B. Origin and Preparation of Data

Field data were recorded originally on magnetic tape using frequency modulation recording. Selected calibration, noise, and signal sections of these tapes were edited onto a master composite tape and a direct record copy made by Geotech personnel. This copy tape was then replayed and demodulated on a Honeywell LAR 7400 f-m tape transport. The analog-output signal was digitized and then digitally recorded on magnetic

tape by a Texas Instruments Digital Field System for subsequent input to the Texas Instruments Data Analysis and Reduction Computer (DARC). Simultaneously, a conventional oscillographic paper record monitor was made.

During the demodulation of the copy tape, a playback speed increase of 20 resulted in a time decrease of 20 and a frequency increase of 20. The analog-output signals were passed through a low-pass filter having an upper-band limit of 180 cps, corresponding to 9 cps on the original frequency scale, before being sampled at a rate of 500 cps and digitized into 12-bit data. The equivalent Nyquist or folding frequency is thus 12.5 cps, at which frequency the low-pass filter response is down 35 db. Accordingly, any effects due to aliasing are minimized. Actually, as the spectral analyses bear out, the recorded events contain little energy above about 5 to 6 cps. Except for the low-pass filtering operation, the demodulated f-m signals were unaltered prior to being digitized.

Further handling of the data prior to processing involved the assembly of digital edit records comprising 2048-word sections

(of 81.92 seconds real time duration) of microseismic noise, from an interval of record just before the onset of the signal, and of the signal. Two sections of each signal event were taken: one containing the P_n and P_g phases, and the other containing the L_g phase. These signal edit records provided the basis for the final amplitude-adjusted and velocity-aligned traces presented for individual phase study.

The 2048-word noise edit records provided the input data for computation of noise-power density spectra, as described in a later section. Autocorrelation functions of the "entire" signal were computed with the original digital tape as input and covered the signal interval of each record from the arrival time of the P_n phase to a point sufficiently far down the record that no evidence of the signal can be visually detected on the paper monitor record. Phase arrival times are predicted on the basis of epicentral distances furnished by Geotech using standard North American velocities and time intercepts.

C. Station Data Processed

Of the 23 LRSM stations that reported receipt of a short-period vertical signal from the ARMADILLO detonation, data from 18 were processed. Table I lists the reporting stations and indicates those deficient such that their data could not be studied.

Table I. ARMADILLO. LRSM Stations Reporting Short-Period Vertical Signal Receipt

Station	Identification	Reason for not Processing
Death Valley, California	DV CL	-
Mina, Nevada	MN NV	-
Kanab, Utah	KN UT	-
Austin, Nevada	AT NV	Time information missing
Bakersfield, California	BF CL	Recording system overdriven
Twentynine Palms, Calif.	TN CL	-
Williams, Arizona	WM AZ	-
Fillmore, Utah	FM UT	-
Flagstaff, Arizona	FS AZ	-
Campo, California	CP CL	-
Winnemucca, Nevada	WI NV	-

Station	Identification	Reason for not Processing
Marysville, California	MV CL	-
Snowflake, Arizona	SF AZ	-
Vernal, Utah	VN UT	-
Springerville, Arizona	SV AZ	-
Venator, Oregon	VT OR	-
Durango, Colorado	DR CO	-
Hailey, Idaho	HL ID	-
Mogollon, New Mexico	ML NM	Time information missing
Truth or Consequences, N.M.	TC NM	-
Pendleton, Oregon	PT OR	Excessively weak signal
Las Cruces, New Mexico	LC NM	-
Sleepy Eye, Minnesota	SE MN	Excessively weak signal

II. PRESENTATION OF DATA

This section presents the data obtained from the digital processing program. Presentation is made in two categories: time domain data and frequency domain data. A description of the processing and computational methods is given in the following section.

A. Time Domain Data

1. Entire Signal Traces

For the purpose of providing an overall view of the entire received short-period vertical signal at each station, figures 1 through 6 present time traces of each signal over a time interval from about 15 to 20 seconds before the predicted P_n arrival to a time beyond which no evidence of the signal is visible. The amplitudes of the traces were chosen solely for convenience and have no particular relationship one to another. Similarly, no effort was made to align the traces in any particular time relationship. An arbitrary time scale is provided for each trace. The traces are grouped in order of increasing distance from NTS.

2. Signal Phase Studies

Figures 7 through 20 present displays by radials of stations of received P_n, P_g and L_g phases. Predicted phase arrival times have been used to align the time traces in accordance with standard velocities of 8.11 km/sec for the P_n phase, 6.0 km/sec for the P_g phase, and 3.5 km/sec for the L_g phase. Distance from NTS is used as the ordinate for each display.

Trace amplitudes have been adjusted to nearly the same maximum values for uniformity and to facilitate waveform examination.

Normalized multiplier factors are provided to place the trace amplitudes in correct perspective for comparison studies. These multiplier factors are computed on the basis that received signal amplitudes vary at each station directly as the gain of the short-period vertical seismometer system, directly as the yield of the nuclear detonation, and inversely as the cube of the distance from NTS. All multipliers are normalized with respect to the gain and distance of the Death Valley, California, LRSM station for the STILLWATER event.

B. Spectral Studies

1. Signal-Energy Density Spectra

Figure B, plates 1 through 18 are energy-density spectra of the entire received signal at each station. The spectra are computed from autocorrelations taken over a time interval of record extending from the predicted P_n arrival to a point beyond which no signal is discernible. Absolute units of spectral intensity are $(\text{millimicrons})^2$ per cycle per second.

2. Noise-Power Density Spectra

Figure B, plates 1 through 18 are power-density spectra of the microseismic background noise at each station. The spectra are computed from autocorrelations of 2048-word data sections (equivalent to 81.92 seconds of real-time data) taken from the record interval just prior to the P_n arrival. Absolute units of spectral intensity are $(\text{millimicrons})^2$ per cycle per second.

Many of the noise spectra will be observed to contain peaks of substantial intensity in the vicinity of 5 to 6 cps and of 9 to 10 cps. These peaks are believed to be caused by "system noise" and are not felt to be seismic in origin. It is likely from the frequencies involved that this extraneous noise has its origin in one or more of the magnetic-tape transports in the system.

3. Signal-to-Noise Ratio Spectra

Figure C, plates 1 through 18 are signal-to-noise density ratio spectra obtained for each station by computing the ratio of the signal-energy density spectrum to the noise-power density spectrum at 0.1 cps frequency intervals. The resulting spectrum provides a measure at each frequency of the

signal-to-noise ratio in an incremental bandwidth centered about that frequency. The ordinate is expressed in decibels, where $db = 10 \log_{10} (S/N)$.

Because the signal and noise spectra do not provide stable spectral estimates in the frequency range 0 to 0.1 cps, the signal-to-noise ratio spectra are not computed below 0.1 cps.

4. Integrated Signal-Energy Density Spectra

Figure A, plates 1 through 18 are octave-band integrations of the signal-energy density spectra obtained by integrating the spectra over octave bandwidths having center frequencies ranging from 0.15 cps to 9.3 cps. The ordinates are given in $(\text{millimicrons})^2$, and represent for any frequency f_c the total signal-energy contained in a bandwidth extending from $2/3\ f_c$ to $4/3\ f_c$.

III. DATA PROCESSING METHODS

In order that maximum utility be available from the data presented in the preceding section, the following description

is presented of the data processing methods and computational techniques employed in the program.

A. Frequency Domain Processing

In this section, the general theory pertaining to spectral analysis is briefly reviewed and the computational techniques employed are described. Methods employed in other areas of spectral data processing are described.

1. Spectral Analysis

The methods of spectral analysis employed in this study are those described in detail by Lee[1] and by Blackman and Tukey[2]. Briefly, for either a noise-power density spectrum or a signal-energy density spectrum, the autocorrelation given generally by

$$\phi_{11}(\tau) = \int_{-\infty}^{\infty} f_1(t)\, f_1(t+\tau)\, dt \qquad (1)$$

[1] Lee, Y. W., Statistical Theory of Communication, John Wiley and Sons, New York, 1960.

[2] Blackman, R. B. and Tukey, J. W., The Measurement of Power Spectra, Dover, New York, 1958.

is first computed for a selected section of sampled digitized data approximately from

$$\Psi_{11}(m\,\Delta T) = \frac{F}{N-m} \sum_{n=1}^{N-m} f_n \cdot f_{n+m} \qquad (-127 \leq m \leq 127) \qquad (2)$$

in which

F = computer scale factor

N = total number of data samples in the data section

T = sampling interval

M = number of time shifts (such that $m\Delta T$ corresponds to in Eq. 1)

f_n = n^{th} sample of the data section (corresponding to $f_1(t)$ in Eq. 1)

f_{n+m} = $(n+m)^{th}$ sample of the data section (corresponding to $f_1(t+\tau)$ in Eq. 1)

Use of this approach requires that the minimum requirements of the sampling and quantization theorems are met, such that the effects of frequency aliasing and the loss of statistics from amplitude quantization are negligible. It is further required that the effects of truncating the original data are negligible; i.e., the length of the data section is large (10 times or greater) compared with the maximum time shift $m\Delta t$ used in computing $\Psi_{11}(m\,\Delta T)$. The effects of truncating $\Psi_{11}(m\,\Delta T)$ by limiting N will be discussed.

The energy-density spectrum of an aperiodic signal is obtained from the autocorrelation by means of the Fourier cosine transform; hence, in general

$$\Phi_{11}(\omega) = \frac{1}{2\pi} \int_{-\infty}^{\infty} \phi_{11}(\tau) \cos \omega \tau \, d\tau \qquad (3)$$

and approximately,

$$\theta_{11}(2\pi m \Delta f) = F_1 \sum_{m=-127}^{127} \psi_{11}(m \Delta T) \cos 2\pi f (m \Delta T) \qquad (4)$$

in which

F_1 = computer scale factor

f_N = Nyquist or folding frequency = $1/(2 \Delta T)$

f = $k f_N / 125$

T = sampling interval

T = $f_N / 125$

The same cosine transformation of the autocorrelation of a time section of seismic noise yields the power-density spectrum of the noise process, if it can be assumed that the process is stationary and ergodic. Hence, noise-power density spectra as well as signal-energy density spectra are computed by Eqs. 2 and 4.

Because the spectra are computed from truncated autocorrelations of only 255 terms, the spectral estimate is impaired, but substantial improvement is gained by smoothing* the raw spectrum obtained by Eq. 4. The smoothing technique employed is known as "hanning" and may be described by

$$A'(f) = 1/4 \, [A(f-\Delta f) + A(f+\Delta f)] + 1/2 \, [A(f)] \qquad kf_N/125 \le f \le f_N - \Delta f, \quad 1 \le k \le 125 \qquad (5)$$

$$A'(f_N) = 1/2 \, [A(f_N) + A(f_N - \Delta f)] \qquad (6)$$

$$A'(0) = 1/2 \, [A(0) + A(f_N/125)] \qquad (7)$$

when smoothing on the same frequency increments as the transform is calculated.

For the numerical parameters involved in the analysis, i.e., an equivalent sampling frequency of 25 cps, the computation of 255 terms of the autocorrelation, and the use of equivalent 0.040 second incremental time shifts in computing the autocorrelation, it turns out that the spectra computed and smoothed on 0.1 cps centers provide a stable reliable estimate of the

* See Blackman and Tukey

true spectra from the folding frequency of 12.5 cps down to a lower frequency limit of about 0.1 cps and provide resolution of spectral peaks 0.2 cps apart.

2. Signal-to-Noise Spectral Density Ratios

An estimate at each station of the ratio of signal energy per unit bandwidth is obtained by forming the ratio at 0.1 cps frequency increments of the signal-energy density spectrum to the noise-power density spectrum. The resulting signal-to-noise ratio spectrum is interpreted as providing at any given frequency a measure of the signal-to-noise ratio existing in an incremental bandwidth centered on that frequency. Note that although dimensionally the concept of bandwidth does not appear explicitly in the ratio, it is not permissable to consider the ratio as existing over any arbitrary bandwidth, even though the same bandwidth is employed with both signal and noise.* The computed ratios are correct only for a very

*Strictly, the signal energy and noise power are both infinitesimal at any given frequency. Nonetheless, their ratio exists and is that given by the signal-to-noise ratio spectrum.

small, incremental bandwidth (in the order of 0.1 cps) centered on each frequency in the ratio spectrum.

3. Integrated Signal-Energy Density Spectra

The integrated signal-energy density spectra provide a means for obtaining from the signal-energy density spectra an estimate of the total signal energy to be found in association with any particular frequency, in a form that is comparable with similar estimates obtained from more conventional visual analysis of paper records.

It has been found that such a visual analysis involves an equivalent band-pass filtering operation characterized usually by an octave bandwidth.* Accordingly, the signal-energy density spectra are integrated over octave bandwidths to yield the total signal energy per octave bandwidth. The center frequency of the octave-band filter is varied in 0.15 cps steps over the range 0.15 cps to 9.3 cps while the band limits vary from 0.1 and 0.2 cps to 6.2 and 12.4 cps, respectively. The integrated spectra have the dimensions of energy per octave bandwidth.

* See, for example, "Instrument Noise in Seismometers", by C. J. Byrne, Bulletin of the Seismological Society of America, Vol. 51, No. 1, Jan. 1961.

B. Time Domain Processing

In this section, the methods are described that are used to prepare time domain presentations of signal phases such that the study of relative amplitudes, waveforms, and departures from standard velocities is facilitated.

1. Arrival Time Studies

Arrival times T_a for the P_n, P_g and L_g phases are computed from the relations

$$T_a = \frac{\Delta}{8.11} + 7.2 \text{ sec} \quad (8)$$

for the P_n phase,

$$T_a = \frac{\Delta}{6.0} \text{ sec} \quad (9)$$

for the P_g phase, and

$$T_a = \frac{\Delta}{3.5} \text{ sec} \quad (10)$$

for the L_g phase, where Δ is the epicentral distance in kilometers (provided by Geotech) and 8.11, 6.0, and 3.5 are standard phase velocities in km/sec.

Time traces of the signal phases are obtained from the digital signal edit records by digital-to-analog conversion and display of the analog signal by oscillographic camera. For presentation, these traces are aligned in time such that all predicted P_n arrival times fall on a vertical line of constant velocity corresponding to 8.11 km/sec and an intercept of 7.2 seconds, all predicted P_g arrival times fall on a slant line corresponding to a constant velocity of 6.0 km/sec, and all predicted L_g arrival times fall on a vertical line corresponding to a constant velocity of 3.5 km/sec. Examination of the signal phase waveforms accordingly allows departures from these standard velocities and corresponding arrival times to be observed.

2. Relative Signal Amplitudes

To facilitate comparisons among the signal phases received at various stations for each nuclear event studied, time traces showing the P_n and P_g and the L_g phases are presented with all traces at about the same maximum amplitude. In this manner, variations in received signal strength and seismometer system magnification from one station to another do not interfere with examination of waveforms.

In order, however, that the phases may be studied in a realistic amplitude perspective, multiplier factors are provided for each trace. These factors are obtained on the premise that signal amplitude at each station varies inversely as the cube of distance from NTS, and directly as the gain of the short-period vertical seismometer system and as the yield of the nuclear detonation. That is,

$$G \propto k \frac{r^3}{G_v W} \tag{11}$$

where k is a scaling constant, r is distance to NTS, G_v is short-period vertical gain, and W is yield.

Actually, since only relative amplitudes are of interest, the gain factors ultimately used are normalized with respect to the gain and distance of the Death Valley, California, station for the STILLWATER detonation. Hence, the normalized relative gain factors are given by

$$G_N = \frac{G_{DV}}{r_{DV}^3} \cdot \frac{W_a}{W} \cdot \frac{r^3}{G_v} \tag{12}$$

where G_{DV} is the Death Valley short-period vertical gain

(332,000), r_{DV} is the distance from NTS (143.7 km), and W_a/W is the ratio of the ARMADILLO yield to the yield for the event being studied: 1 for STILLWATER and 1/2 for STILLWATER.

Table II lists the short-period vertical channel magnification, distance from NTS, and G_N value used for each station processed. The operating gain for each station is taken to be numerically equal to the short-period vertical magnification measured during the last system calibration before arrival of the signal. Even though the actual numerical gain (measured from an earth-motion displacement at the seismometer to the output of the Digital Field System digitizer) very likely differs from the magnification, it is related by a constant which is the same for all stations. Thus, when the normalized gain factors G_N are computed, this gain-magnification constant cancels and the desired results are obtained.

Because the G_N are generally awkward multipliers with which to work, the trace multiplier factors are chosen for convenience and the actual trace amplitudes are adjusted to compensate. For example, for the Kanab, Utah, Station, G_N = 19.93. A

Table II. ARMADILLO. Distance from NTS, short-period vertical gain, and normalized gain factor

DV CL	134.4 km	297.0	4.40
MN NV	241.8	38.5	20.92
KN UT	285.8	61.3	19.93
TN CL	315.8	254.0	6.33
WM AZ	388.2	207.0	14.63
FM UT	413.7	221.0	17.22
FS AZ	479.1	362.0	16.17
CP CL	479.1	352.0	1.53
WI NV	493.7	314.0	22.25
MV CL	521.1	316.0	2.20
SF AZ	577.2	202.3	4.76
VN UT	680.3	159.0	9.61
SV AZ	700.6	84.2	19.81
VT OR	707.6	349.0	50.85
DR CO	733.7	384.0	4.96
HL ID	748.8	358.9	7.61
TC NM	890.9	136.0	25.25
LC NM	1005.5	392.0	12.60

multiplier of 15.0 is chosen for convenience and the trace amplitude is made 1.329 times as large as that of the normalising Death Valley trace. In this manner, inconvenient multiplying factors are avoided, and yet all traces are made to have nearly the same maximum amplitude for uniformity of presentation.

C. Absolute Calibration of Spectra

To permit comparisons among signal and noise spectra computed for various stations and to facilitate interpretation of the data, it is desirable to present energy density and power-density spectra in terms of absolute earth motion, the spectral ordinates having the dimensions of $(\text{millimicrons})^2$ per cps. Absolute calibration is obtained from weight-lift calibration data and from manufacturer's shake-table measurements made on the seismometer and phototube amplifier.

1. Calibration Method

From shake-table data, the peak-to-peak seismometer base displacement, for sinusoidal motion at a frequency of 1 cps, is found that produces the same output voltage amplitude as that of the voltage pulse produced when a given weight is lifted. From this empirical relation between a weight-lift input to the

seismometer system and a base-displacement input, and from a knowledge of the final system output produced from a given weight-lift input, the overall system calibration is obtained.

It should be noted carefully that this procedure relies for its validity upon the premise that the system being calibrated has an amplitude and phase response substantially identical (except for a constant multiplier) to that of the seismometer and phototube amplifier from which the shake-table data were originally taken. For the composite system under consideration in this program - the LRSM Field System, the Honeywell F-M Playback System, and the TI Digital Field System - it is a fair assumption that indeed the overall system response is controlled by the seismometer and phototube amplifier, particularly over the restricted frequency range of interest.

It is important to realize also that application of this calibration technique results only in the assignment of absolute units of earth motion to the spectral ordinates. The spectra are still viewed as it were, through the response function of the seismometer and phototube amplifier, and do not represent true earth

motion. For the purposes of this program, where principal interest is in comparisons among station outputs, it is believed that omission of seismometer response equalisation neither compromises the results nor limits the usefulness of the data.

2. Multi-Channel, Two-Level Recording and Gain Ratios

Because the ball-lift calibrations almost invariably were of such amplitude as to cause overdriving of the f-m recording system on Channel 5, the high-gain short-period vertical recording channel, it was frequently necessary to rely upon channel 6, the low-gain, short-period vertical channel, for ball-lift amplitude information.

Two practical problems of substantial magnitude made this alternative difficult, however. First, channel 6 had a substantial content of "system noise" evidently acquired during the making of the master composite and copy tapes. The presence of this noise made suspect the amplitude of a single ball-lift pulse and necessitated taking the average of several amplitudes. Second, the gain ratio between channels 5 and 6 while nominally 10 to 1 was found to vary from values as low

as 6.6 to as high as 13.0, the average being 10.7. Accordingly, before calibration information from channel 6 could be used for the absolute calibration of channel 5, it was necessary to determine for each station from the data on hand what gain ratio existed at the time of the nuclear event.

These gain ratios were determined after substantial effort by means of the following method. First, the paper monitor records of each event at each station were examined to determine the location of a time region on channel 5 in which a large signal-to-noise ratio existed, but where no system overdriving was detectable, for a period of time sufficiently long to contain about 150 peaks or troughs. Second, DARC was programmed to search within each of these selected regions, find 128 peaks or troughs, and at the time corresponding to each compute the ratio of the channel 5 amplitude to the channel 6 amplitude, and average these 128 ratios.

It was found upon examination of the statistical distribution of the gain ratios that extreme skewing was sometimes present such that the average of the ratios did not accurately reflect the mean of their distribution. To correct this effect, it was

necessary to cast out those computed ratios which fell outside an interval approximately 4σ in extent and adjust the averages accordingly. This procedure led to meaningful averages.

3. Calibration Data

Table III presents a summary of the calibration data for the ARMADILLO event, including the channel gain ratios described above.

Table III. ARMADILLO. Calibration Data

Station	Signal Channel	Gain Ratio	Ball Wts. (mg)	Equiv. mμ	Ball Lift Amp	Output Number per mμ at 1 cps
DV CL	6	11.0	255.3	319.0	232	0.727
MN NV	6	11.5	255.3	319.0	212	0.665
KN UT	6	10.9	130.5	163.2	1791	1.007
TN CL	6	10.5	130.5	163.2	175	1.072
WM AZ	6	10.7	130.5	163.2	432	2.647
FM UT	6	11.3	55.0	578.0	1245	0.191
FS AZ	6	11.0	130.5	163.2	164	1.005
CP CL	5	11.4	130.5	163.2	1707	10.460
WI NV	6	11.6	130.5	163.2	177	1.085
MV CL	5	9.9	130.5	163.2	257	15.590
SF AZ	6	10.3	130.5	163.2	181	1.109
VN UT	5	11.5	55.0	578.0	585	11.639
SV AZ	5	6.6	255.3	319.0	157	3.248
VT OR	6	10.3	130.5	163.2	241	1.477
DR CO	5	13.0	55.0	578.0	517	11.628
HL ID	5	12.3	130.5	163.2	3°3	25.097
TC NM	5	10.5	130.5	163.2	233	14.990
LC NM	5	8.4	130.5	163.2	343	17.654

NOTE: All noise data were taken from Channel 5 of the f-m magnetic tape.

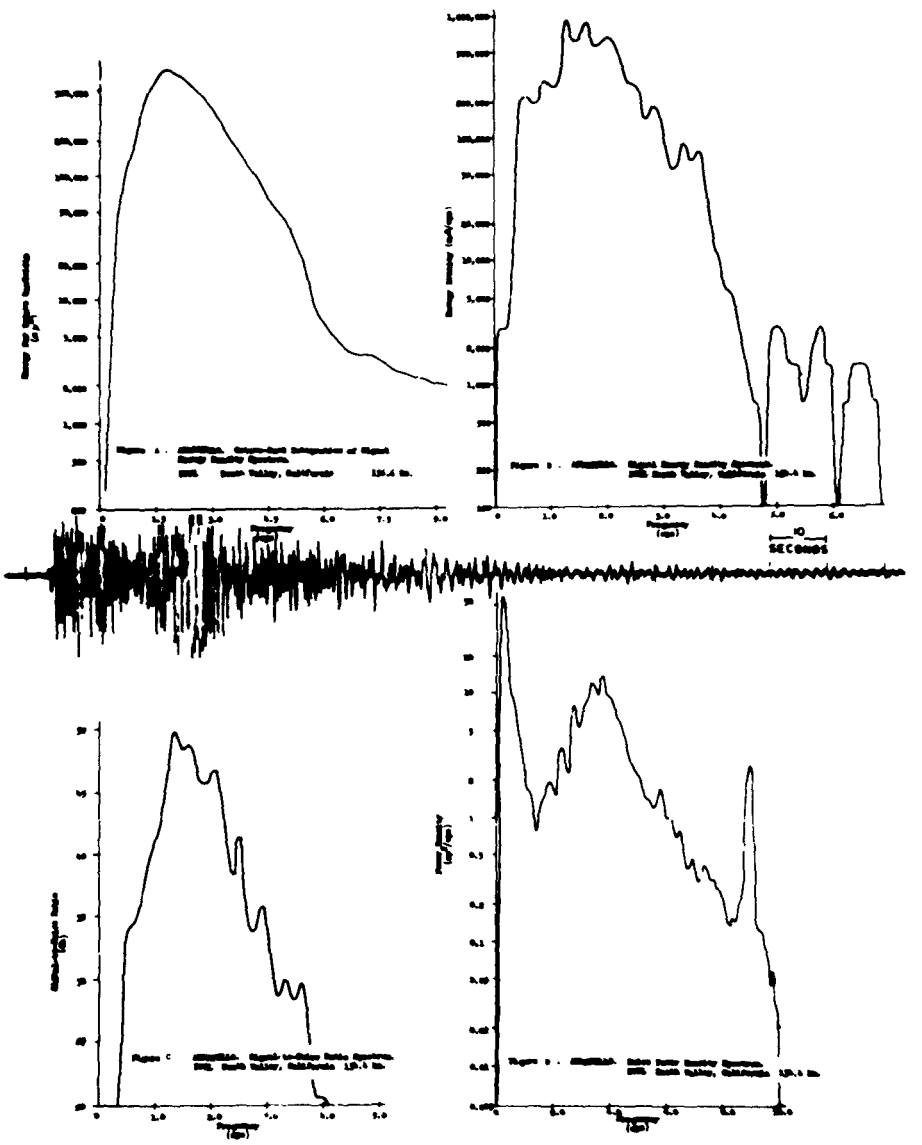

Plate 1. ARMADILLO. DV CL, 134.4 km

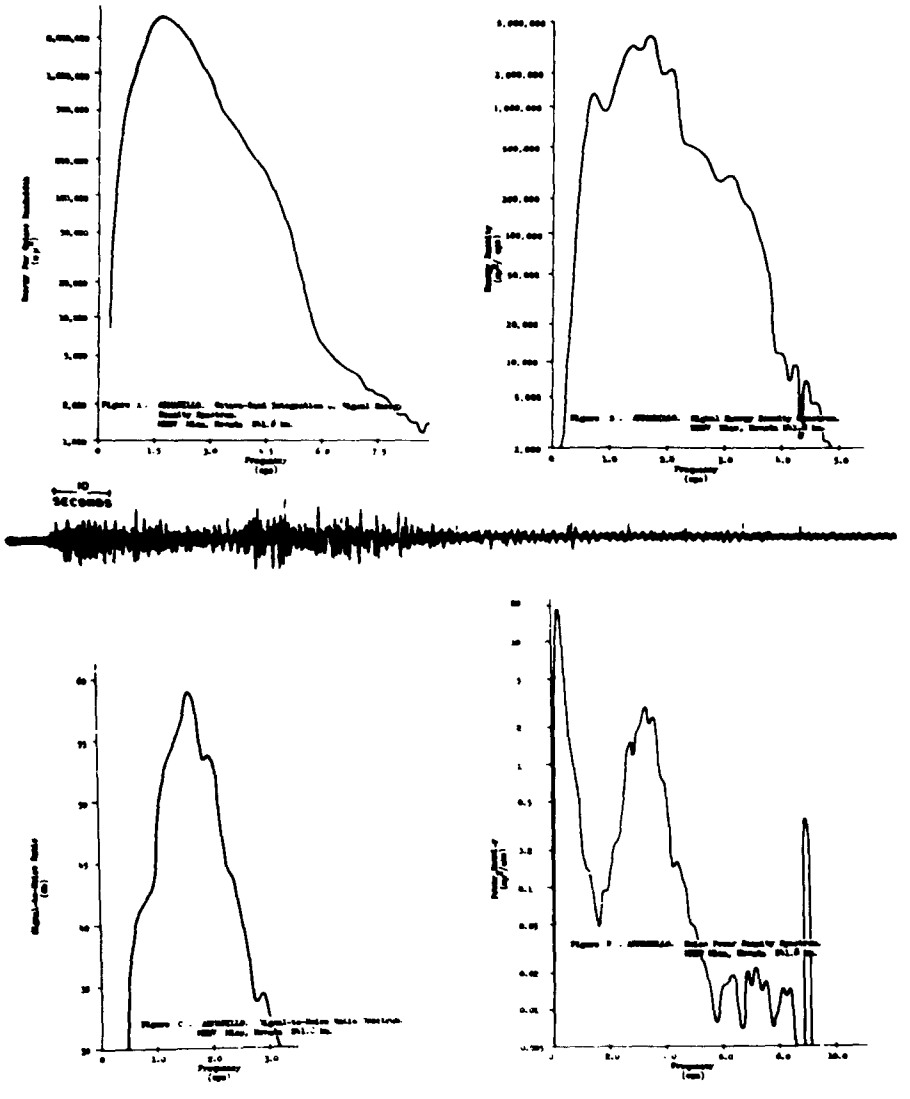

Plate 2. ARMADILLO. MN NV, 241.8 km

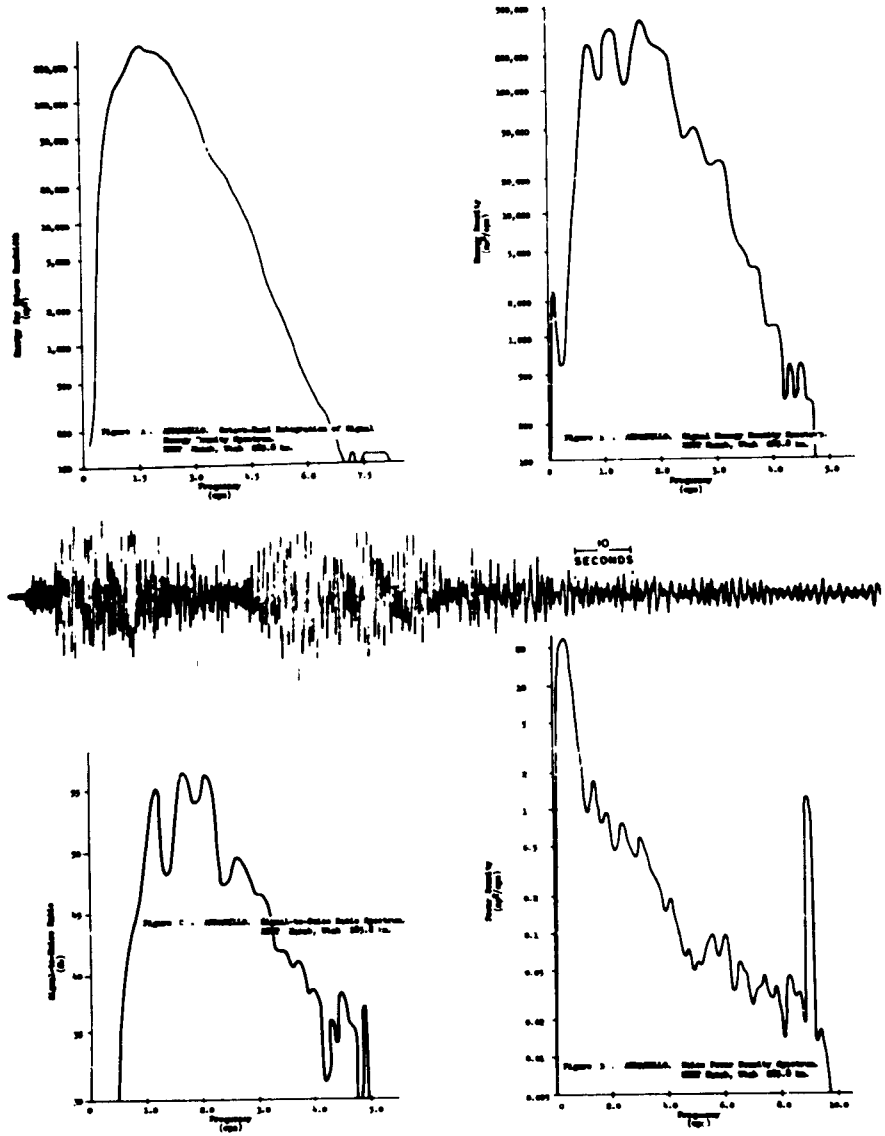

Plate 3. ARMADILLO. KN UT, 285.8 km

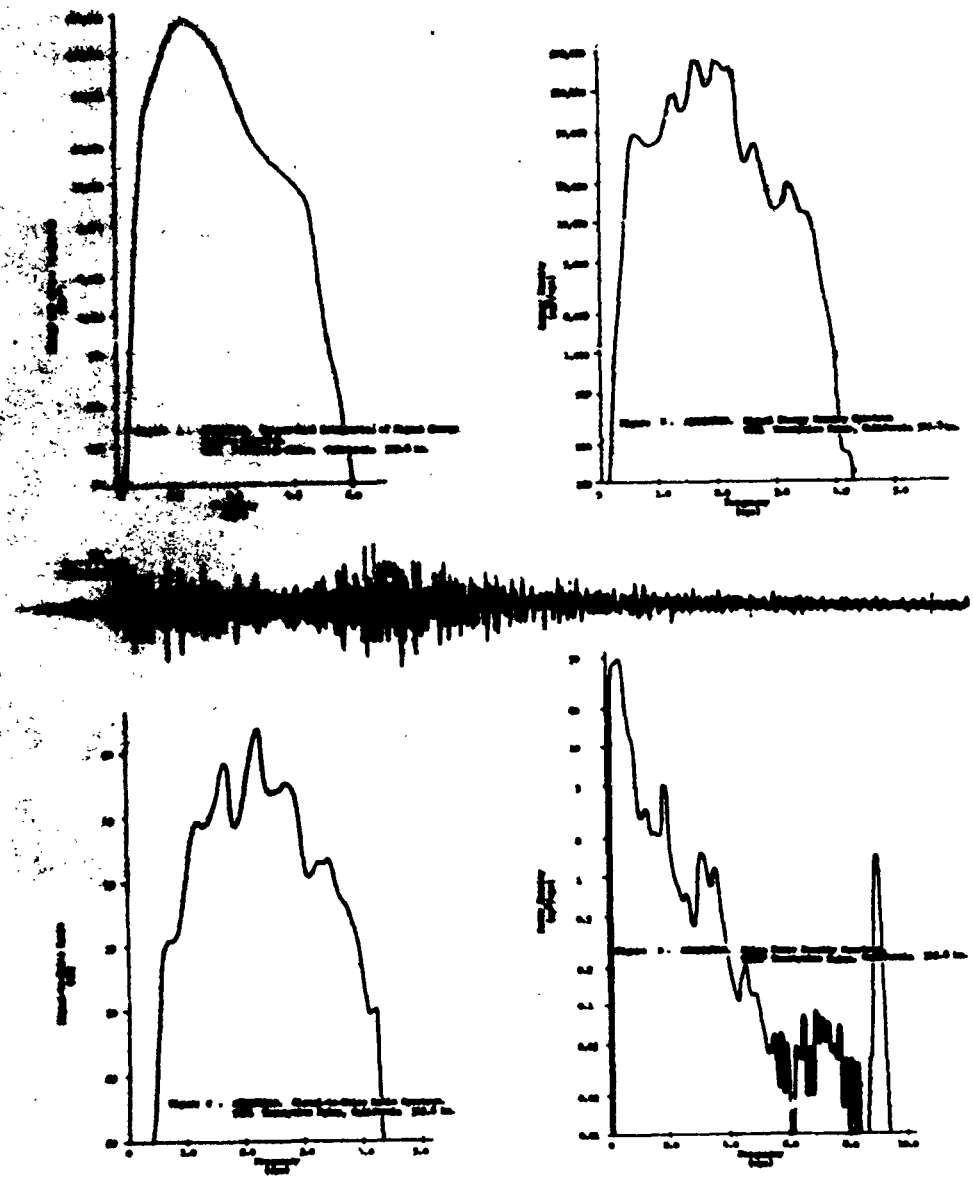

Plate 4. ARMADILLO. TN CL, 315.8 km

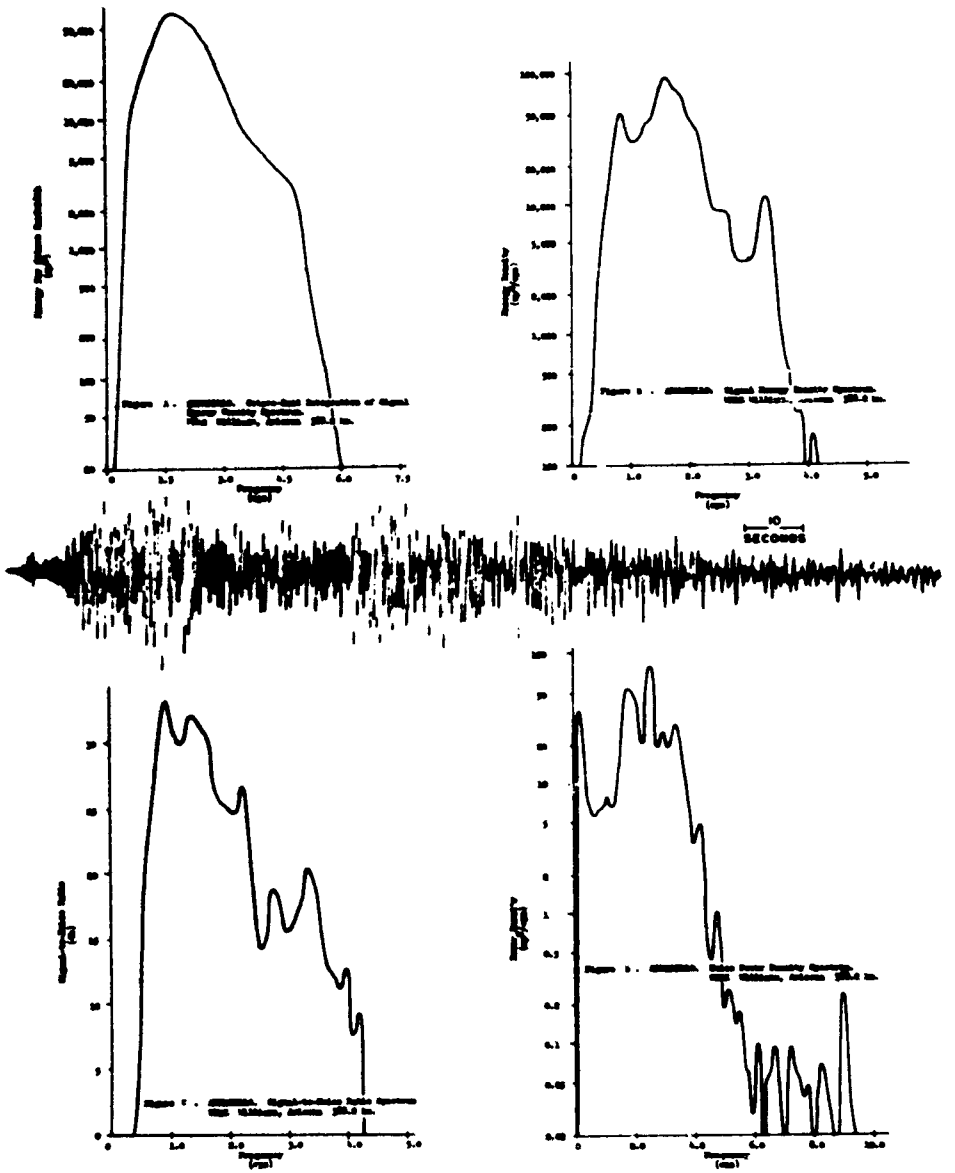

Plate 5. ARMADILLO. WM AZ, 388.2 km

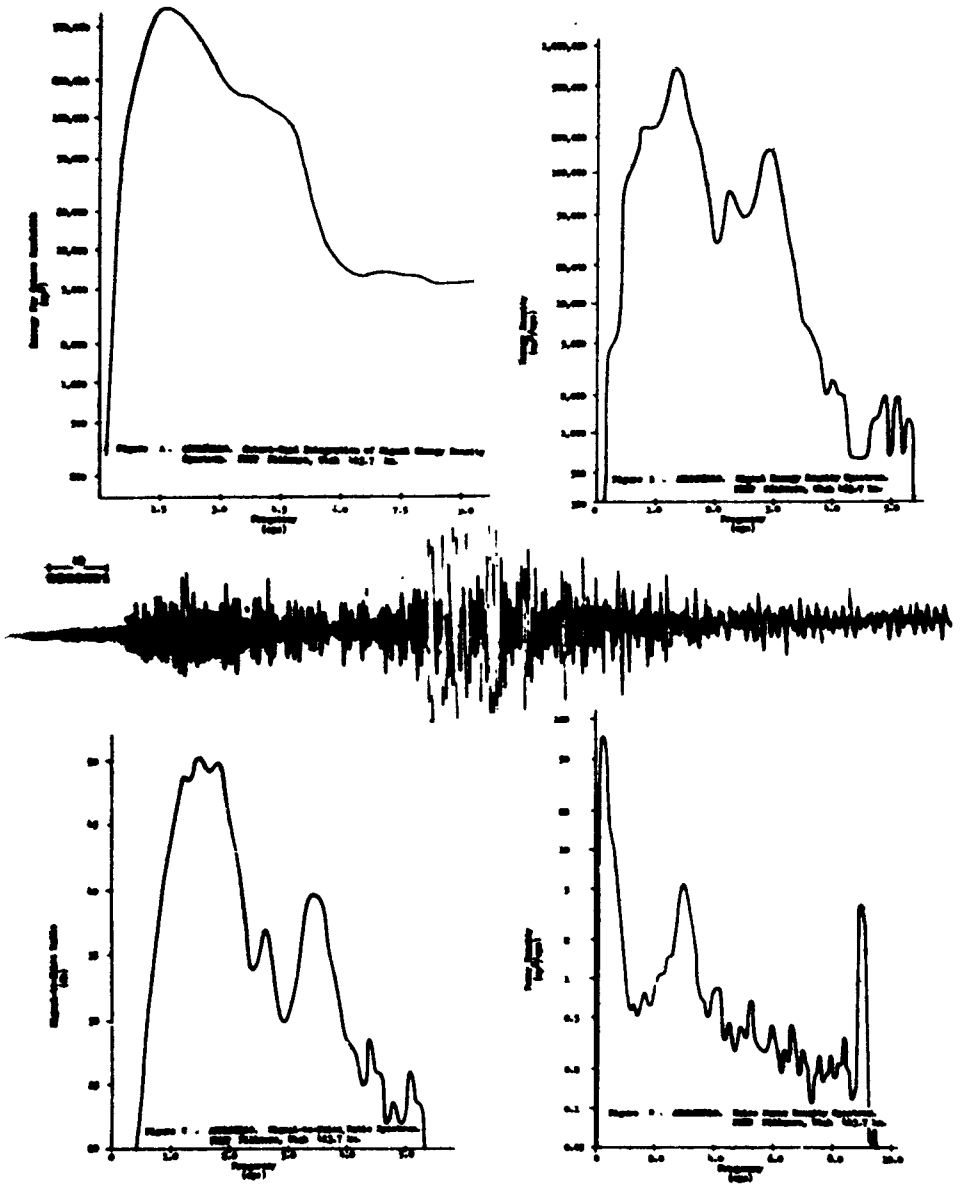

Plate 6. ARMADILLO. FM UT, 413.7 km

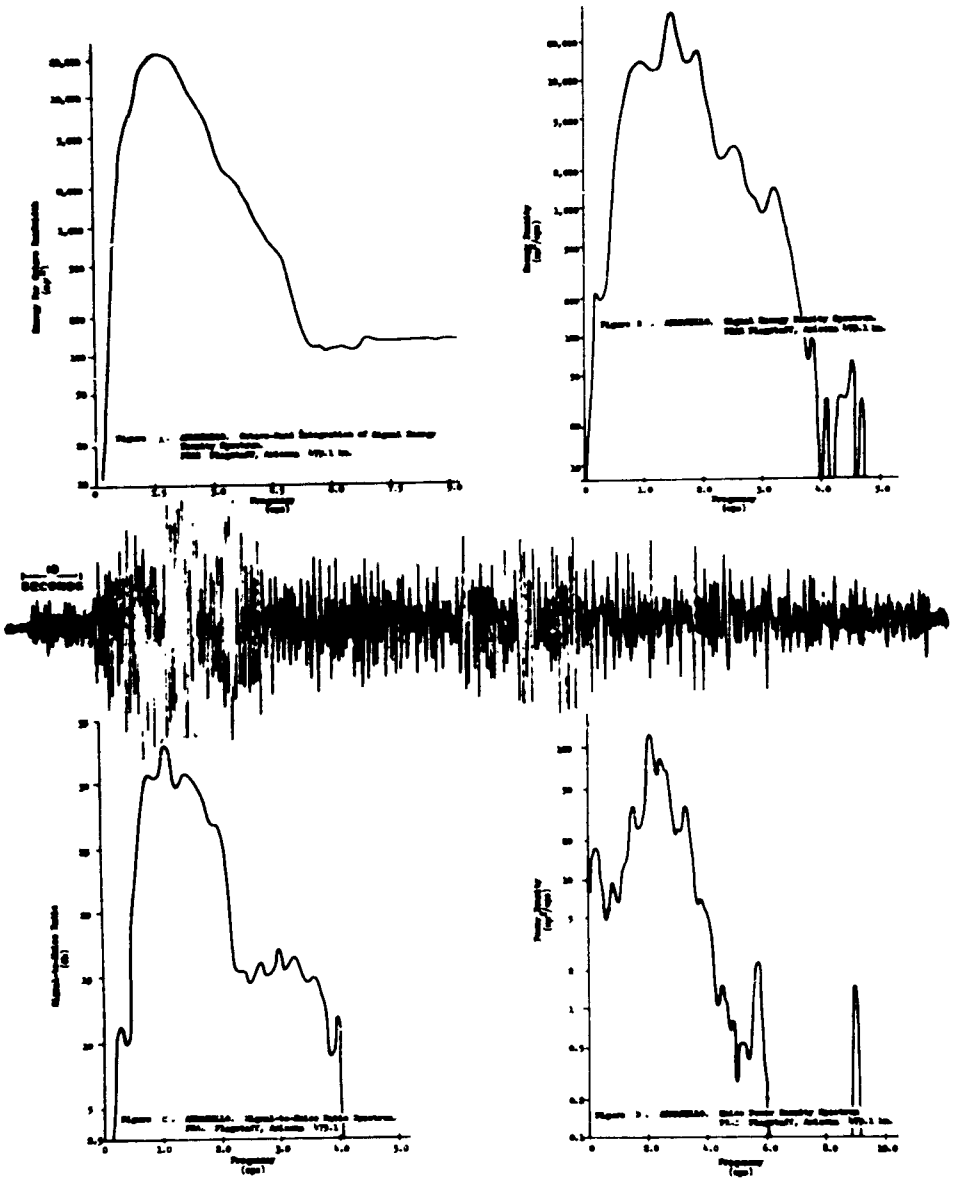

Plate 7. ARMADILLO. FS AZ, 479. 1 km

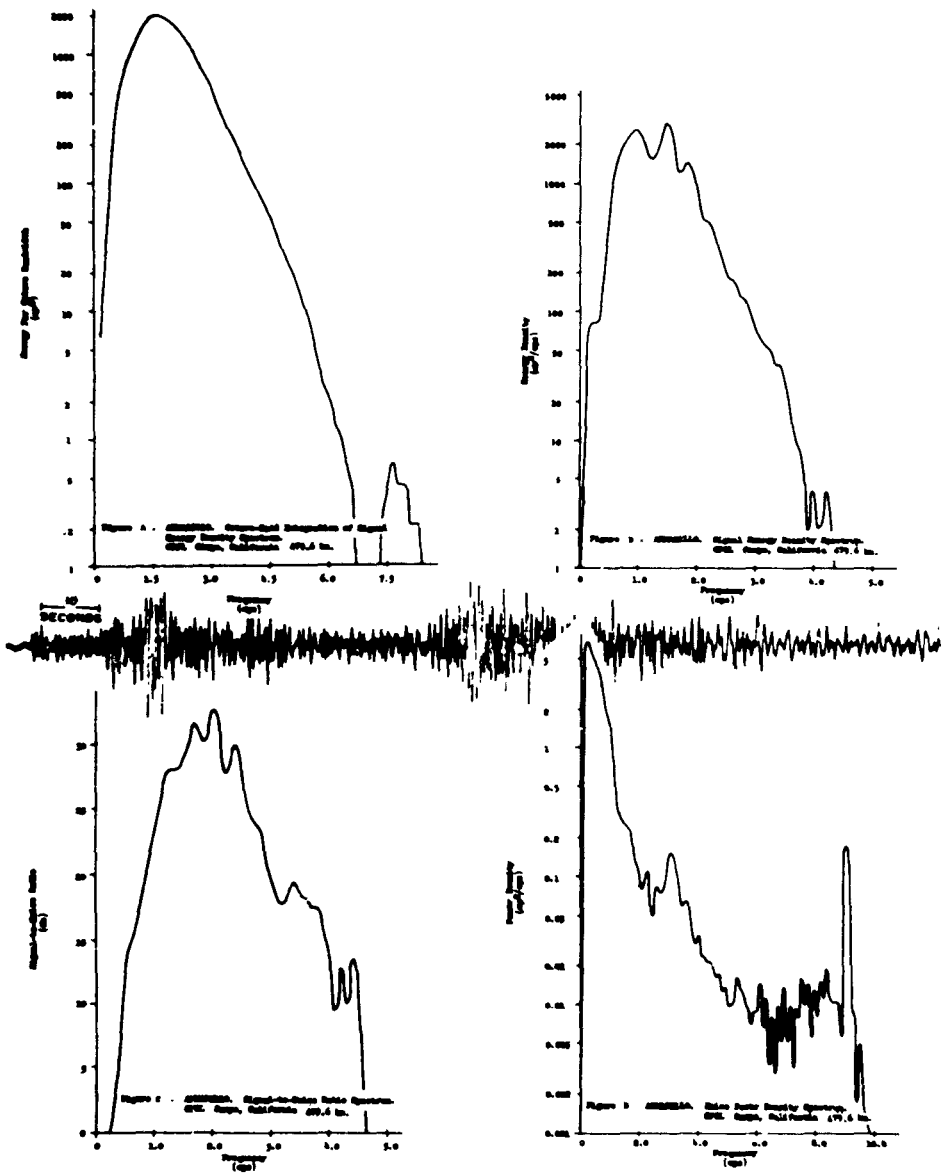

Plate 8. ARMADILLO. CP CL, 479.6 km

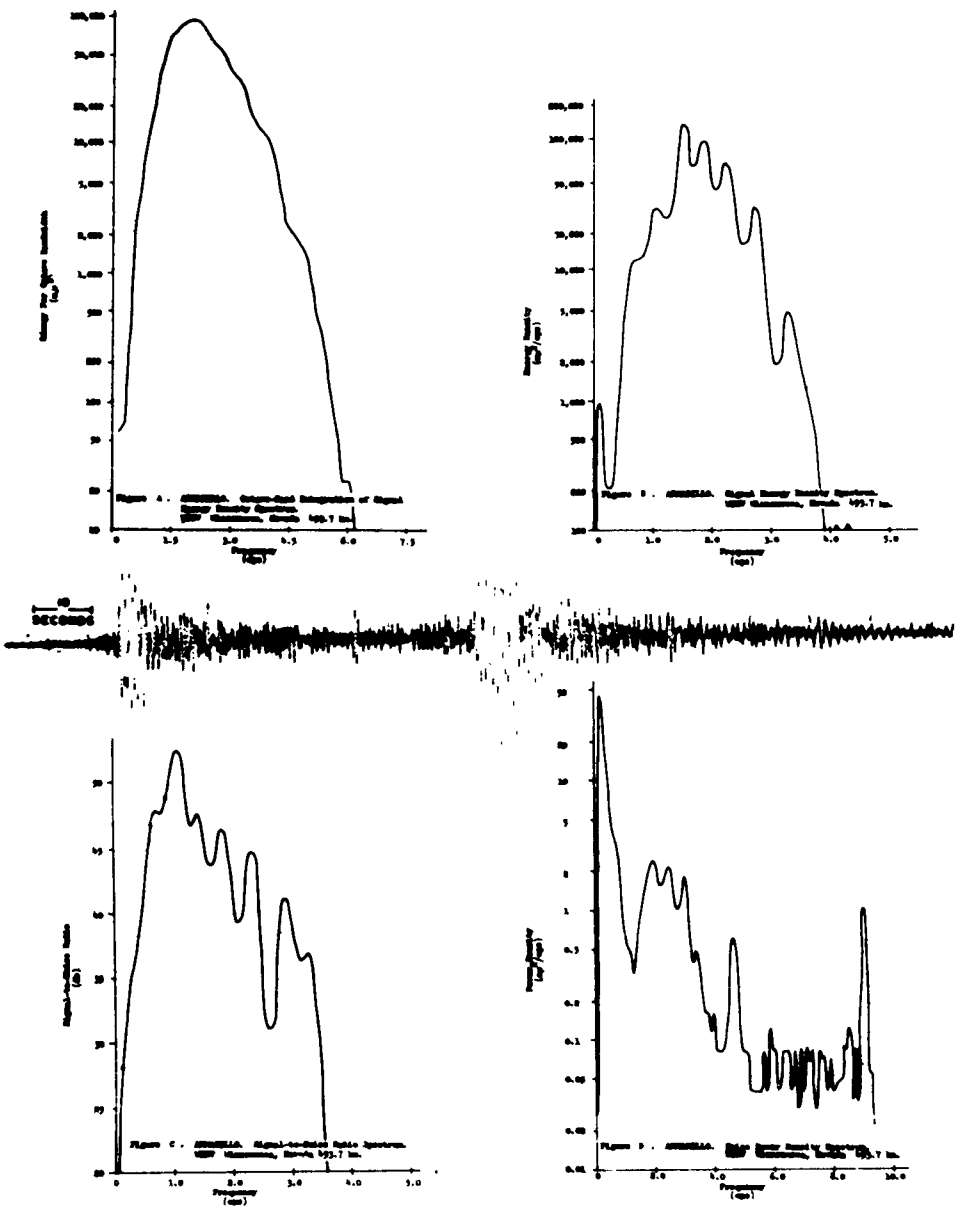

Plate 9. ARMADILLO. WI NV, 493.7 km

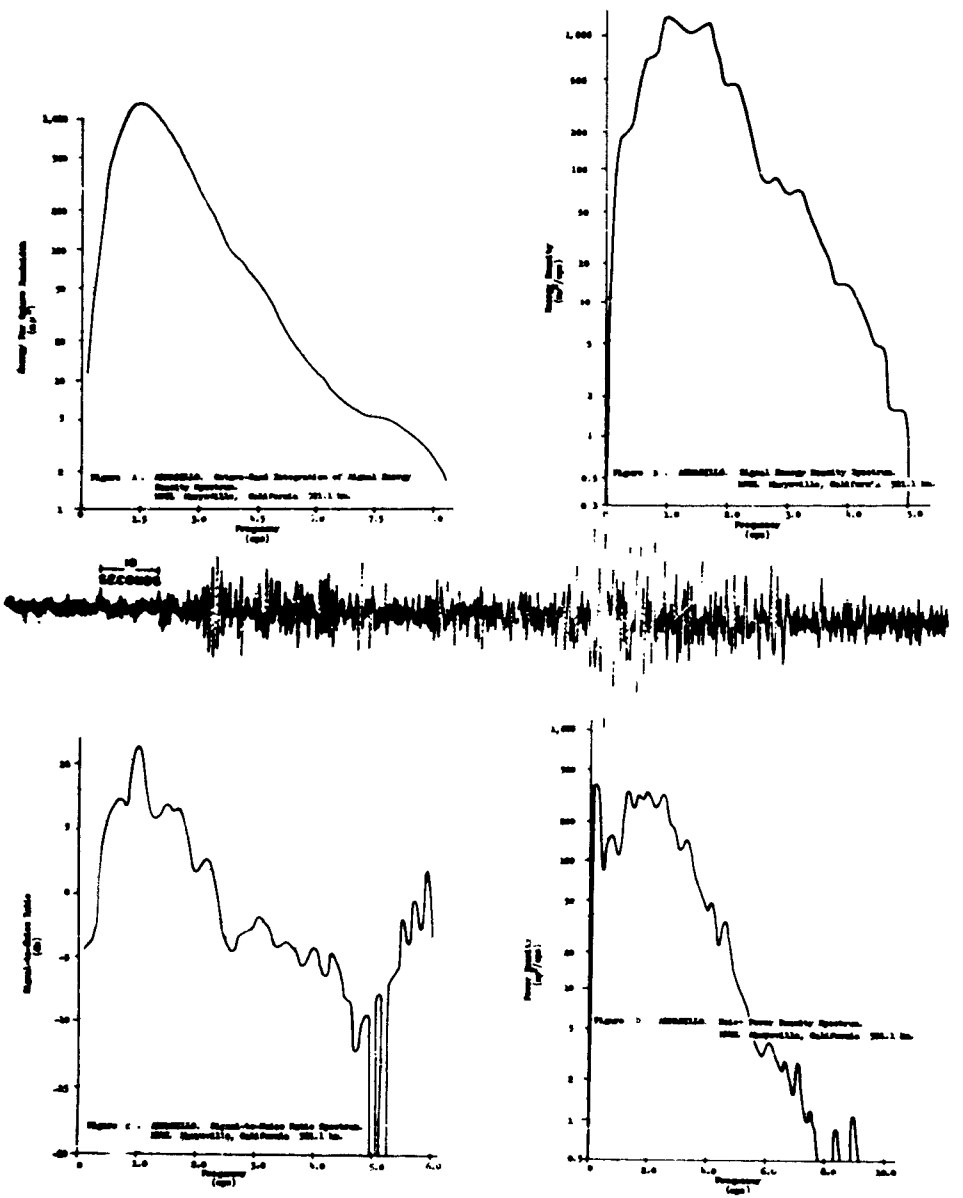

Plate 10. ARMADILLO. MV CL. 521. 1 km

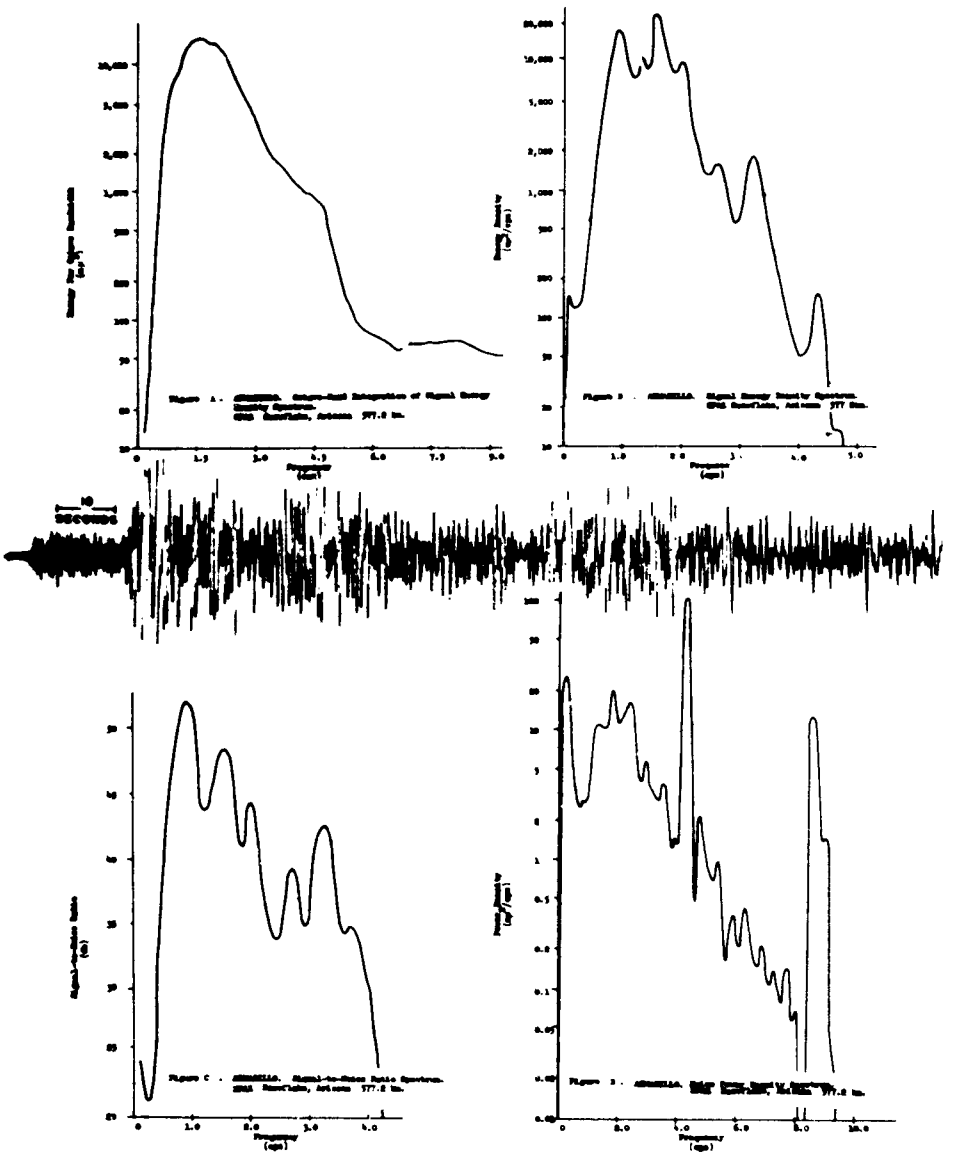

Plate 11. ARMADILLO. SF AZ, 577. 2 km

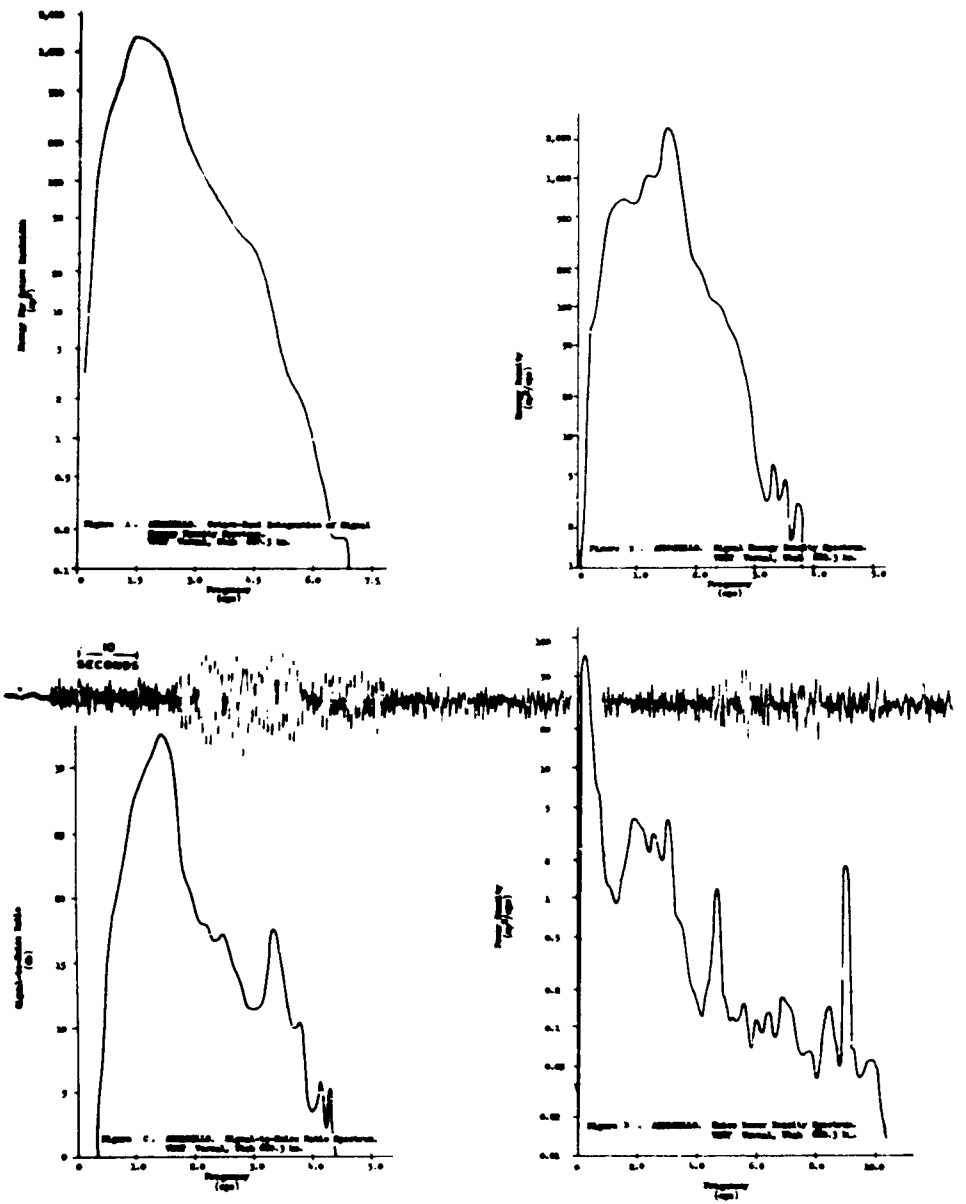

Plate 12. ARMADILLO. VN UT, 680.3 km

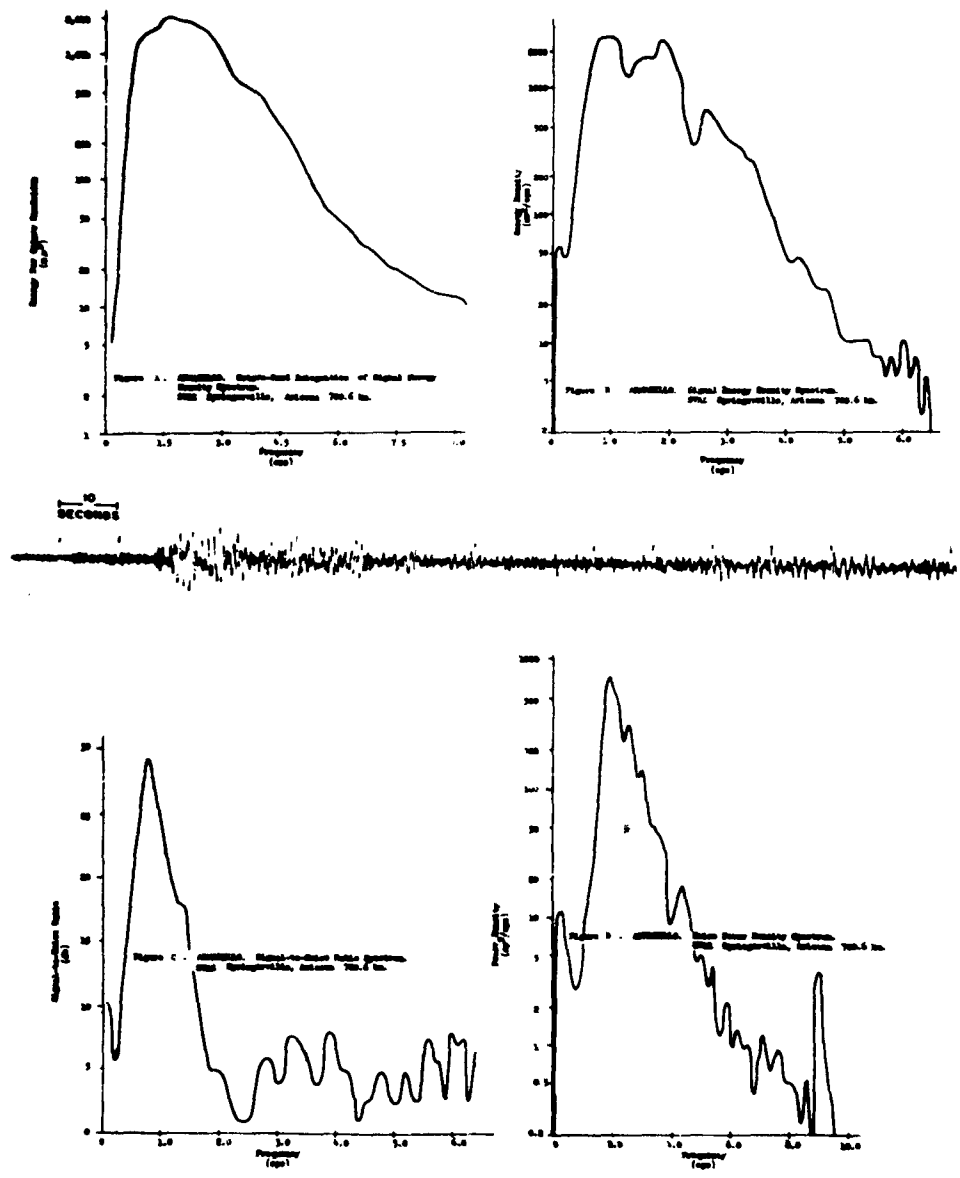

Plate 13. ARMADILLO. SV AZ, 700.6 km

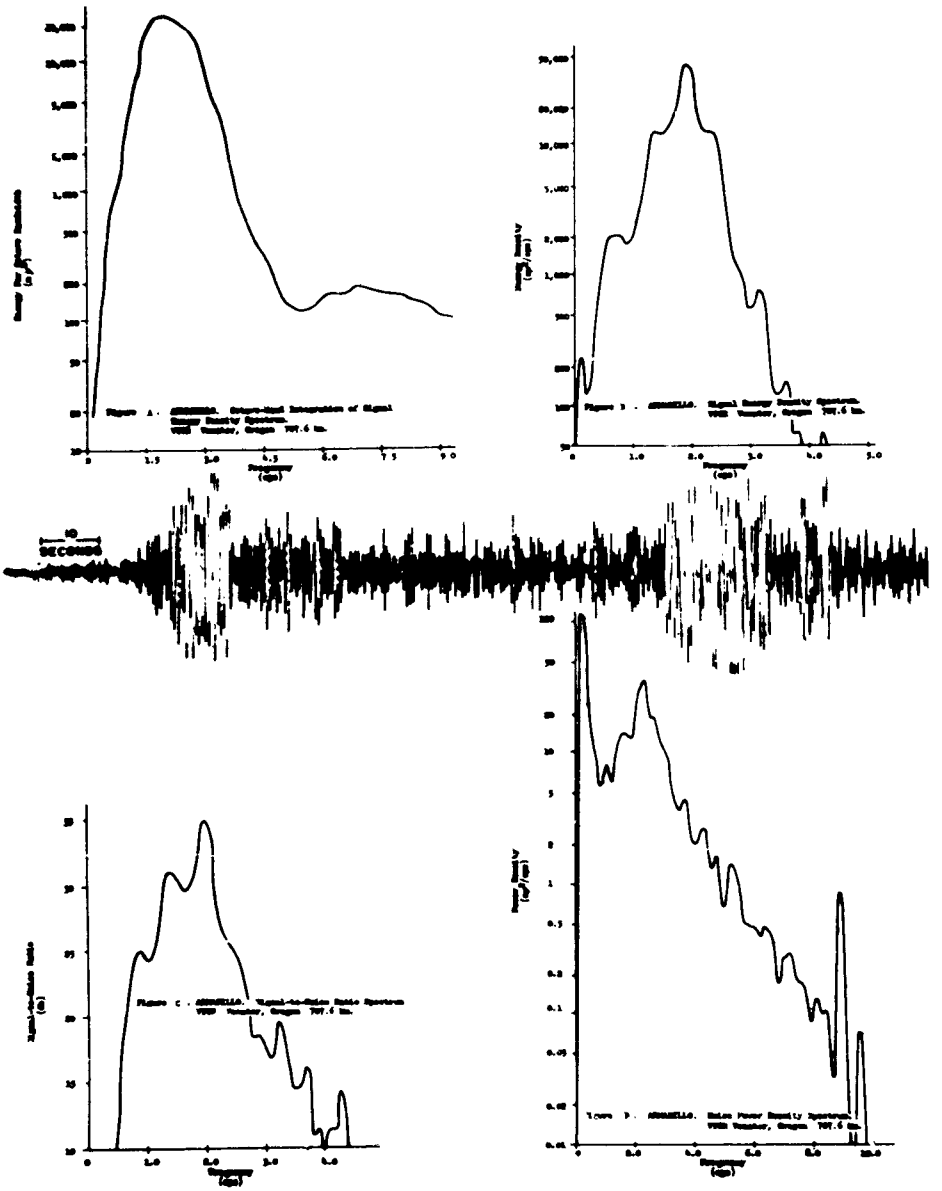

Plate 14. ARMADILLO. VT OR, 707.6 km

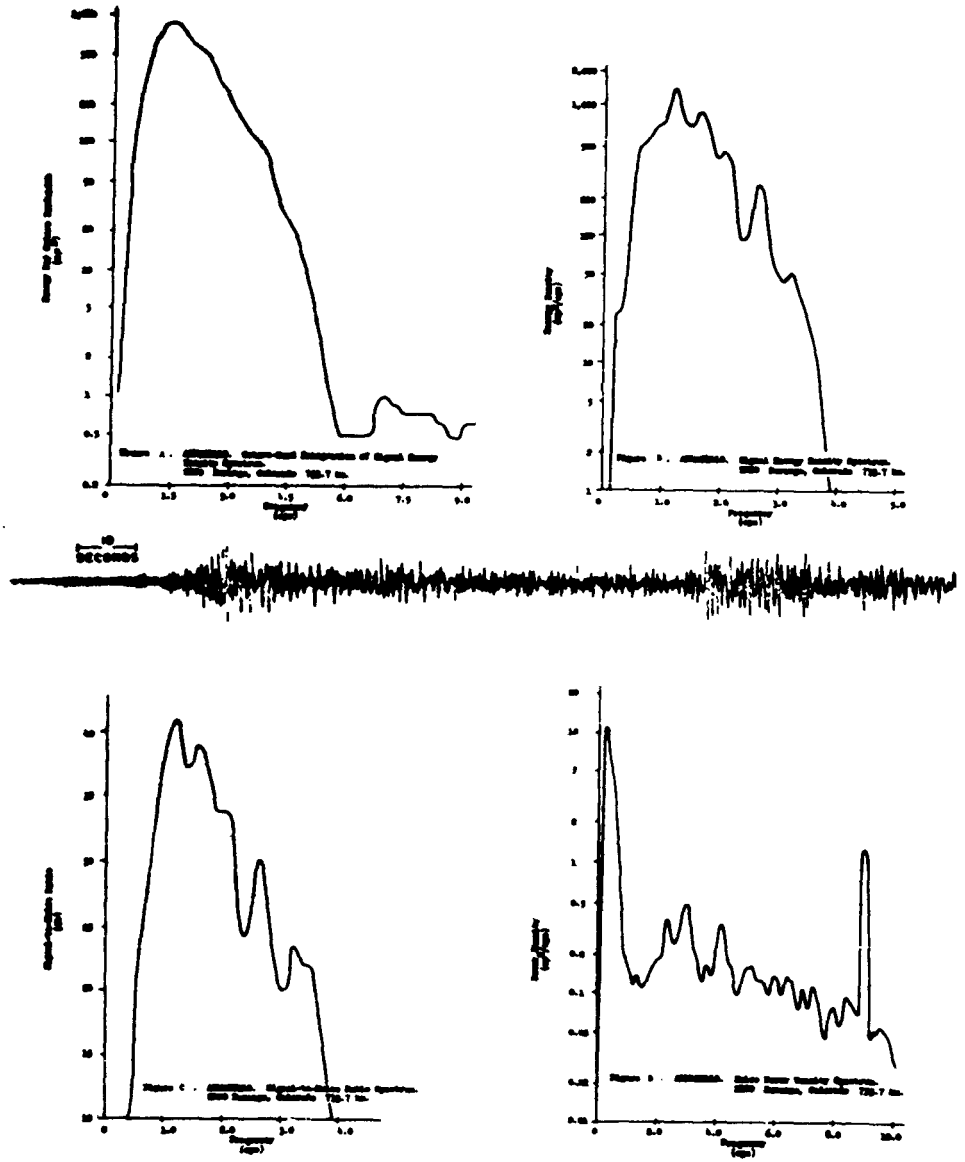

Plate 15. ARMADILLO. DR CO, 733.7 km

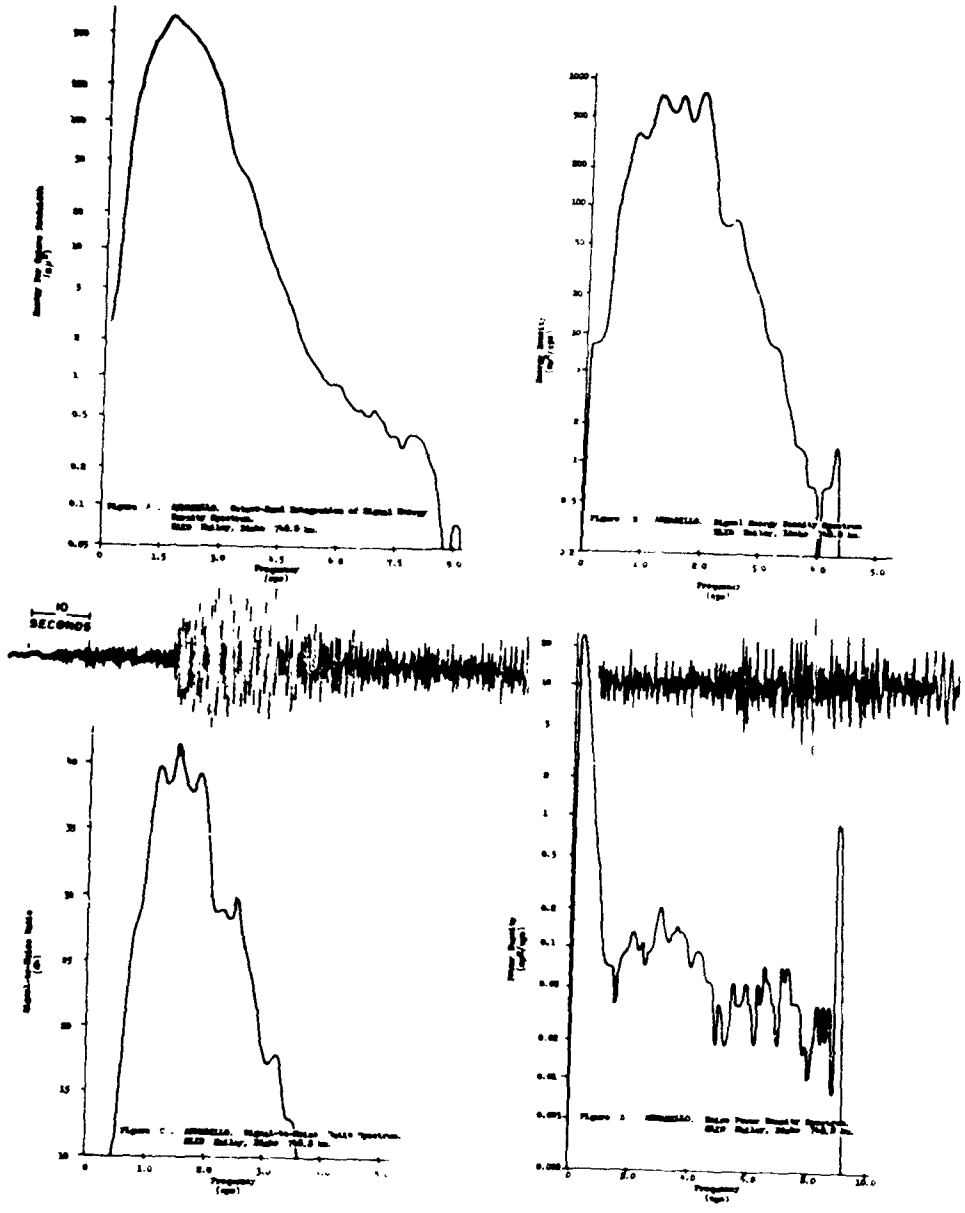

Plate 16. ARMADILLO. HL ID, 748.8 km

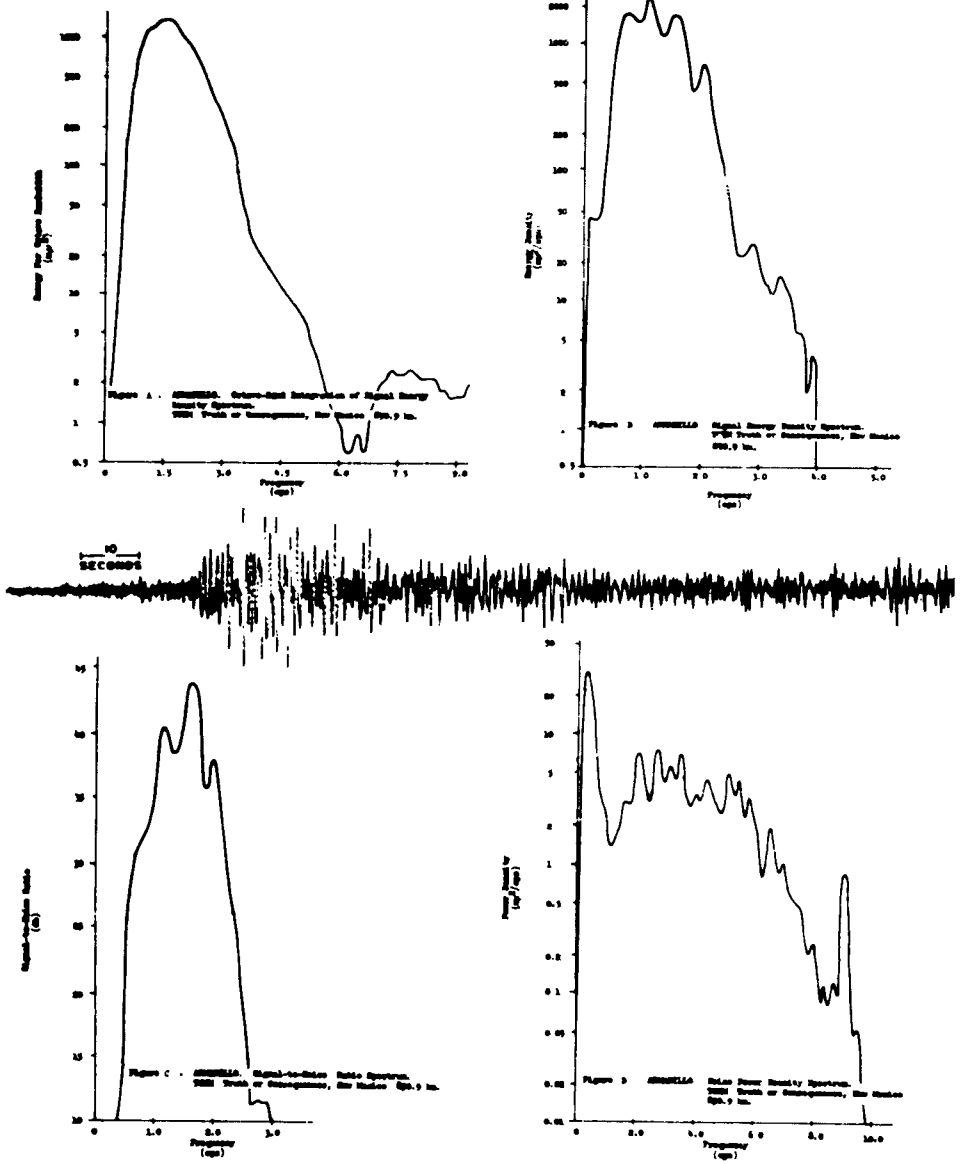

Plate 17. ARMADILLO. TC NM, 890.9 km

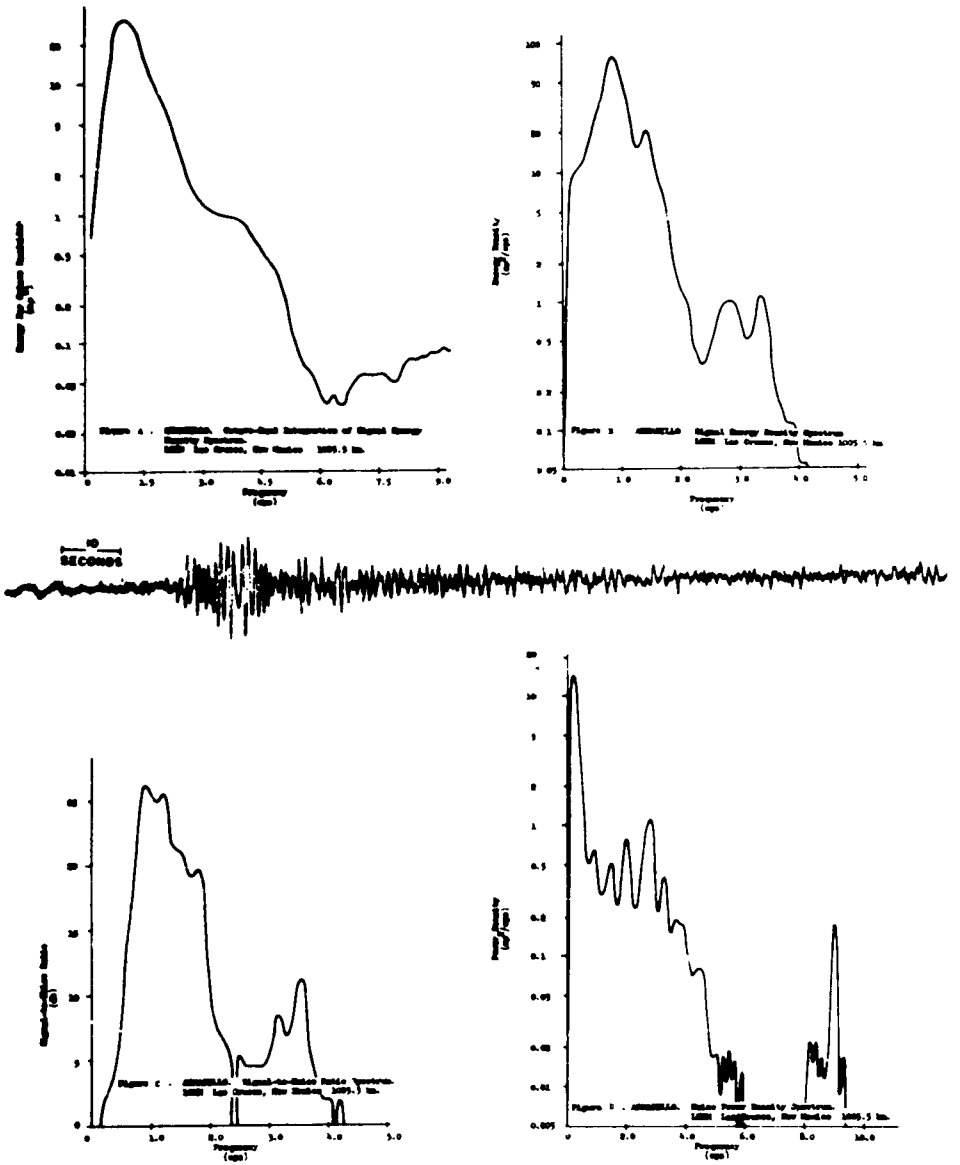

Plate 18. ARMADILLO, LC NM, 1005.5 km